MONTHLY NOTICES

OF THE

ROYAL ASTRONOMICAL SOCIETY

Vol. 116 No. 1 1956

ANNUAL CONTRIBUTIONS OF FELLOWS

By decision of the Annual General Meeting of the Society, held on 1956 February 10, the annual contribution of Fellows was increased to £4 4*s*. 0*d*. as from 1957 January 1. Fellows are reminded that the annual contribution becomes due and is payable in advance on January 1 of each year.

Published and Sold by the

ROYAL ASTRONOMICAL SOCIETY

BURLINGTON HOUSE

LONDON, W.1

Price Thirteen Shillings and Sixpence

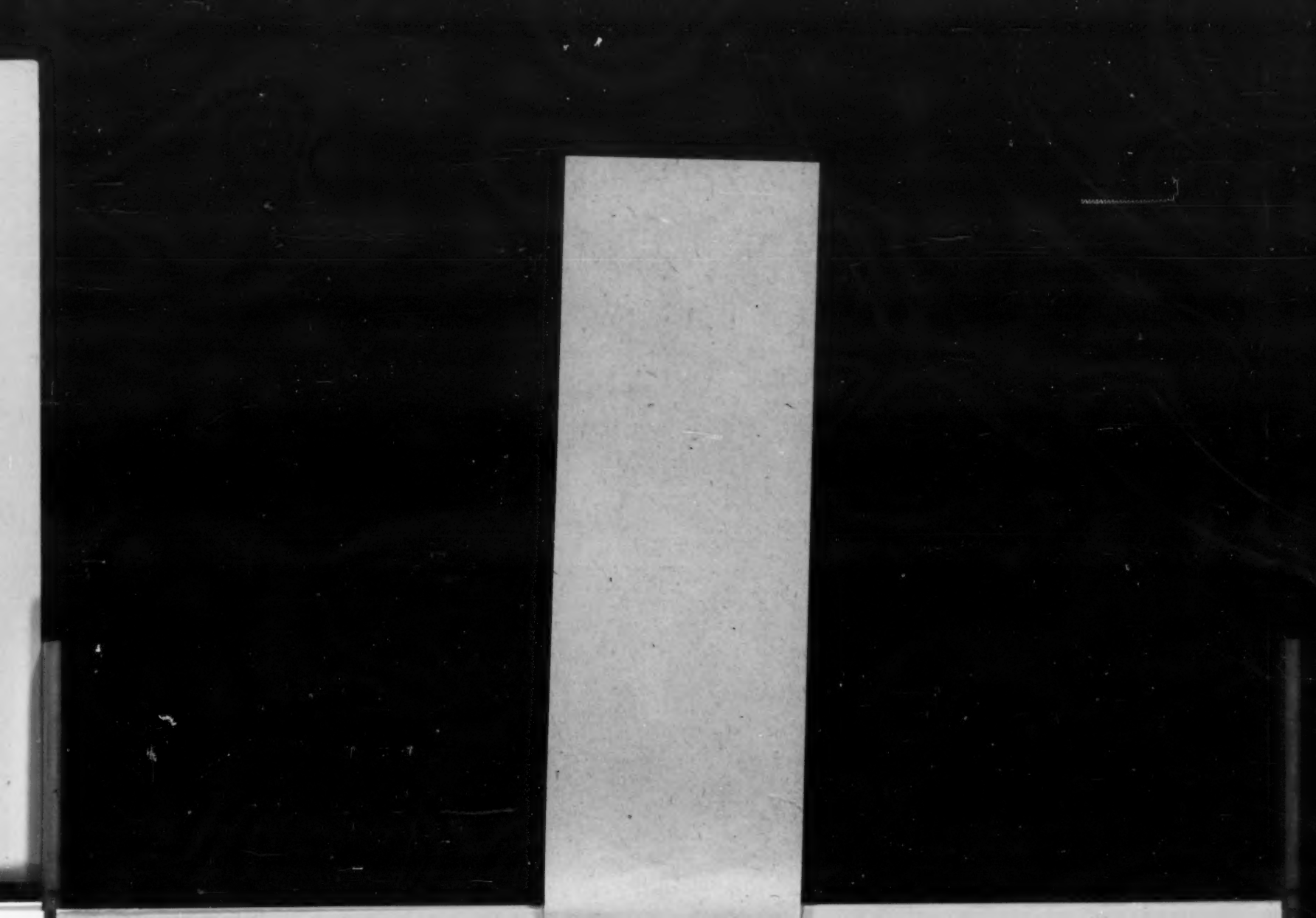

MONTHLY NOTICES

OF THE

ROYAL ASTRONOMICAL SOCIETY

Vol. 116 No. 1 1956

Published and Sold by the
ROYAL ASTRONOMICAL SOCIETY
BURLINGTON HOUSE
LONDON, W.1

Price Thirteen Shillings and Sixpence

NOTICE TO AUTHORS

1. *Communications.*—Papers must be communicated to the Society by a Fellow. They should be accompanied by a summary at the *beginning* of the paper conveying briefly the content of the paper, and drawing attention to important new information and to the main conclusions. The summary should be intelligible in itself, without reference to the paper, to a reader with some knowledge of the subject; it should not normally exceed 200 words in length. **Authors are requested to submit MSS. in duplicate. These should be typed using double spacing and leaving a margin of not less than one inch on the left-hand side. Corrections to the MSS. should be made in the text and not in the margin.** Unless a paper reaches the Secretaries more than seven days before a Council meeting it will not normally be considered at that meeting. By Council decision, MSS. of accepted papers are retained by the Society for one year after publication; unless their return is then requested by the author, they are destroyed.

2. *Presentation.*—Authors are allowed considerable latitude, but they are requested to follow the general style and arrangement of *Monthly Notices*. References to literature should be given in the standard form, including a date, for printing either as footnotes or in a numbered list at the end of the paper. Each reference should give the **name and initials** of the author cited, irrespective of the occurrence of the name in the text (some latitude being permissible, however, in the case of an author referring to his own work). The following examples indicate the style of reference appropriate for a paper and a book, respectively :—

A. Corlin, *Zs. f. Astrophys.*, **15**, 239, 1938.
H. Jeffreys, *Theory of Probability*, 2nd edn., section 5.45, p. 258, Oxford, 1948.

3. *Notation.*—For technical astronomical terms, authors should conform closely to the recommendations of Commission 3 of the International Astronomical Union (*Trans. I.A.U.*, Vol. VI, p. 345, 1938). Council has decided to adopt the I.A.U. 3-letter abbreviations for constellations where contraction is desirable (Vol. IV, p. 221, 1932). In general matters, authors should follow the recommendations in *Symbols, Signs and Abbreviations* (London : Royal Society, 1951) except where these conflict with I.A.U. practice.

4. *Diagrams.*—**These should be designed to appear upright on the page, drawn about twice the size required in print and prepared for direct photographic reproduction except for the lettering, which should be inserted in pencil. Legends should be given in the manuscript indicating where in the text the figure should appear.** Blocks are retained by the Society for 10 years; unless the author requires them before the end of this period they are then destroyed.

5. *Tables.*—**These should be arranged so that they can be printed upright on the page.**

6. *Proofs.*—Costs of alteration exceeding 5 per cent of composition must be borne by the author. Fellows are warned that such costs have risen sharply in recent years, and it is in their own and the Society's interests to seek the maximum conciseness and simplification of symbols and equations consistent with clarity.

7. *Revised Manuscripts.*—When papers are submitted in revised form it is especially requested that they be accompanied by the original MSS.

Reading of Papers at Meetings

8. When submitting papers authors are requested to indicate whether they will be willing and able to read the paper at the next or some subsequent meeting, and approximately how long they would like to be allotted for speaking.

9. Postcards giving the programme of each meeting are issued some days before the meeting concerned. Fellows wishing to receive such cards whether for Ordinary Meetings or for the Geophysical Discussions or both should notify the Assistant Secretary.

MONTHLY NOTICES

OF THE

ROYAL ASTRONOMICAL SOCIETY

Vol. 116 No. 1

MEETING OF 1956 JANUARY 13

Professor Sir Harold Jeffreys, President, in the Chair

The President announced the death of Professor W. M. H. Greaves, Past President of the Society and Astronomer-Royal for Scotland, and read the following Resolution, passed by the Council that afternoon, the Fellows standing :—

" With the untimely death of William Michael Herbert Greaves, British astronomy has suffered a severe loss. Whilst he will be remembered chiefly for his pioneer work on stellar spectrophotometry, his contributions to dynamical astronomy and to geomagnetism were substantial.

" He was always glad to serve the Society : he was a member of Council for an aggregate of 16 years, being Secretary for 7 years and holding the office of President from 1947 to 1949. Always an active member of the national and international committees on which he served, his considered advice will be greatly missed."

The President announced that the Council had awarded the Gold Medal of the Society to Professor Thomas George Cowling for his distinguished contributions to theoretical astrophysics and particularly for his work on the stability of stars.

The election by the Council of the following Fellows was duly confirmed :—

Bruce Alan Bolt, M.Sc., Department of Applied Mathematics, University of Sydney, Australia (proposed by K. E. Bullen);

*Michael William Walter Farrow, Trinity College, Cambridge (proposed by H. Jeffreys);

Victor Walter Raymond Charles Lionheart-Richardson, 213 Milkwood Road, Herne Hill, London, S.E.24 (proposed by J. F. H. Carr-Gregg);

Richard Fred Pashley, M.A., 72 Brocklehurst Avenue, Norton, Sheffield 8 (proposed by R. R. S. Cox);

Geoffrey Turner, 43 Green Street, Sandbach, Cheshire (proposed by W. H. Steavenson); and

*Roger D. Wade, 76 Starford Road, Hoddesdon, Hertfordshire (proposed by P. Moore).

* Transferred from Junior Membership.

Ninety-eight presents were announced as having been received since the last meeting, including :—

O. C. Mohler, *A table of solar spectrum wave-lengths* (presented by the McMath-Hulbert Observatory);

G. van den Bergh, *Periodicity and variation of solar (and lunar) eclipses* (presented by the Editor of *Physics Abstracts*);

A. Dauvillier, *Cosmologie et Chemie* (presented by the author);

W. J. Luyten, *A catalogue of* 1849 *stars with proper motions exceeding* 0″·5 *annually* (presented by the author); and

V. de Callatay, *Atlas du Ciel* (presented by M. A. de Visscher).

SPECTROSCOPIC AND PHOTOMETRIC OBSERVATIONS OF S DORADUS

A. J. Wesselink

(Communicated by the Radcliffe Observer)

(Received 1956 January 12)

Summary

The P Cygni character of the spectrum of S Dor has been confirmed. The radial velocity does not vary during the three years covered by the observations. The mean emission-line velocity is +295 km/sec and therefore the membership of the Large Magellanic Cloud is beyond question. The mean displacement of the absorption lines is 82 km/sec towards the violet; this is unusually small for a P Cygni star. The presence of helium is doubtful. The spectral type is A0. The Ca II lines are mainly stellar. Lines due to H and Ca II are strong. For 74 lines wave-lengths and intensities are presented together with probable identifications. Photoelectric observations in an interval of seventeen months show a decline in brightness of $0^m.8$ without change in colour. During this same interval the emission character of the spectrum became more pronounced, while forbidden lines of Fe II, which are diffuse, strengthened with respect to the permitted lines. In 1955 February the apparent photographic magnitude was $10^m.8$; the corresponding absolute magnitude is $-9^m.2$. S Dor is not an eclipsing variable but varies irregularly.

---

1. The present paper presents wave-lengths and identifications of lines measured in the spectrum of S Dor with the 2-prism Cassegrain spectrograph attached to the 74-inch Radcliffe reflector.

TABLE I

Plate and Dispersion	Date	Exp. Time (min)	Emulsion Kodak	Region Measured	Radial velocity Emission km/sec	Absorption km/sec
c 404	1951 Nov. 9	60	103aO	3973–4866	+297	+191
c 418	1951 Nov. 13	75	,,	3934–4924	296	196
c1740	1953 Oct. 14	80	,,	3892–4866	306	214
b1763	1953 Oct. 29	126	,,	4105–4866	296	227
b1779	1953 Nov. 16	63	,,	3936–4894	295	226
c1796	1953 Nov. 29	120	103aF	3936–6568	315	220
b1830	1954 Jan. 19	130	103aO	3936–4929	293	224
b1848	1954 Feb. 3	135	,,	3892–5023	293	228
c2274	1955 Jan. 5	70	103aB	3913–6566	291	215
c2279	1955 Jan. 8	90	103aO	4104–4866	289	208
c2281	1955 Jan. 11	35	,,	3973–4866	285	196
c2285	1955 Jan. 14	120	,,	3840–5023	283	214
					+295	+213

Table I presents the journal of the spectrographic observations. The prefix to the plate number shows which camera was used; the dispersions at $H\gamma$ of the corresponding spectra are as follows: (b) 29, (c) 49 A/mm. The various columns

are self-explanatory. The last two columns give the radial velocity as derived from emission and absorption lines respectively.

TABLE II

Mean wave-lengths and intensities of emission and absorption lines

Wave-length	Type	Intensity '51	53/54	'55	*n*	Main Contributor Element R.M.T.	Minor Contributor Element R.M.T.
3837·64	*a*			,1	1	H 5·39;	
3889·13	*ea, a*		,1	1,2	3	H 9·05;	
3933·66	*ea, a*	1,1	1,2	1,1	8	Ca II (1) 3·66;	
3968·38	*ea, a*		2,2		6	Ca II (1) 8·47;	
3970·21	*ea*	2,1	1,2	2,2	9	H (1) 0·07;	Fe II (3) 9·40
4101·76	*ea*	6,6	5,3	6,4	12	H (1) 1·74;	
4122·03	*e*		1,		1	Fe II (28) 2·64;	
4128·67	*ea, a*		1,0		2	Fe II (27) 8·74;	
4173·19	*ea, e, a*	1,1	1,1	1,	5	Fe II (27) 3·45;	
4178·82	*ea, e*	2,1	1,1	1,	7	Fe II (28) 8·86;	Fe II (23F) 8·95
4233·02	*ea, e*	2,2	2,1	1,	11	Fe II (27) 3·17;	Fe II (21F) 1·56
4243·30	*ea, e, a*		,1	2,2	4	Fe II (21F) 3·98;	Fe II (21F) 4·81
4257·46	*ea, a*		1,1		3	Fe II (28) 8·16;	
4276·25	*e*		1,	1,	3	Fe II (21F) 6·83;	Cr II (31) 5·57
4287·11	*e*		1,	2,	5	Fe II (7F) 7·40;	
4289·85	*a*		,0		3	Ti II (41) 0·22;	
4296·20	*ea, e, a*		1,1	,1	4	Fe II (28) 6·57;	
4300·05	*ea, a*		1,1		3	Ti II (41) 0·05;	
4303·05	*ea*	1,1	0,1		5	Fe II (27) 3·17;	
4314·29	*e*			1,	1	Fe II (32) 4·29;	Ti II (41) 4.98
4340·39	*ea, e*	10,3	11,6	11,6	12	H 0·47;	
4351·67	*ea, e*	2,1	1,1	1,2	11	Fe II (27) 1·76;	Fe II (21F) 2.78
4358·59	*ea, e*			2,2	4	Fe II (7F) 9·34;	Fe II (21F) 8·37
4384·82	*ea*	1,1			1	Fe II (27) 5·38;	
4388·67	*ea, a*			0,1	2	?He I (51) 7·93;	
4394·92	*a*	,1	,1		5	Ti II (19) 5·03;	Ti II (51) 4·06
4413·77	*e*	1,0	1,0	2,	4	Fe II (7F) 3.78;	Fe II (32) 3.60
4416·65	*ea, e, a*	,2	0,0	1,	6	Fe II (6F) 6·27;	Fe II (27) 6·82
4443·70	*ea, a*	,1	1,1		2	Ti II (19) 3·80;	
4468·25	*ea, a*	,4	1,1		6	Ti II (31) 8·49;	
4471·56	*a,*	,1	,1		2	?He I (14) 1·48;	
4472·98	*a*		1,	,2	2	Fe II (37) 2·92;	
4476·18	*e, a*	,1		2,	2		
4481·68	*a*	,4	,3	,2	11	Mg II (4) 1·26;	
4489·02	*e*		1,		1	Fe II (37) 9·18;	Fe II (6F) 8·75
4490·99	*ea, a*			0,0	2	Fe II (37) 1·40;	
4508·04	*ea, e, a*	2,1	1,1	2,2	8	Fe II (38) 8·28;	
4515·31	*ea, e*	2,1	1,1		5	Fe II (37) 5·34;	
4519·99	*ea, e*		1,0		2	Fe II (37) 0·22;	
4522·65	*ea, a*	1,1	1,2		5	Fe II (38) 2·63;	
4533·79	*ea, e, a*	0,1	1,1		3	Fe II (37) 4·17;	Ti II (50) 3·97
4541·23	*ea, a*		1,0		2	Fe II (38) 1·52;	
4549·45	*ea, e, a*	2,1	1,		11	Fe II (38) 9·47;	Ti II (82) 9·62
4555·58	*ea, e, a*	1,1	1,1	1,	6	Fe II (37) 5·89;	Cr II (44) 5·02
4558·89	*ea, a*	,1	1,1		3	Cr II (44) 8·66;	
4571·95	*ea*		1,0		1	Ti II (82) 1·97;	
4576·12	*ea, a*		1,0		2	Fe II (38) 6·33;	
4580·34	*e, a*		1,		2	Fe II (26) 0·05;	
4583·85	*ea, e*	3,3	3,2	2,	11	Fe II (38) 3·83;	
4588·52	*ea, a*	0,1	,1		2	Cr II (44) 8·22;	

Wave-length	Type	Intensity '51	53/54	'55	*n*	Main Contributor Element R.M.T.	Minor Contributor Element R.M.T.
4592·07	*e*		1,		1	?Cr II (44) 2·09;	
4616·99	*e*		1,		1	Cr II (44) 6·64;	
4620·12	*ea, e*		1,		3	Fe II (38) 0·51;	
4628·96	*ea, e*	1,1	1,	2,	8	Fe II (37) 9·34;	
4633·86	*e, a*		1,1		2	Cr II (44) 4·11;	
4657·93	*e*			1,	1	?Fe III (3F) 8·1;	
4666·23	*ea*		1,0		1	Fe II (37) 6·75;	
4730·89:	*e*		2,0		1	Fe II (43) 1·44;	
4814·16	*e, a*			1,	3	Fe II (20F) 4·55;	
4861·60	*e*	15,	15,	15,	12	H 1·33;	
4923·69	*ea, e*	1,1	1,1	1,1	6	Fe II (42) 3·92;	
5017·85	*ea, e*		2,2	2,1	4	Fe II (42) 8·43;	
5168·66	*e,*			1,	1	Fe II (42) 9·03;	
5262·77	*e*			1,	1	Fe II (19F) 1·6;	
5275·73	*e*			1,	1	Fe II (49) 5·99;	
5317·14	*e*			3,	1	Fe II (49) 6·61;	Fe II (48) 6·78
5467·06	*e*		2,		1	Fe II 6·94;	unclassified
5890·55	*a*		,3		1	Na (1)	
5990·02	*e*		2,		1	Fe II (46) 1·38;	
6330·20	*e*		2,		1	Fe II (199) 1·97;	
6431·14	*e*		1,		1	Fe II (40) 2·65;	
6493·79	*e*		2,		1	Fe II	unclassified
6516·10	*e*		2,		1	Fe II (40) 6·05;	
6560·31	*e*		20		2	H 2·8;	

2. Table II presents the results of measurements in the spectrum of S Dor.

First column: The mean wave-length after reduction for radial velocity. A colon indicates uncertainty in the measures.

Second column: The various types of the line that have been found on at least one plate: *ea* means a P Cygni line, thus showing emission and absorption, *e* means emission without absorption, whereas *a* indicates that the line occurs in absorption only.

Third column: Mean estimated intensity. It was found difficult to represent the intensities of the lines for all the plates on the same scale because of the variations that took place with time. The estimates on the various plates were adjusted so that those lines that were measured on all the plates showed no variation. The intensities are given for three groups of plates taken respectively during the 1951–52, 1953–54 and 1954–55 oppositions. The intensity of the emission line is always to the left of that of the absorption component, the two values being separated by a comma. Though these intensities are only rough, they are usually sufficiently accurate to indicate the behaviour in time of a particular line relative to the other lines.

Red-sensitive plates were only used in the second of the three intervals. The absence of intensities for lines with wave-lengths larger than 4900 A in the first and third intervals does not therefore necessarily mean these lines to be either weak or absent.

Fifth column: Number of plates on which the line was recorded.

Sixth column: Suggested identifications giving the responsible ion followed by the multiplet number in the *Revised Multiplet Table* and wave-length (also from the *R.M.T.*). Forbidden lines are distinguished by F following the multiplet

number. In the case of blends the probable major contributor is given first. The identifications were arrived at in the usual manner by systematic searches for the strongest lines of each ion in the *R.M.T.*

3. Not only is the emission character of the spectrum on later Radcliffe plates more pronounced than on the earlier plates but there is evidence that [Fe II] emission has strengthened relative to permitted Fe II in the course of time. As an instance we mention the relative intensity of [Fe II] 4244 and Fe II 4233. The effect is clearly visible in Plate 1 where an early (*c*) and a late (*d*) spectrum are shown. It is very remarkable that the forbidden lines are definitely more diffuse than the permitted ones; so far we have been unable to find a satisfactory explanation for this fact.

Dr A. D. Thackeray, in a recent study (**1**) of the spectrum of RR Tel, finds the ratio of [Fe II] 4244 and Fe II 4233 to increase steadily with time while the emission lines of higher stages of ionization have been emerging. There is no evidence that [Fe II] lines in RR Tel are more diffuse than Fe II (as they are in S Dor) but increasing diffuseness in RR Tel is shown by the lines of higher ionization. If the diffuseness of [Fe II] lines in S Dor is to be attributed to turbulent broadening then one seems driven to conclude that the sharp Fe II lines originate in an entirely different atmospheric level relatively free from turbulence. Both the lines 4471 and 4388 are very weak and have provisionally been attributed to He I. The presence of He is therefore rather doubtful and consequently the usual classification of the star as Be (**2**) does not seem to accord with Radcliffe spectra. It is, however, possible that the evidence for He has been stronger in the early Harvard spectra; for the present we classify the star as A0. Our plates show the lines H and K of Ca II in emission as well as in absorption. This observation shows conclusively that the lines are mainly stellar. H. J. Smith (*Harvard Thesis*, 1955) has the same opinion about the origin of these lines, though he has found them only in absorption. His inference must be based on their great strength and the advanced spectral type of the star. It is further remarkable that Smith finds Hϵ only in absorption whereas all the Radcliffe spectra show the line in absorption as well as in emission. As a possible explanation of this difference in results we suggest the higher dispersion of our plates. The line 4481 Mg II appears strong and in absorption only. In contrast with the other absorption lines 4481 is very diffuse and much less displaced. This behaviour of 4481 seems to be similar in other stars of the P Cygni class (**3**).

Miss Cannon (**4**) found S Dor to be a P Cygni star on objective prism plates. H. Shapley (**5**) then concluded, from the position of the star in the sky and from fact that galactic P Cygni stars are strongly concentrated towards the galactic plane, that S Dor was a member of the Large Magellanic Cloud.

According to Beals (**2**) it is very difficult to determine the true radial velocity of a P Cygni star as the position of the lines is not uniquely determined by the velocity. The intrinsic displacement is however smallest for the emission lines. The mean value of the radial velocity derived from the emission lines is +295 km/sec. This result is sufficiently close to the radial velocity of the Large Magellanic Cloud at the position of S Dor to prove its membership without question. The absorption-line velocities given in Table I are systematically higher when derived from spectra with the larger dispersion. This is undoubtedly a consequence of the greater resolution obtained with the higher

dispersion. The mean difference between the emission and absorption velocities given in Table I is −82 km/sec. This is unusually small for a P Cygni star.

TABLE III

Ion	Mean displacement with respect to emission lines km/sec
Fe II	−82
Ti II	−96
Cr II	−85
H	−62
Ca II	−76
Mg II	−21

4. In Table III the mean displacements of the absorption lines are given for the different ions. It is seen that there is little or no significant variation with the ion, with the exception of Mg II for which the figure is due to 4481, already discussed in Section 3. Beals (**2**) found clear evidence of stratification in the atmosphere of P Cygni manifesting itself as a variation of the displacement with the ionization potential. Such a relation could not be found from the measures in the spectrum of S Doradus, probably because of the small range in ionization potential of the ions present.

5. *Photoelectric photometry.*—On several occasions the brightness of S Dor was measured with the Cassegrain photoelectric photometer. A few remarks on this photometer seem to be called for. When the telescope is used for spectroscopy, the light of the star reaches the spectrograph slit direct from the Cassegrain mirror. In the case of Cassegrainian photoelectric photometry a flat mirror a few inches above the spectrograph slit deflects the light sideways into the photometer. In order to focus the stellar image on the diaphragm in the photometer it is necessary to move the Cassegrain mirror about half an inch

TABLE IV

Brightness of S Doradus

Date	JD	S_{pg}	S_{pv}	S_{CI}
		m	m	m
30. 9.1953	2434651	9·22	9·41	−0·19
17. 9.1954	5003	9·56	9·75	−0·19
13.12.1954	5090	9·94	10·13	−0·19
16.12.1954	5093	9·91	10·11	−0·20
6. 2.1955	5145	10·04	10·23	−0·19

closer to the primary mirror. Table IV shows the photographic and photovisual magnitudes, so far obtained, reduced to the Cape S system (**5**). The brightness is seen to vary markedly during recent years; the star is of photographic magnitude $10^m{\cdot}0$ in 1955 February. The colour-index ($-0^m{\cdot}19$ in the Cape S system) is seen to be remarkably constant. Its value in the international system is $-0^m{\cdot}07$ After reduction for galactic reddening we obtain an intrinsic colour index of $-0^m{\cdot}19$ in the international system; this is rather blue for an Ao star. The brightness of $10^m{\cdot}0$ photographic is about $0^m{\cdot}8$ fainter than the faintest brightness

recorded by S. Gaposchkin (7). Though part of this amount may be due to a difference in photometric system, it may also be caused by the light of neighbouring stars contributing to that of S Dor on the small-scale Harvard photographs used by him. The recent drop in brightness is inconsistent with the ephemeris given by Gaposchkin on the hypothesis that the star is an eclipsing variable. The suggestion of Hubble and Sandage that S Dor belongs to the same class of bright blue variables as discovered by them in M 31 and M 33 seems more likely (8).

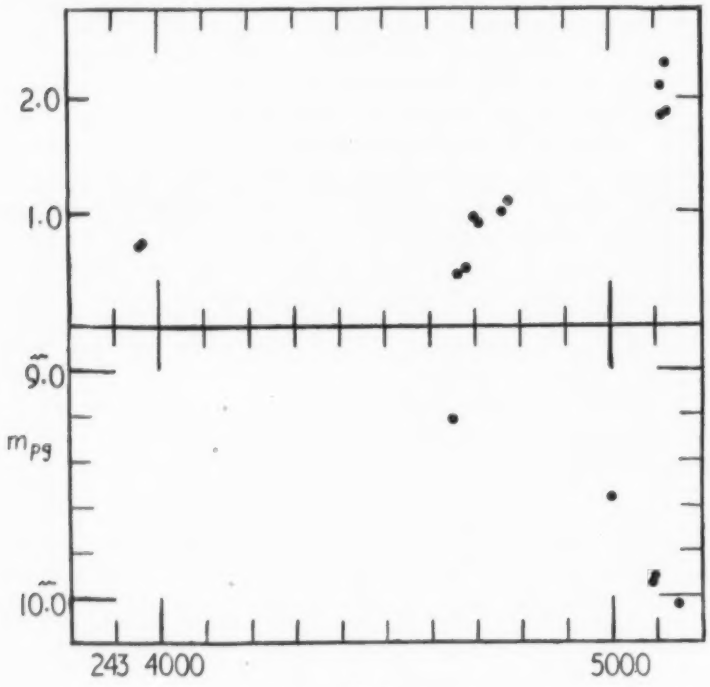

FIG. 1

Ordinate: in upper part, the number of emission lines divided by the number of absorption lines; in lower part, the photographic magnitude.
Abscissa: in either part, the Julian Date.

The gradual fading of the light of S Dor in recent times is shown graphically in the lower half of Fig. 1. The upper half of the diagram exhibits the ratio between the number of emission lines to the number of absorption lines measured on Radcliffe spectra. The marked increase of the ratio with time could of course be attributed to the general fading of the continuum as shown by the photoelectric measures, the emission remaining constant; but other explanations seem to be possible.

The author wishes to record his indebtedness to Dr A. D. Thackeray and Dr M. W. Feast for invaluable advice. I am deeply indebted to H.M. Astronomer at the Cape, Dr R. H. Stoy, for the use of an amplifier and to Dr A. W. J. Cousins for much support in photoelectric matters.

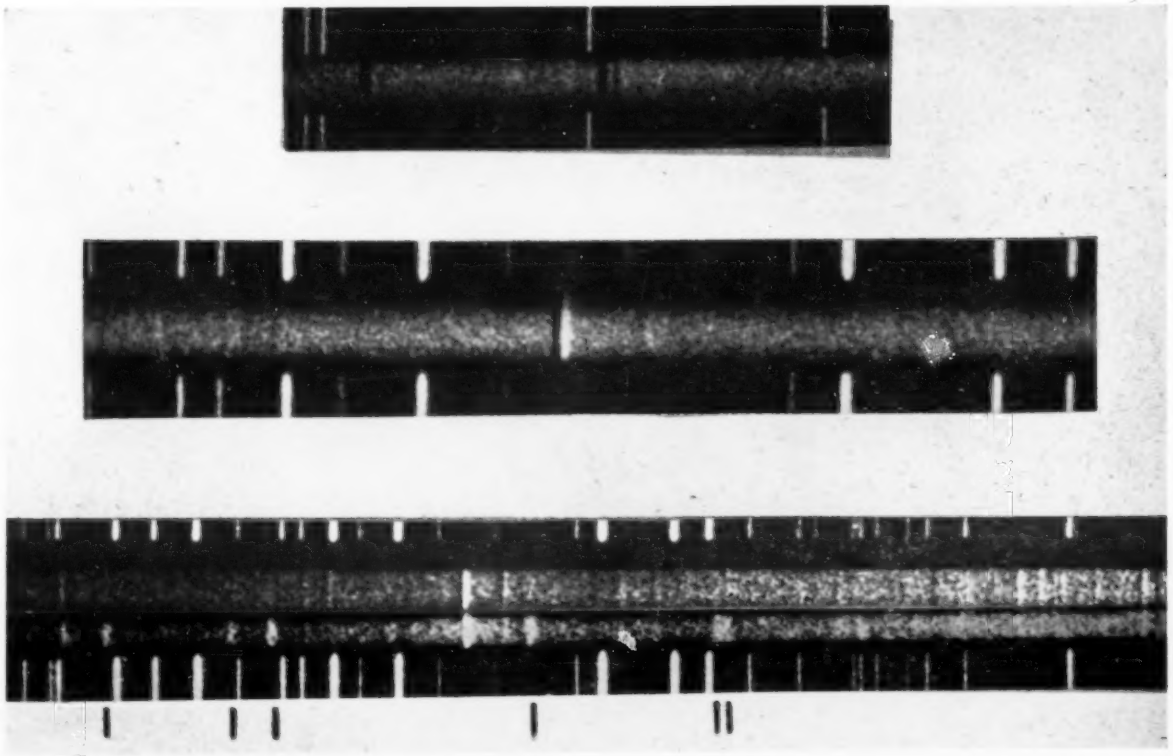

A. J. Wesselink, Spectroscopic and photometric observations of S Doradus.

Spectra of S Doradus.

(*a*) 1953 *Oct.* 14 *Region of H and K.*
(*b*) 1954 *Feb.* 3 *Region of Hγ.*
(*c*) 1951 *Nov.* 9 } *Region 4212–4560 with [Fe II] 4244 to 4416 marked.*
(*d*) 1955 *Jan.* 14 }

References

(1) A. D. Thackeray, *M.N.*, **115**, 236, 1955.
(2) C. S. Beals, *Publications Dominion Astrophysical Observatory*, Vol IX, 1, page 124, 1951.
(3) Compare for instance Struve, *Ap. J.*, **72**, 343, 1930; Struve and Swings, *Ap. J.*, **75**, 177, 1932; Struve and Roach, *Ap. J.*, **90**, 727, 1939; these authors find a similar behaviour of 4481 in 17 Leporis.
(4) A. J. Cannon, *Harvard Bulletin* No. 801, Table II, 1924.
(5) H. Shapley, *Harvard Bulletin* No. 814, 1925. See also H. Shapley and H. H. Wilson, *Harvard Circular* No. 271, 1925.
(6) *Cape Mimeogram* No. 3; Standard Magnitudes in the E regions.
(7) S. Gaposchkin, *Ap. J.*, **97**, 166, 1942.
(8) E. Hubble and A. Sandage, *Ap. J.*, **118**, 353, 1953.

RESULTS OF A SEARCH FOR BRIGHT β CEPHEI VARIABLES IN THE SOUTHERN SKY

B. E. J. Pagel

(Communicated by the Radcliffe Observer)

(Received 1956 January 3)

Summary

The radial velocities of seven bright southern early B-type stars, known to have variable velocity, have been systematically examined at the Radcliffe Observatory in an effort to detect the presence of short periods (3 to 7 hours) characteristic of β Cephei variables. Positive results were obtained for three stars: β Cru ($0<2K<14$ km/sec), τ^1 Lup ($2K=11$ km/sec), and α Lup ($2K=15$ km/sec). Definitive periods have been derived for τ^1 Lup and α Lup, while a provisional period is suggested for β Cru.

β Cru and τ^1 Lup have been observed photoelectrically by the staff of the Cape Observatory and found to have short-period variations in light with a range of about $0^m{\cdot}04$. In the case of τ^1 Lup, the light variation shows the same period as the velocity variation, with the phase relationship typical of β Cephei variables. In the case of β Cru, all that can be said is that the light variation has approximately the period of the velocity variation. α Lup was observed photoelectrically by A. B. Muller at the Leiden Observatory Southern Station; no variation in excess of $0^m{\cdot}01$ has so far been detected.

τ^1 Lup fits closely the period–luminosity relations derived for β Cephei variables by Blaauw and Savedoff and by Petrie. It is clearly a typical member of the group with constant velocity amplitude. α Lup comes tolerably near to the period–luminosity relation, but, until some variation in light can be established, one cannot quite exclude the possibility that it is a single-lined spectroscopic binary. β Cru, in spite of its early spectral type (B0), would seem to be related to the β Cephei group, though it is anomalous in a number of ways.

---

1. *Introduction.*—In recent years, there has been a revival of interest in variable stars of the β Cephei or β Canis Majoris group. These are early B-type stars, somewhat above the main sequence in the HR diagram, which vary in light and radial velocity with periods between 3 and 7 hours. At present, ten stars visible from northern observatories are known to be members of this class (see, for example, Struve, 1955 b) and have been studied extensively. They appear to fit a period–luminosity curve consistent with the normal period–density relation for pulsating stars (Blaauw and Savedoff, 1953; Petrie, 1954 a) and a period–colour relation (McNamara and Williams, 1955), and their variations in light and radial velocity can usually be described by one-sine or two-sine curves; in each component oscillation, light maximum is closely coincident with the descent of the radial-velocity curve through its mean value.

Together with these general features, there is an immense variety in individual behaviour. Three stars with small variations in velocity and light—γ Peg, δ Cet and ξ^1 CMa—behave in a comparatively simple fashion with a single period and apparently constant velocity amplitude (McNamara, 1955). On the other hand,

β Cep has an irregularly varying amplitude and five other members of the group have a well-marked secondary oscillation giving rise to a beat phenomenon (Struve, 1952). These latter, and BW Vul (Petrie, 1954b; McNamara, Struve and Berthiau, 1955; Odgers, 1955), show a periodic variation in line width —identified with high dispersion as doubling of the lines—together with departures from a sinusoidal velocity curve (e.g. a stillstand or intermediate branch on the descending portion) and a phase lag between the velocities determined from the hydrogen and other lines (Struve, 1955c); in a few cases, a secular variation in period has been detected (Struve, 1955a).

The general features of the group suggest a radial pulsation analogous to that of cepheids and this hypothesis fits well with observations of β Cep in six colours (Stebbins and Kron, 1954). However, a similar investigation of BW Vul has been inconclusive (Walker, 1954a), and the pulsation hypothesis seems to break down completely for 16 Lac (Walker, 1954b).

This variety of phenomena suggests a need for further efforts to identify and study new β Cephei variables. The high time resolution required for the elucidation of details of the velocity curves sets a limiting magnitude to variables detectable spectroscopically with a given telescope and dispersion; hence a study of bright early B-type stars of known variable velocity in the southern sky immediately suggests itself. In this paper, we describe a spectrographic study of a few promising stars carried out at the Radcliffe Observatory between 1955 February and 1955 July; in individual cases, the radial-velocity data were supplemented with photoelectric observations carried out by the staff of the Cape Observatory and by A. B. Muller at the Leiden Observatory Southern Station.

2. *Observational details.*—The spectra were obtained with the two-prism Cassegrain spectrograph of the Radcliffe 74-inch reflector, using the *a* camera (*f*/8: dispersion 21 A/mm at Hγ) with slit width 0·030 mm (projected width 0·017 mm). Emulsions were selected to give exposure times between 5 and 10 minutes. Comparison spectra were obtained from an iron arc exposed for equal periods at the beginning and end of each stellar exposure and the plates calibrated by means of a tube sensitometer. The plates were measured using the Casella projection instrument of the Radcliffe Observatory, each set of measurements being repeated with the plate reversed. Lines were selected for measurement in accordance with current practice at the Radcliffe Observatory (Feast, Thackeray and Wesselink, 1955)—based on the I.A.U. standards and on the recommendations of Petrie (1953b)—but with a few modifications. Details of the lines measured and wave-lengths adopted in this investigation are given in Table I.

The effective wave-lengths of the lines λ4088 Si IV and λ4471 He I were chosen empirically to bring about the best possible agreement between the radial velocities derived from these lines and from the others (for the wave-length of λ4471, cf. Petrie, 1953b). The spectral classes in the fourth column of Table I are the MKK classes of stars for which the relevant line was found useful in this particular investigation and are not intended as general recommendations.

The reductions to the Sun were carried out by the method of Schlesinger (1899) in the form described by Wesselink (1952). The standard diurnal correction was also applied.

TABLE I

Lines used for Radial velocity measurement

Laboratory wave-length	Identification	Adopted wave-length	Range of spectral type	Remarks
3918·977	C II	3918·977	B 2, 3	I.A.U. standards not in Petrie's list.
3920·677	C II	3920·677	B 2, 3	
3933·664	Ca II	3933·664	B 2, 3	
3964·727	He I	3964·727	all	
3970·075	H ϵ	3970·075		ξ^2 Cen only.
3994·996	N II	3994·996	all	
4026·189	He I	4026·189	all	Lab. wave-length seems satisfactory.
4069·794	O II	4069·794	all	
4088·862	Si IV	4088·998	B o	Not in Petrie's list. Lab. wave-length increased by 0·136 A (10 km/sec).
4101·738	H δ	4101·738	all	
4116·103	Si IV	4116·103	B o	Not in Petrie's list.
4120·837	He I	4120·812	all	I.A.U. wave-length used.
4143·759	He I	4143·759	all	
4267·167	C II	4267·160	all	
4340·468	H γ	4340·466	all	
4387·928	He I	4387·928	all	
4437·549	He I	4437·549	all	I.A.U. standard not in Petrie's list.
4471·477	He I	4471·552	all	Lab. wave-length increased by 0·075 A (5 km/sec).
4481·228	Mg II	4481·228	B 2, 3	
4552·662	Si III	4552·622	all	
4567·841	Si III	4567·841	all	

As a check on the general procedure of measurement, occasional plates of three I.A.U. standard stars of late spectral type were taken and measured, using standard wave-lengths recommended by Petrie (1946), apart from the line λ4494·575 Fe I, which was found to be unreliable and therefore rejected.

TABLE II

Measured radial velocities of standard stars

Star	Spectral Type	Date, U.T.		Measured R.V. km/sec.	R.V. (Wilson) km/sec.
693 (6 Cet)	F 5	1955 July	9·181	+12·9 ± 1·0	+14·8
81797 (α Hya)	gK 5	1955 March	16·748	−4·7 ± 0·4	−4·3
		March	30·777	−4·1 ± 0·4	
		April	7·822	−7·1 ± 0·7	
		April	13·747	−6·9 ± 0·4	
		May	18·700	−5·7 ± 0·5	
		May	21·702	−5·3 ± 0·5	
		Mean		−5·6 ± 0·5	
150798 (α Tri A)	K 2	1955 March	1·121*	−2·7 ± 0·9	−3·6
		May	1·174	−1·3 ± 0·5	
		May	22·015	−2·4 ± 1·0	
		Mean		−2·1 ± 0·6	

* Taken with the *b* dispersion (29 A/mm).

The results are given in Table II, where they are compared with those given in R. E. Wilson's catalogue (R. E. Wilson, 1953). The errors given in this and later tables are standard deviations per plate.

The data are too few in number for a detailed analysis of the residuals, but it is satisfactory to note that they can be of either sign, and that they are of the order of magnitude of the uncertainty in the catalogue values (1–2 km/sec).

3. *Results of radial-velocity and photoelectric measurements.*—The selection of promising stars for investigation was based on a list supplied by D. H. McNamara. They are early B-type stars noted as variable velocity stars in the Lick Observatory Catalogue (Lick Observatory, 1932). The stars considered are given in Table III, together with a summary of the results obtained from radial-velocity measurements. The MKK spectral types given in the table have been taken from Cape Mimeogram 1 (Stoy, 1953).

TABLE III

Summary of results of radial-velocity measurements

Star	1950 α	1950 δ	Spectral Type (MKK)	No. of plates	No. of nights	Conclusions
28873 (δ Cae)	$04^h\,29^m\cdot3$	$-45°\,04'$	B 3‡			Not observed owing to unsuitable R.A.
106490* (δ Cru)	$12^h\,12^m\cdot5$	$-58°\,28'$	B 2 V	8	3	Lines too diffuse for velocity measurements of adequate accuracy.
111123 (β Cru)	$12^h\,44^m\cdot8$	$-59°\,25'$	B 0 III	79	10	Sharp lines: definite variation with period between $0^d\cdot15$ and $0^d\cdot2$; exact period doubtful (may be variable). $2K$ variable, sometimes reaching 14 km/sec.
113791 (ξ^2 Cen)	$13^h\,04^m\cdot0$	$-49°\,38'$	B 3‡	8	2	Sharp lines: single-line spectroscopic binary (orbit by Neubauer, 1931) with no velocity variation detectable during period of observation.
126341* (τ^1 Lup)	$14^h\,22^m\cdot9$	$-45°\,00'$	B 2 (IV)†	76	16	Sharp lines: definite variation with period $0^d\cdot177365 \pm 15$. $2K = 10\cdot6$ km/sec.
129056 (α Lup)	$14^h\,38^m\cdot6$	$-47°\,10'$	B 2 II	74	16	Sharp lines: definite variation with period $0^d\cdot259882 \pm 20$. $2K = 14\cdot7$ km/sec.
132200 (κ Cen)	$14^h\,55^m\cdot9$	$-41°\,54'$	B 2 V	14	5	Sharp lines: no velocity variation detectable during period of observations.
134687 (θ Lup)	$15^h\,09^m\cdot5$	$-44°\,19'$	B 3‡	4	2	Double-line spectroscopic binary with sharp and diffuse components. Velocity of sharp component varies from night to night, but not on one night.

* Added to McNamara's list by A. D. Thackeray.

† Derived by the writer from a single low-dispersion spectrum. The luminosity class is uncertain.

‡ H.D. spectral class; MKK class not available.

The results indicate that the three stars β Cru, τ^1 Lup and α Lup definitely possess a short-term variation in radial velocity, which suggests that they may be β Cephei variables of small amplitude (comparable with γ Peg, ξ^1 CMa and δ Cet). The spectroscopic binaries ξ^2 Cen and θ Lup definitely are not, while the lines in the spectrum of δ Cru are too diffuse for any conclusion to be drawn. κ Cen merits further detailed study, since variability is suggested by the early Lick observations (Campbell and Moore, 1928), but a short period seems to be excluded by the present observational material.

We now give the detailed results for individual stars.

(i) *ξ^2 Cen, κ Cen and θ Lup.* The measured radial velocities of these stars, together with the velocities in Wilson's catalogue, are given in Table IV.

TABLE IV

Radial velocities of ξ^2 Cen, κ Cen, *and* θ Lup

Star	Mean Velocity (Wilson)	Date, U.T.			Observed Velocity
ξ^2 Cen	+14·3	1955	April	30·927	+29·2±0·6
				30·949	+28·4±0·4
				30·974	+30·3±0·5
				30·999	+20·9±0·6
			May	18·742	+29·2±0·7
				18·768	+28·6±0·8
				18·827	+24·9±1·0
				18·882	+26·3±1·0
κ Cen	+9·1	1955	April	4·149	+3·9±0·8
				14·154	+5·0±0·7
				30·069	+6·3±0·9
				30·109	+2·7±0·8
				30·135	+2·9±0·8
				30·156	+5·8±0·6
				30·174	+4·9±0·7
			May	11·963	+5·1±0·8
				11·980	+5·7±0·8
				12·031	+5·8±1·1
				12·075	+6·9±0·9
				12·137	+6·6±1·3
				18·815	+4·0±1·0
				18·870	+4·8±0·6
θ Lup (sharp component)		1955	April	4·137	+19·9±0·8
				4·163	+18·5±1·2
				30·097	−7·2±1·8
				30·120	−7·7±1·8

(ii) *β Cru.* The measured radial velocities of β Cru are presented graphically in Figs. 1, 2. The epochs were converted into heliocentric Julian days using Prager's tables (Prager, 1932); as the exposure times were between 5 and 10 minutes, the epochs are accurate to about $0^d{\cdot}001$. Considerable difficulty was experienced in determining a period. The amplitude is variable (Fig. 1), and the apparent departures from strict periodicity may be either genuine or due to errors of observation in cycles when the amplitude was small. The radial-

velocity observations have been supplemented by photoelectric observations carried out at the Cape Observatory on four nights when conditions were not considered good enough for the general photometric programmes. On one of these nights (1955 March 25 = J.D. 2435192), both photoelectric and radial-velocity measurements were carried out; these data suggest that light maximum coincides approximately with radial velocity descending through γ. If we assume that this always holds, we obtain a period $P = 0^d{\cdot}160474 \pm 50$, but this period is not established with any certainty. The deviations are large (Fig. 2) and it has not proved possible to find any interfering oscillation that explains them. It is quite possible that the oscillations of β Cru are not strictly periodic; neither the radial-velocity data nor the photometric data are sufficiently accurate or numerous to decide this point. When combined by means of the period given above, the radial-velocity observations scatter about a symmetrical curve; the sine curve obtained by least squares is

$$V = +12{\cdot}44 + 2{\cdot}20 \sin(2\pi t/0^d{\cdot}160474), \quad \pm 0{\cdot}25 \pm 0{\cdot}50 \qquad (1)$$

$$t = \text{J.D.} - (2435211^d{\cdot}357 + 0^d{\cdot}160474E), \quad \pm 0^d{\cdot}006 \qquad (2)$$

where E is an integer (Fig. 2). Owing to the considerable discrepancies in the phases, the amplitude in equation (1) is somewhat less than the mean of the observed amplitudes. The r.m.s. residual is 2·2 km/sec.

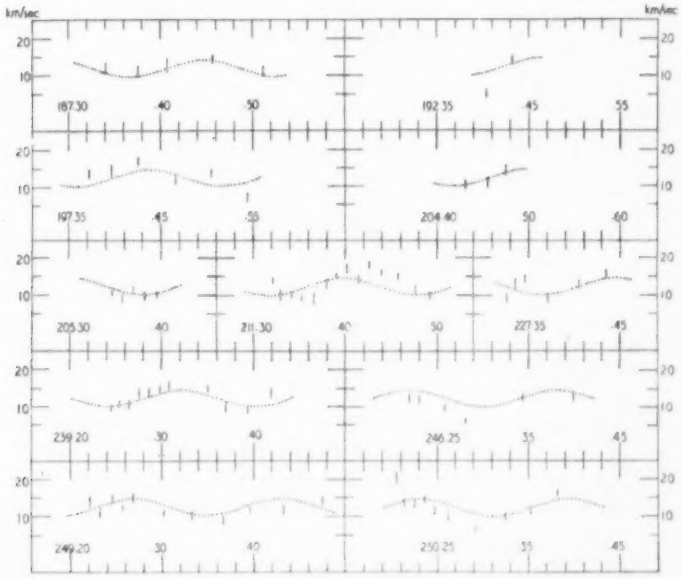

FIG. 1.—*Observed radial velocities of β Cru*
Abscissae: Heliocentric J.D.—2435000.
Ordinates: Radial velocity.
Vertical lines represent the observations, with the standard error estimated for each plate; the dotted curve represents the least-squares solution, assuming the period $0^d{\cdot}160474$.

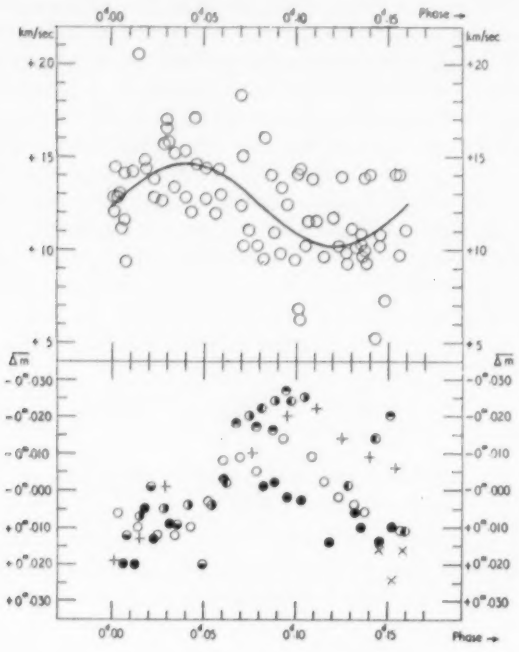

◐	Cycle beginning JD 2435			188.949
◑	,,	,,	,,	188.409
○	,,	,,	,,	192.261
×	,,	,,	,,	195.149
●	,,	,,	,,	195.310
○	,,	,,	,,	195.470
+	,,	,,	,,	212.390
◒	,,	,,	,,	212.480

FIG. 2.—*Radial-velocity and photoelectric observations of β Cru, combined into one cycle.*
Abscissae: Phase, in days.
Ordinates: Upper figure, radial velocity.
Lower figure, $\overline{\Delta m}$.
The circles and crosses represent the observations; the full line in the upper figure represents the least-squares solution. The limitations of the solution are obvious.

The results of the Cape photoelectric observations, combined into one cycle with the aid of equation (2), are illustrated in the lower half of Fig. 2. γ Cen, δ Cen and ρ Cen were used as comparison stars and observations were carried out in blue and yellow light (on the natural colour system of the photometer). The ordinate in the diagram is $\overline{\Delta m}$, the mean of the departures in blue and yellow light from the respective mean magnitudes $m_b = 0^m{\cdot}793$ and $m_y = 1^m{\cdot}650$; the uncertainty in the zero-points ranges from $0^m{\cdot}01$ to $0^m{\cdot}03$.

The scatter in the individual observations of this series is too large to make any definite deductions concerning the shape and periodicity of the light curve, but they are sufficient to demonstrate a range of about $0^m{\cdot}04$ between maximum and minimum and a period between $0^d{\cdot}15$ and $0^d{\cdot}20$, in agreement with the

radial velocity observations. More definite conclusions must be postponed until a greater number of simultaneous photoelectric and spectrographi observations can be carried out on first-class photometric nights.

No changes were observed in the appearance of the spectrum of β Cru.

(iii) τ^1 *Lup.* The measured radial velocities of τ^1 Lup are given in Figs. 3, 4. The observations show a well-defined periodicity with $P = 0^d.177365 \pm 15$, and, when combined into one cycle, lie close to a simple sine curve (Fig. 4). The curve obtained by least squares is

$$V = -21.51 + 5.31 \sin(2\pi t/0^d.177365), \quad \pm 0.22 \pm 0.40 \tag{3}$$

$$t = \text{J.D.} - (2435250^d.394 + 0^d.177365E), \quad \pm 0^d.002 \tag{4}$$

where E is an integer (Fig. 4). The r.m.s. residual from the least-squares solution is 1·9 km/sec, slightly larger than might be expected from observational inaccuracy; if the discrepancies are genuine, they could represent either an interfering cycle of a variation in amplitude, but they are clearly not large enough to deserve detailed analysis.

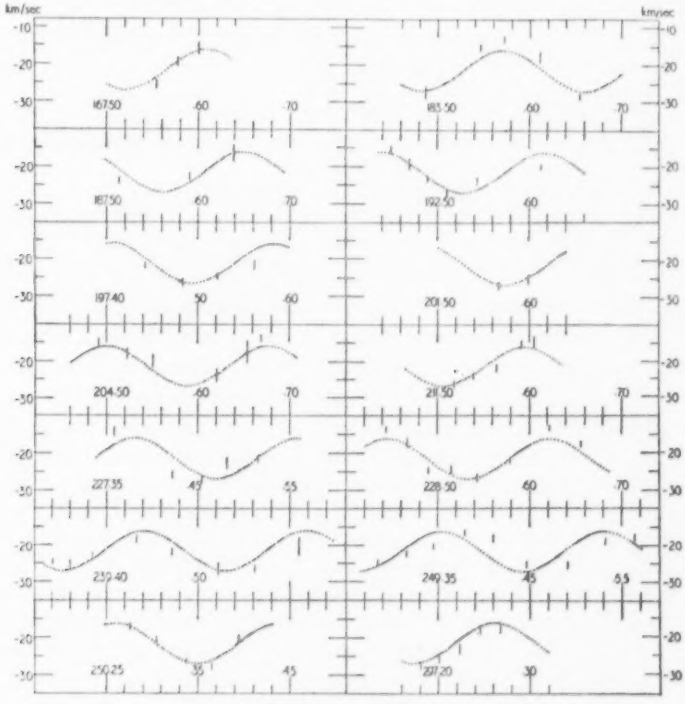

FIG. 3.—*Observed radial velocities of* τ^1 *Lup.*
Abscissae: Heliocentric J.D. −2435000.
Ordinates: Radial velocity.
Vertical lines represent the observations, with the standard error estimated for each plate; the dotted curve represents the least-squares solution, assuming the period $0^d.177365$.

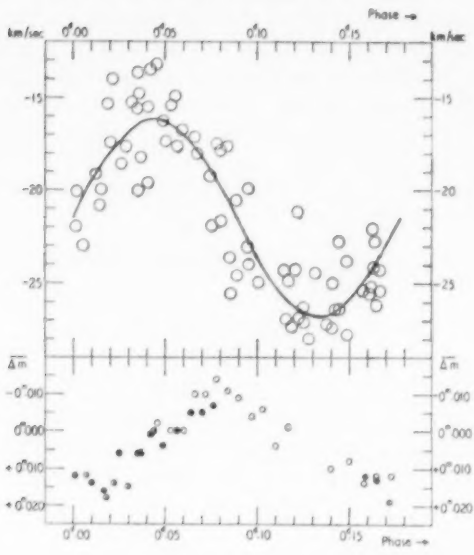

● Cycle beginning JD 2435 241.171
◐ ,, ,, ,, 241.348
○ ,, ,, ,, 242.235
● ,, ,, ,, 242.413

FIG. 4.—*Radial-velocity and photoelectric observations of* τ^1 *Lup, combined into one cycle.*
Abscissae: Phase, in days.
Ordinates: Upper figure, radial velocity.
Lower figure, $\overline{\Delta m}$.
The circles represent the observations; the full line in the upper figure represents the least-squares solution. The phase relationship between the light and velocity curves is clearly visible.

τ^1 Lup was observed photoelectrically in two colours at the Cape Observatory on 1955 May 13 and 14, and the means of the results obtained with blue and yellow filters are illustrated in Fig. 4. $\overline{\Delta m}$ is the mean departure from $m_b = 4^m{\cdot}127$ and $m_y = 4^m{\cdot}637$. The uncertainty in the zero-point is about $0^m{\cdot}01$.

The photoelectric observations indicate a range of $0^m{\cdot}03$ in $\overline{\Delta m}$ and a period in perfect agreement with that derived from the radial-velocity data; furthermore the phase of light maximum coincides with that of the descent of the radial-velocity curve through the γ value (Fig. 4), in accordance with the typical behaviour of β Cephei variables. τ^1 Lup has thus been shown to be a β Cephei star of small amplitude, similar in behaviour to γ Peg, δ Cet and ξ^1 CMa. The scatter in individual observations is too large for the detection of any change in colour during the cycle. A comparison of the results of 1955 May 14 (= J.D. 2435242) with some Fabry photometric observations carried out during the past few years suggests that the range in light may vary by $\pm 0^m{\cdot}02$ (A. W. J. Cousins, private communication).

The velocity amplitude of the star is 40 per cent below the value corresponding to the linear period–amplitude relation found by McNamara (1955).

A visual examination of the spectrum of τ^1 Lup shows a slight intensification of the O II doublet $\lambda 4415$ at light maximum (suggesting slightly earlier spectral

type) during certain cycles. Such intensification was found on April 6 (=J.D. 2435204), April 29 (=J.D. 2435227), May 11 (=J.D. 2435239), and July 8 (=J.D. 2435297), but not on the other nights when spectra were taken. No changes were observed in the shapes of line profiles.

(iv) α *Lup.* The measured radial velocities of α Lup are illustrated in Figs. 5, 6. The observations show a well-defined periodicity with $P = 0^{d}\cdot259882 \pm 20$, and when combined into a single cycle, line close to a simple sine curve (Fig. 6). The curve obtained by least squares is

$$V = +3\cdot98 + 7\cdot33 \sin(2\pi t/0^{d}\cdot259882), \quad \pm 0\cdot22 \pm 0\cdot37 \tag{5}$$

$$t = \text{J.D.} - (2435297^{d}\cdot409 + 0^{d}\cdot259882\,E), \quad \pm 0^{d}\cdot002 \tag{6}$$

where E is an integer (Fig. 6). The r.m.s. residual from the least-squares solution

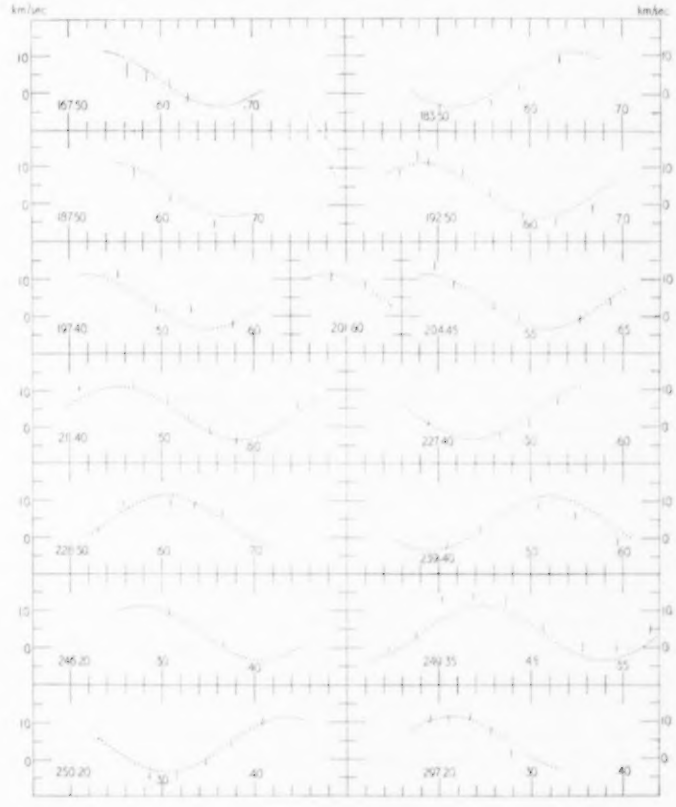

FIG. 5.—*Observed radial velocities of α Lup.*
Abscissae: Heliocentric J.D. −2435000.
Ordinates: Radial velocity.
Vertical lines represent the observations, with the standard error estimated for each plate; the dotted curve represents the least-squares solution, assuming the period $0^{d}\cdot259882$.

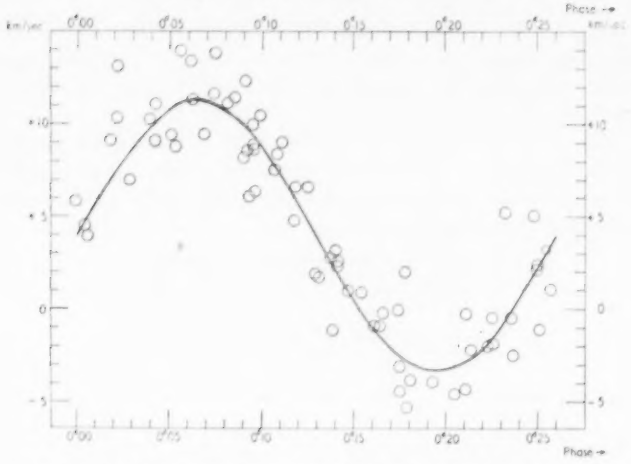

FIG. 6.—*Radial-velocity observations of α Lup, combined into one cycle.*
Abscissae: Phase, in days.
Ordinates: Radial velocity.
The open circles represent the observations; the full line represents the least-squares solution.

is 1·8 km/sec, closely similar to that obtained for τ^1 Lup. This coincidence suggests that the discrepancies are probably due to observational inaccuracy in both cases.

α Lup was observed photoelectrically in yellow light on 1955 July 20 by A. B. Muller at the Leiden Observatory Southern Station, using the neighbouring fifth-magnitude star HD 129858 for comparison, α Lup being measured through a $2^m{\cdot}5$ neutral filter. The observations were continued for $3\frac{1}{2}$ hours, during which time α Lup was not found to vary by more than $\pm 0^m{\cdot}01$; even this variation behaves in such a random fashion that a systematic variation of more than $\pm 0^m{\cdot}005$ can be ruled out. The apparent constancy in light of α Lup is confirmed by reference to some earlier observations of this star carried out at the Cape Observatory in 1948 and 1950 (A. W. J. Cousins, private communication). A. B. Muller's observations, averaged in groups of five successive measurements, are given in Table V.

It is conceivable that α Lup has variable light amplitude, like ξ^1 CMa (McNamara, 1955), so that some variation might be detectable on a more favourable occasion; however, the present data indicate constancy in light to a remarkably high accuracy and would be perfectly consistent with the hypothesis that α Lup is a spectroscopic binary.

4. *Absolute magnitudes of β Cru, τ^1 Lup and α Lup.*—The purpose of the present section is to determine the absolute magnitudes of the three stars that have been found to have a short-period variation in radial velocity and to compare the results with the two period–luminosity relations that have been obtained for β Cephei variables. Owing to the very small range in intrinsic colour of the group, it is not possible at present to determine the intrinsic colours of the three stars on the *U, B, V* system sufficiently accurately for a detailed comparison with the results of McNamara and Williams (1955), apart from remarking that β Cru must be intrinsically much bluer than any well-established β Cephei star.

TABLE V

Leiden Photoelectric measurements of α Lup

Heliocentric J.D. −2435000	Δm (yellow filter) −3m·395 +	Heliocentric J.D. −2435000	Δm (yellow filter) −3m·395 +
1955 *July* 20		1955 *July* 20 (*continued*)	
309·286	−10	309·362	1
·290	3	·367	0
·296	11	·372	0
·301	−7	·377	2
·306	−6	·383	3
·311	−2	·389	0
·316	4	·394	−3
·321	0	·401	−5
·326	−2	·406	−1
·351	2	·412	−2
·357	3	·418	1

β Cru and α Lup belong to the Scorpio–Centaurus stream, and their absolute magnitudes have been determined by Blaauw (1946). However, these magnitudes may require some correction for interstellar absorption; the correction may be estimated in an indirect manner using the equation

$$\Delta m = 7(E_1 + 0^m{\cdot}05) \tag{7}$$

where E_1 is the colour excess on the scale of Stebbins, Huffer and Whitford (1940). Equation (7) is based on the work of Oort (1938) and Oosterhoff (1951). A comparison of the colour excesses derived by Stebbins and his collaborators with those of Johnson and Morgan (1953) suggests the approximate relation

$$E_1 + 0^m{\cdot}05 = \tfrac{1}{2}E_y \tag{8}$$

where E_y is the colour excess in $(B-V)$ of an early B-type star. From the colour index C_{pe} given in Cape Mimeogram 1, we can now find $(B-V)$ using the relation

$$C_{pe} = 0{\cdot}964(B-V) - 0^m{\cdot}188 \tag{9}$$

(Stoy, 1953) and compare it with the normal value for its spectral class given by Johnson and Morgan (1953). Equation (9) was tested for seven early B stars common to both lists and found to give a maximum error of $0^m{\cdot}01$.

τ^1 Lup does not belong to the Scorpio–Centaurus stream, and no parallax is available. Its absolute visual magnitude has therefore been estimated from the equivalent width of Hγ, following Petrie (1953a). For this purpose, the Hγ line in suitable spectra of τ^1 Lup and of a number of other stars of known absolute magnitude (Blaauw, 1946; corrected for absorption) was traced with the microphotometer at the Radcliffe Observatory (using 24 calibration spots from the tube sensitometer on each plate) and the magnitudes calculated from Petrie's formula. The results are given in Table VI.

Unfortunately, the stars studied are so intrinsically luminous that the magnitudes determined from Hγ are very sensitive to errors in the equivalent width; the results do show, however, that the absolute magnitude of τ^1 Lup is not likely to differ from that estimated from the Hγ measurements by much more

TABLE VI

Magnitudes, colours, and Hγ *measurements of six southern stars*

Star	Spectral type	M_{vis} (Blaauw 1946)	C_{pe}	$(B-V)$ (Eqn. (9))	E_y	M_{vis} (adopted)	No. of Hγ plates	E.W. of Hγ (ångströms)	M_{vis} (from Hγ)	$M - M_{H\gamma}$
β Cru	Bo III	$-3^m\cdot83 \pm 0^m\cdot15$	$-0^m\cdot44$	$-0^m\cdot26$	$0^m\cdot06$	$-4^m\cdot0$	5	$2\cdot5 \pm 0\cdot3$	$-4^m\cdot4 \pm 0^m\cdot5$	$+0^m\cdot4$
ξ^2 Cen	B 3	$-1^m\cdot60 \pm 0^m\cdot19$	$-0^m\cdot37$	$-0^m\cdot19$	$0^m\cdot01$	$-1^m\cdot6$	4	$5\cdot1 \pm 0\cdot6$	$-1^m\cdot8 \pm 0^m\cdot4$	$+0^m\cdot2$
τ^1 Lup	B 2 (IV)		$-0^m\cdot36$	$-0^m\cdot18$	$0^m\cdot06$		8	$3\cdot75 \pm 0\cdot2$	$-2^m\cdot9 \pm 0^m\cdot2$	
α Lup	B 2 II	$-3^m\cdot53 \pm 0^m\cdot18$	$-0^m\cdot41$	$-0^m\cdot23$	$0^m\cdot01$	$-3^m\cdot6$	6	$2\cdot7 \pm 0\cdot3$	$-4^m\cdot2 \pm 0^m\cdot5$	$+0^m\cdot6$
κ Cen	B 2 V	$-2^m\cdot95 \pm 0^m\cdot18$	$-0^m\cdot40$	$-0^m\cdot22$	$0^m\cdot02$	$-3^m\cdot0$	2	$4\cdot5 \pm ?$	$-2^m\cdot2 \pm ?$	$-0^m\cdot8$
τ Sco	B 0 V	$-3^m\cdot60 \pm 0^m\cdot13$	$-0^m\cdot45$	$-0^m\cdot27$	$0^m\cdot05$	$-3^m\cdot7$	1	$2\cdot8 \pm ?$	$-4^m\cdot0 \pm ?$	$+0^m\cdot3$

than the standard error determined from their intrinsic scatter. Furthermore, our value for the equivalent width of Hγ in the spectrum of τ Sco is in tolerable agreement with Petrie's value (3·3 A). We may therefore use the results of Table VI to compare the observational data for β Cru, τ^1 Lup and α Lup with the period–luminosity relations of Blaauw and Savedoff (1953) and of Petrie (1954a). This is done in Fig. 7; it is seen that τ^1 Lup fits either of the two curves very well, α Lup comes tolerably close to that of Petrie, and β Cru departs from both curves by more than a magnitude.

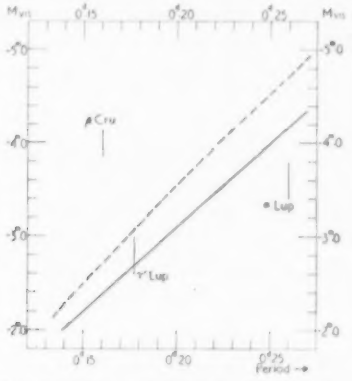

FIG. 7.—*Periods and luminosities of β Cru, τ^1 Lup, and α Lup.*
Abscissae: Period, in days.
Ordinates: Absolute visual magnitude.
The vertical lines represent the observational results for the three stars, with estimated limits of error.
Broken line: Period-luminosity curve of Blaauw and Savedoff (1953).
Full line: Period-luminosity curve of Petrie (1954a).

These results suggest the following conclusions.

(i) τ^1 Lup appears to be a typical small-amplitude β Cephei star.

(ii) In view of the failure of all efforts hitherto to establish a variation in light of α Lup, it is not possible to conclude from the velocity variation that it is definitely an intrinsic variable rather than a single-lined spectroscopic binary. However, if we assume the mass of the primary component to be of the order of 10 solar masses, it is easily shown that a binary system completing an orbit in $0^d{\cdot}26$ would have positive total energy if the mean mutual distance of the centres of the components were greater than $3{\cdot}3 \times 10^{11}$ cm, or about 5 solar radii. As the radius of a B2 giant is probably of the order of 10 solar radii (cf. the discussion of β Cep by Stebbins and Kron, 1954), it is clear that the binary hypothesis is not a very likely one. Clearly further studies of α Lup are needed. If it should turn out to be a β Cephei star, it would be of great significance in fixing the period–luminosity relation because its period is the longest known and its parallax relatively well determined.

(iii) As has been mentioned, it is possible that the period of β Cru may require revision in the light of future observations; alternatively, the anomalies that have been found here may be connected with its early spectral type, which suggests that β Cru cannot in any case be a "typical" β Cephei star. Further study of this star involving simultaneous observations of light and radial velocity, would be of the greatest interest (see note overleaf).

It is a pleasure to acknowledge the writer's indebtedness to Dr A. D. Thackeray for suggesting this investigation and for his continuous interest and advice during its progress; to Dr R. H. Stoy, Dr A. B. Muller and Dr A. W. J. Cousins for their cooperation in supplying photometric observations of the exceptional quality required for the detection of changes of the order of $0^{m}\cdot005$; to D. D. H. McNamara for supplying a list of "promising" stars; and to Dr A. Beer, Dr M. W. Feast, Professor J. B. Irwin and Dr A. J. Wesselink for useful discussion of various points connected with the investigation. The writer is also greatly indebted to the Radcliffe Trustees for the award of a Radcliffe Studentship and to the Master and Fellows of Sidney Sussex College, Cambridge, for a Research Fellowship.

Sidney Sussex College,
Cambridge:
1956 *January* 2.

Note added in proof.—Since the completion of this paper, a measurement of the radial velocity of α Lup, carried out by W. Buscombe at the Mount Stromlo Observatory, Canberra, has been brought to my notice. Buscombe's result, for 1954 March 24.701 U.T. (heliocentric J.D. 2434826.204), is $(-2\pm1\cdot2)$ km/sec, in perfect agreement with equation (5). I am grateful to Dr Buscombe for his permission to quote this result.

References

Blaauw, A., 1946, *Pub. Kapteyn Astr. Lab. Groningen*, No. 52.
Blaauw, A., and Savedoff, M. P., 1953, *B.A.N.*, **12,** 69.
Campbell, W. W., and Moore, J. H., 1928, *Pub. Lick Obs.*, **16,** 218.
Feast, M. W., Thackeray, A. D., and Wesselink, A. J., 1955, *Mem. R.A.S.*, **67,** 51.
Johnson, H. L., and Morgan, W. W., 1953, *Ap. J.*, **117,** 313.
Lick Observatory, 1932, *Catalogue of Radial Velocities of Stars and Nebulae*, *Pub. Lick Obs.*, **18.**
McNamara, D. H., 1955, *Ap. J.*, **122,** 95.
McNamara, D. H., and Williams, A. D., 1955, *Ap. J.*, **121,** 51.
McNamara, D. H., Struve, O., and Berthiau, F. C., 1955, *Ap. J.*, **121,** 326.
Neubauer, F. J., 1931, *Lick Obs. Bull.*, **15,** 107.
Odgers, G. J., 1955, *Pub. D.A.O.*, **10,** No. 9.
Oort, J. H., 1938, *B.A.N.*, **8,** 233.
Oosterhoff, P. Th., 1951, *B.A.N.*, **11,** 299.
Petrie, R. M., 1946, *J.R.A.S. Canada*, **40,** 325; *D.A.O. Contr.* No. 4.
Petrie, R. M., 1953 a, *Pub. D.A.O.*, **9,** No. 8.
Petrie, R. M., 1953 b, *ibid.*, **9,** No. 10.
Petrie, R. M., 1954 a, *J.R.A.S. Canada*, **48,** 185; *D.A.O. Contr.* No. 38.
Petrie, R. M., 1954 b, *Pub. D.A.O.*, **10,** No. 2.
Prager, R., 1932, *Kleine Veröff. Univ. Sternwarte Berlin-Babelsberg*, No. 12.
Schlesinger, F., 1899, *Ap. J.*, **9,** 159.
Stebbins, J., Huffer, C. M., and Whitford, A. E., 1940, *Ap. J.*, **91,** 20. *Mt. Wilson contr.* No. 621.
Stebbins, J., and Kron, G. E., 1954, *Ap. J.*, **120,** 189.
Stoy, R. H., 1953, *Cape Mimeogram*, No. 1.
Struve, O., 1952, *Ann. d'ap.*, **15,** 157.
Struve, O., 1955 a, *Pub. A.S.P.*, **67,** 31.
Struve, O., 1955 b, *ibid.*, **67,** 135.
Struve, O., 1955 c, *ibid.*, **67,** 173.
Walker, M., 1954 a, *Ap. J.*, **119,** 631.
Walker, M., 1954 b, *ibid.*, **120,** 58.
Wesselink, A. J., 1952, *Monthly Notes S. African Astr. Soc.*, **11,** 39.
Wilson, R. E., 1953, *General Catalogue of Stellar Radial Velocities* (Washington, D.C.: Carnegie Inst. of Washington Pub. No. 601).

THE EVOLUTION OF UNMIXED STARS

R. J. Tayler

(Received 1955 November 10)

Summary

The earlier treatment of this problem by Roy is shown to suffer from difficulties with regard to the transfer of energy in the convective core. These can be eliminated if Roy's assumed discontinuity of composition is replaced by a continuous gradient of molecular weight. Six such models have been obtained with central hydrogen content changing from 99 to 2 per cent. The evolutionary tracks of these models are compared with those obtained by Roy's method and there is seen to be no significant change in the observable properties of the stars. The H. R. Diagram for stars of varying masses but of the same age gives qualitative agreement with the lower part of the observed H. R. Diagram for globular clusters.

---

1. *Introduction.*—This paper may be regarded as a sequel to one on the evolution of massive stars. [Tayler (**18**). This will be referred to as Paper I in what follows.] It is also a reconsideration of a problem previously studied by Roy (**14**). Paper I contains a list of references to previous papers on stellar evolution; papers that have appeared since include Härm and Schwarzschild (**7, 8**), Hoyle and Schwarzschild (**9**) and Reiz (**13**).

If a star evolves without mixing currents, and either it possesses no convective core or the size of the convective core decreases as it evolves, a region with a continuous gradient of molecular weight will be set up in the star. Sequences of models obtained by Schönberg and Chandrasekhar (**16**), Roy (**14**), and Tayler (**17**) have assumed a discontinuity of composition at the surface of the core, but all these series of models have decreasing convective cores so that zones of variable composition must be present. In Paper I models have been obtained for massive stars with zones of variable composition, but for electron scattering opacity (which predominates in such stars) no models with a discontinuous change in composition at the surface of the core can exist. Hence no estimate could be made of the effect of the neglect of a transition zone. In this paper models are obtained similar to those of (**14**) but with a zone of variable composition replacing the discontinuity. At the same time a difficulty in the transport of energy, which occurs in the cores of some of the models of (**14**), is removed. This will be discussed in the next section.

2. *Outline of problem.*—In (**14**) Roy considered the evolution of unmixed stars with a photoelectric opacity law and with convective cores. He assumed that as the stars evolved, with conversion of hydrogen into helium in the energy-producing regions, a discontinuity of composition was built up at the surface of the convective core. The outer envelope retained its initial composition while the helium content of the core gradually increased. As was pointed out in Paper I, the assumption of a discontinuity of composition is essentially approximate,

when the convective core mass decreases as the star evolves. In this case convection dies out in the outer regions of the core and, as this material has already converted some of its hydrogen into helium, a radiative zone of variable composition is formed. Since the change in size of the convective core in the models of (**14**) is very small, one might expect that the replacement of the zone of variable composition by a discontinuity would have little effect on the models. There is however another difficulty associated with the transfer of energy in the core.

At the surface of the convective core all the energy flowing out from the centre of the star must be carried by radiation. One of the conditions used at the surface of discontinuity of models in (**14**) is that the flow of radiation should be continuous across the interface and equal to the surface luminosity. Because of this the energy carried by radiation at any point of the convective core must be less than that at the surface of the core; otherwise convection currents would be required to transport energy against the temperature gradient. The convective core is the Lane–Emden polytrope ($n = 3/2$) which is tabulated in (**4**) and for any given opacity law we can plot the radiative energy flux against Emden radius (or the Bondis' variable S used in Paper I (**14**) and the present paper). The transfer of radiant energy in convective cores has previously been considered by Öpik (**12**) and the results shown here are essentially those given by him. Fig. 1 shows the results for Electron and Kramers opacity laws. We see from

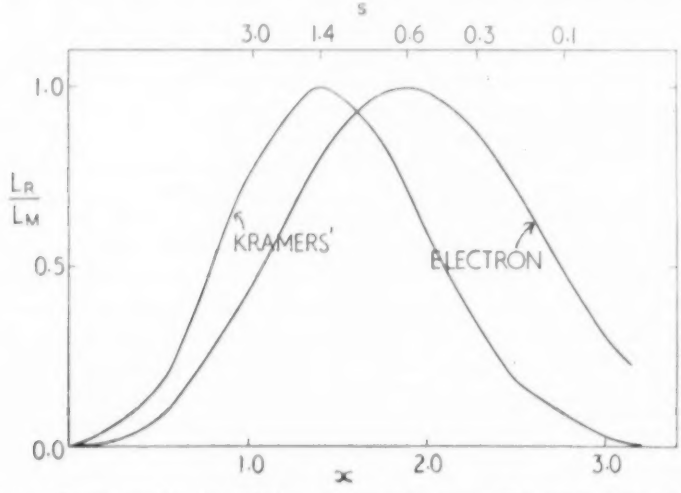

FIG. 1.—*Energy transfer by radiation in convective cores. The curves show the energy carried by radiation at points in the convective core of a star for two different opacity laws. For each curve the flux is expressed in terms of its maximum value and is plotted against the Emden radius x and the homology variable S.*

this figure that there is a maximum value of the Emden radius at which the boundary of the core can occur; for the two opacity laws we have

Electron $x < 1{\cdot}893$, $S > 0{\cdot}6$,
Kramers $x < 1{\cdot}409$, $S > 1{\cdot}4$.

This condition in a more refined form has been used by Naur and Osterbrock (**11**)

to obtain a necessary condition for the existence of convective cores in stars. They require that the energy flow by radiation inside the core must be less than the flow across the surface of the core by an amount at least equal to that produced in the intervening region. We shall assume that we are dealing with sufficiently concentrated energy production for this correction to our criterion to be unimportant.

An equivalent way of looking at this problem is that of examining the radiative equations near the interface. At the interface the value of $N\,(=1/(n+1))$ jumps to the convective value 0·4, but in order that convective conditions shall persist N must remain greater than or equal to 0·4 as we go further into the core. The radiative equations for Kramers' opacity give (**14**)

$$\frac{dN}{dS} = \frac{N(S+2-8{\cdot}5N)}{S(1+2S-4Q)}. \tag{2.1}$$

When $N=0{\cdot}4$ on the Emden solution, $1+2S-4Q>0$ and

$$\frac{dN}{dS} = \frac{0{\cdot}4(S-1{\cdot}4)}{S(1+2S-4Q)}. \tag{2.2}$$

Thus if $S<1{\cdot}4$, dN/dS is negative just inside the core, and the temperature gradient gives stability against convection once again. This condition that, at the boundary of a convective region, the radiative temperature gradient must remain unstable has been previously stated by Ledoux (**10**). In (**14**) we have Kramers' opacity and after the first three models of the sequence the convective core boundary occurs with $S<1{\cdot}4$, implying convective transport of energy against the temperature gradient.

In (**17**) it was shown that this same difficulty occurs with models having a modified Kramers' opacity law $\kappa \propto \rho^{0{\cdot}75}/T^{3{\cdot}5}$ but no attempt was made to remove the difficulty. In the present paper, by taking account of the zone of variable composition formed when the convective core shrinks in size, we have also obtained models in which there is no difficulty about the energy transport in the core. Kramers' rather than modified Kramers' opacity has been used to facilitate direct comparison with (**14**).

3. *Assumptions and equations.*—The models here considered consist of a helium enriched core in convective equilibrium surrounded by a zone of variable composition in radiative equilibrium and an envelope of constant composition also in radiative equilibrium. The following assumptions have been made.

(1) Energy production is by the carbon cycle and is confined to the convective core.
(2) Except in the convective regions there is no mixing.
(3) Only photoelectric opacity is important.
(4) The initial composition is 99 per cent hydrogen and 1 per cent heavy elements.
(5) The central temperature remains constant as the star evolves.
(6) Radiation pressure is negligible.
(7) Degeneracy never becomes important.

Homology variables. The solutions were obtained in homology variables introduced by Bondi and Bondi (**2**) and defined by

$$S=\frac{4\pi Pr^4}{GM^2}, \quad Q=\frac{Pr}{GM\rho}, \quad \mathcal{N}=\frac{P}{T}\frac{dT}{dP} \tag{3.1}$$

where the third variable replaces the Bondi variable $N = 1 - (P/\rho)(d\rho/dP)$ to which it reduces when the composition is uniform.

Subscripts. s = surface; c = centre; 1 = inner interface between the convective core and the zone of variable composition; 2 = outer interface between intermediate zone and envelope.

Equations. In a region of variable composition, the hydrostatic equation and the equation of mass conservation take the form

$$\frac{S}{Q}\frac{dQ}{dS} = \frac{S + \mathcal{N} - Q}{1 + 2S - 4Q} + \frac{5S}{2{\cdot}99 + 5X}\frac{dX}{dS} \tag{3.2}$$

where

$$\mu = \frac{4}{2{\cdot}99 + 5X}. \tag{3.3}$$

In a radiative region with opacity

$$\kappa = \kappa_{00} Z(1 + X)\rho/T^{3{\cdot}5}, \tag{3.4}$$

$$\frac{S}{\mathcal{N}}\frac{d\mathcal{N}}{dS} = \frac{S + 2 - 8{\cdot}5\mathcal{N}}{1 + 2S - 4Q} - \frac{2{\cdot}01S}{(1 + X)(2{\cdot}99 + 5X)}\frac{dX}{dS}. \tag{3.5}$$

While, in a convective region,

$$\gamma = 5/3, \quad \mathcal{N} = 0{\cdot}4. \tag{3.6}$$

Limit of convection. The condition for instability against convection will be (cf. (**18**))

$$\left(\frac{dT}{dr}\right)_{\text{rad}} > \left(\frac{dT}{dr}\right)_{\text{adiab}}. \tag{3.7}$$

This relation reduces to

$$\mathcal{N}_{\text{rad}} > \mathcal{N}_{\text{adiab}} = 0{\cdot}4. \tag{3.8}$$

At the boundary of the convective core

$$\mathcal{N} = 0{\cdot}4. \tag{3.9}$$

4. *Method of solution.*—The method of construction of the models is essentially the same as that used in Paper I. The equations for the envelope possess a one-parameter family of solutions. In (**14**) Roy has solved these in terms of the variable

$$u = -\ln(M/M_s) \tag{4.1}$$

and near the surface ($u = 0$)

$$\left.\begin{aligned} S &= u[1 - 3{\cdot}23810\theta + 2{\cdot}75240\theta^2 + 0{\cdot}82594\theta^3 + u + \ldots] \\ Q &= \theta[1 - 1{\cdot}011905\theta - 0{\cdot}35224\theta^2 - 0{\cdot}01172\theta^3 + 0{\cdot}84314u + \ldots] \\ \mathcal{N} &= 0{\cdot}235294 + u[0{\cdot}078431 - 0{\cdot}15700\theta - 0{\cdot}05655\theta^2] \end{aligned}\right\} \tag{4.2}$$

where $\theta = Au^{4{\cdot}17}$. Roy has obtained envelope solutions for eight values of the parameter A and we use these solutions in the construction of our models.

In the convective regions there is a single solution satisfying the central boundary conditions

$$\left.\begin{aligned} Q &= S/3 + O(1), \\ \mathcal{N} &= 0{\cdot}4. \end{aligned}\right\} \tag{4.3}$$

This is the Lane–Emden solution for polytropic index $n = 1{\cdot}5$. This is tabulated in (**4**), and Roy has tabulated it in terms of Bondi variables in (**14**). We have both used Roy's table and retabulated the function for smaller intervals of the Bondi variables, at different stages in the problem.

For one value of the parameter A, the envelope solution will fit smoothly to the core solution, and provide a model for a homogeneous star. Such a model has been obtained by several authors including Bondi and Bondi (**2**) and Gardiner (**6**). Roy extrapolated from his calculated solutions to obtain the homogeneous model which was the starting model for his evolutionary sequence (he obtained good agreement with the model of Gardiner) and we adopted the same procedure.

Once the homogeneous model has been obtained ($A \simeq 0{\cdot}234$), the second model of the sequence was constructed as follows. An envelope with slightly higher $A(=0{\cdot}2415)$ was taken and was used to the point at which it contained the same mass as the radiative part of the first model; this point was reached before condition (3.9) for convective instability was satisfied. Beyond this point we are integrating through a region which was originally in the convective core and has therefore converted some of its hydrogen into helium, and thus we are in a zone of variable hydrogen content. As a first approximation to the variation in this zone we assume that the hydrogen content X is linear with u, so that in the transition zone

$$\frac{dX}{du} = \text{const.}$$

$$\frac{dX}{dS} = \frac{1}{1+2S-4Q}\frac{dX}{du}. \tag{4.4}$$

The integration was carried out for a trial value of dX/du. Initially our solution lies above the Lane–Emden solution in the $S-Q$ plane. For some values of dX/du, the variable $\mathcal{N}$ reaches the value 0·4 while our solution still lies above the Emden solution; for other values the curve crosses the Emden solution before $\mathcal{N}=0{\cdot}4$. For one value of dX/du, $\mathcal{N}=0{\cdot}4$ at the point at which the solution crosses the Emden solution. At this point all the conditions for a fit to a convective core are satisfied. Several trial values of dX/du must be used and the required result obtained by interpolation between them.

The variation of composition in this transition zone defines the variation in the first part of the transition zone of the next model, and the remainder of the transition zone is constructed as above. In all, including the homogeneous starting model, six models have been obtained and the mathematical characteristics of the models are listed in Table I. It may be noted that in each case the fit to a convective core occurs with $S>1{\cdot}4$ so that there is no maximum of radiative energy transfer inside the core. Fig. 2 shows the change in hydrogen content

TABLE I

	I	II	III	IV	V	VI
A	0·234	0·2415	0·2513	0·2568	0·2635	0·2680
S_2	2·120	1·7757	1·3655	1·1559	0·9212	0·7774
Q_2	0·821	0·8104	0·7895	0·7740	0·7507	0·7318
$\mathcal{N}_2$	0·4000	0·3846	0·3636	0·3515	0·3362	0·3259
u_2	1·9215	1·9215	1·9215	1·9215	1·9215	1·9215
S_1		1·8269	1·5035	1·4538	1·4970	1·4523
Q_1		0·7220	0·6130	0·5960	0·6106	0·5954
$\mathcal{N}_1$		0·4000	0·4000	0·4000	0·4000	0·4000
u_1		1·9548	2·0448	2·2073	2·5690	2·8790
$-(dX/du_1)$		6·30	2·863	0·915	0·554	0·503
X_c	0·9900	0·7802	0·5225	0·3738	0·1734	0·0175

and the retreat of the convective core as the star evolves. It can be seen that as the first fifty per cent of the central hydrogen is burnt the transition zone is fairly adequately represented by a discontinuity; after that the size of the transition region increases rapidly.

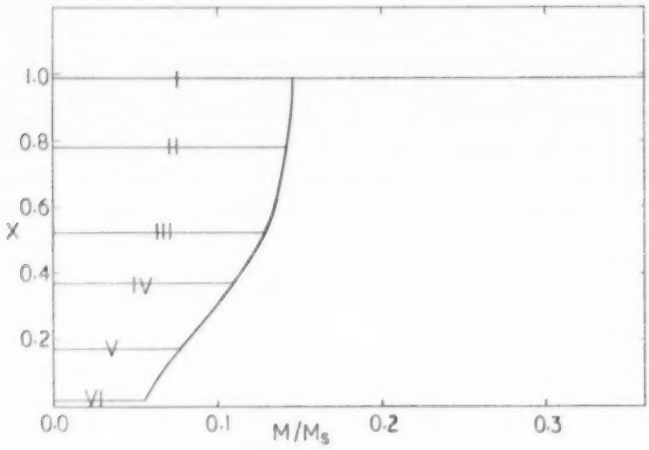

FIG. 2.—*The variation of hydrogen content from centre (left) outwards. The composition of the envelope is constant for all models of the sequence, and this is shown by the horizontal line at the right of the figure. The numbered horizontal lines at the left show the hydrogen content and extent of the convective cores of the successive models. The horizontal lines are joined by a curve showing the varying composition in the intermediate zone.*

5. *Physical properties of models.*—Once we have obtained our solutions in terms of homology variables, we require to pass to the solution in physical variables. If the total mass, M_s, and the central temperature, T_c, are given, we require expressions for L_s, P_c, ρ_c, r_s and T_e. From the definitions of the homology variables

$$\ln Q_1 = \ln \frac{P_c r_s}{G\rho_c M_s} + \ln \frac{r_1}{r_s} + \ln \frac{P_1}{P_c} - \ln \frac{M_1}{M_s} - \ln \frac{\rho_1}{\rho_c} \tag{5.1}$$

$$\ln S_1 = \ln \frac{4\pi P_c r_s^4}{GM_s^2} + \ln \frac{P_1}{P_c} + 4 \ln \frac{r_1}{r_s} - 2 \ln \frac{M_1}{M_s} \tag{5.2}$$

where we have taken these relations at the boundary of the convective core. In this equation

$$\ln (M_1/M_s) = -u_1,$$

$\ln (P_1/P_c)$, $\ln (\rho_1/\rho_c)$ are tabulated in the B.A. Tables (**4**) [B and A in those tables] and

$$\ln (r_1/r_s) = -\int_0^{u_1} (Q/S)\, du \tag{5.3}$$

must be obtained by quadrature. Using

$$P_c = \mathscr{R}\rho_c T_c/\mu_c \tag{5.4}$$

we obtain expressions for r_s, P_c, ρ_c.

L_s is obtained from the "Mass Luminosity" relation which in this case takes the form

$$\frac{4}{17}A^{8\cdot5}=\frac{3\kappa_{00}Z_s(1+X_s)}{16\pi ac}\left(\frac{\mathscr{R}}{\mu_s G}\right)^{7\cdot5}\frac{1}{(4\pi)^2}L_s r_s^{1/2}M_s^{-5\cdot5}. \tag{5.5}$$

The effective temperature can then be found from the relation

$$L_s=\pi a c r_s^2 T_s^4. \tag{5.6}$$

The total mass of hydrogen that has been converted into helium (mass burned) for any model of the sequence can be obtained by integrating the hydrogen content over the mass

$$M_B=\int_0^{M_s}(0\cdot99-X)\,dM. \tag{5.7}$$

The time taken in the evolution is found from

$$\text{Time}=0\cdot007c^2\int dM_B/L. \tag{5.8}$$

Once values are taken for κ_{00}, T_c and M_s, the physical properties of the models are completely determined. However the application of this particular combination of opacity and law of energy generation to any model is uncertain (3), and in Table II we have expressed the physical properties non-dimensionally showing changes from a zero point which is only fixed when κ_{00}, T_c and M_s are given. We could have fitted our models to some of the solar parameters but that might have given quite misleading values for other solar properties.

TABLE II

	I	II	III	IV	V	VI
r_s/r_{sI}	1·00	1·15	1·42	1·65	2·08	2·60
$-\delta M_{\text{BOL}}$	0·00	0·21	0·46	0·58	0·69	0·73
$-\delta \text{ Log}_{10}\, T_e$	0·000	0·008	0·029	0·049	0·088	0·133
ρ_c/ρ_{cI}	1·00	0·96	0·91	0·88	0·86	0·86
M_{core}/M_s	0·146	0·142	0·129	0·110	0·077	0·056
r_{core}/r_s	0·170	0·150	0·121	0·100	0·071	0·051
X_{core}	0·9900	0·7802	0·5225	0·3738	0·1734	0·0175
Mass burned/M_s	0·000	0·030	0·065	0·083	0·101	0·112
$\frac{\text{Time}}{10^9 \text{ years}}\frac{L_{sI}}{M_s}$	0·00	5·44	10·56	12·77	14·77	15·90
$\ln\frac{P_c}{G\rho_c M_s}\frac{r_s}{M_s}$	−0·1083	−0·1113	−0·1043	−0·0990	−0·0980	−0·1001
$\ln\frac{4\pi P_c r_s^4}{GM_s^2}$	4·595	4·965	5·559	5·971	6·642	7·312

By calculating $\int_0^u (Q/S)du$ for values of u other than u_1, and by using equations (5.1) and (5.2), we can obtain the variation of r, P and ρ with M for different models of the sequence. Table III shows the results for Models II–V. Model I has been omitted because of the extrapolation involved, and Model VI because its very low central hydrogen content implies that some of our basic assumptions are invalid. In Fig. 3 we plot the actual movement of mass shells against mean composition of the models. We see that most of the increase in radius occurs for the outer 60 per cent of the mass as would be expected from the small change in central density.

TABLE III

Model M/M_s	II r/r_s	II ρ/ρ_c	II P/P_c	III r/r_s	III ρ/ρ_c	III P/P_c
0·00	0·000	1·000	1·000	0·000	1·000	1·000
0·01	0·058	0·941	0·904	0·048	0·929	0·885
0·02	0·073	0·908	0·843	0·061	0·889	0·821
0·05	0·102	0·830	0·734	0·084	0·796	0·684
0·10	0·131	0·733	0·595	0·109	0·680	0·525
0·129	—	—	—	0·121	0·620	0·450
0·142	0·150	0·667	0·509	—	—	—
0·146	0·152	0·572	0·500	0·129	0·414	0·412
0·20	0·175	0·506	0·410	0·153	0·353	0·334
0·30	0·212	0·397	0·286	0·191	0·266	0·213
0·40	0·246	0·307	0·198	0·226	0·200	0·142
0·50	0·280	0·230	0·132	0·260	0·146	0·091
0·60	0·316	0·163	0·083	0·297	0·102	0·056
0·70	0·358	0·107	0·047	0·339	0·066	0·031
0·80	0·409	0·063	0·024	0·391	0·037	0·014
0·90	0·487	0·030	0·007	0·471	0·015	0·004
0·95	0·555	0·011	0·0024	0·540	0·006	0·0014
1·00	1·000	0·000	0·000	1·000	0·000	0·000

Model	IV			V		
0·00	0·000	1·000	1·000	0·000	1·000	1·000
0·01	0·042	0·920	0·870	0·034	0·900	0·833
0·02	0·053	0·873	0·799	0·043	0·842	0·752
0·05	0·074	0·769	0·645	0·060	0·711	0·567
0·077	—	—	—	0·071	0·619	0·449
0·10	0·097	0·636	0·470	0·080	0·458	0·367
0·110	0·100	0·612	0·441	—	—	—
0·146	0·116	0·316	0·352	0·101	0·209	0·251
0·20	0·141	0·255	0·250	0·127	0·166	0·179
0·30	0·180	0·199	0·169	0·166	0·117	0·108
0·40	0·215	0·161	0·110	0·201	0·085	0·068
0·50	0·249	0·105	0·069	0·236	0·060	0·042
0·60	0·286	0·073	0·042	0·274	0·040	0·025
0·70	0·328	0·046	0·023	0·316	0·025	0·013
0·80	0·381	0·026	0·010	0·369	0·014	0·006
0·90	0·461	0·010	0·003	0·450	0·006	0·0016
0·95	0·532	0·004	0·001	0·522	0·002	0·0005
1·00	1·000	0·000	0·000	1·000	0·000	0·000

We can also consider the relation between luminosity and mean molecular weight for the models of the sequence. It is found that all but Model VI quite closely follow a power law

$$L_s \propto M_s^5 \mu_{\text{mean}}^{9\cdot9}. \tag{5.9}$$

This result can be compared with the mass–luminosity–molecular weight relation for unmixed stars of the same opacity, and with results for both mixed and unmixed stars with electron opacity. These results previously considered in (**19**) are shown in Table IV. It will be seen that for both opacity laws the increase in brightness is more rapid for the unmixed stars, the effect being larger in the case of Kramers' opacity.

We are now in a position to consider the validity of the assumptions made in Section 3. As has been mentioned previously, it is uncertain whether the combination of Carbon Cycle energy production and photoelectric opacity considered in this paper does occur in any stars. Bondi (**3**) considers that Carbon

Cycle production predominates in stars somewhat less massive than the Sun and in these stars photoelectric opacity would be most important. On the other hand Epstein (**5**) believes that the $P-P$ reaction predominates in the Sun. Bound up with this uncertainty is that of the existence and size of convective cores. For these reasons we shall not attempt to justify our choice of laws of energy generation and opacity; we have been interested in the possible effects of replacing a discontinuity by a transition zone, and we have chosen conditions agreeing

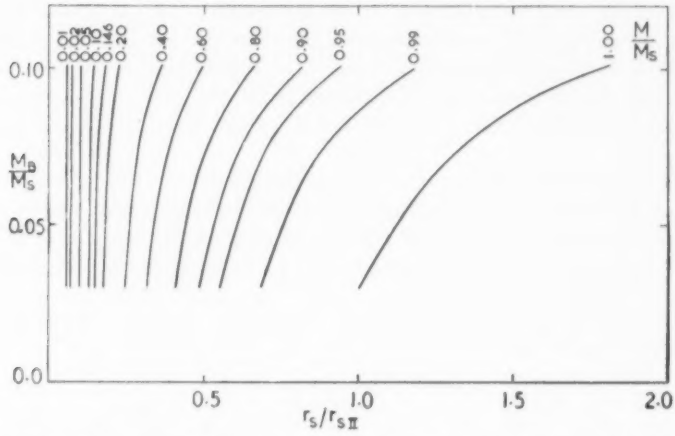

FIG. 3.—*Motion of mass shells during the evolution. The curves show the motion during the evolution of surfaces containing given fractions of the star's mass. Radial distance, in terms of the radius of Model II, is plotted against fractional mass of hydrogen converted into helium. The numbers at the top show the percentage of the mass contained within the surfaces considered.*

with those used in (**14**), and avoiding the mathematical difficulties of mixed opacities and energy generation. In Paper I, where the opacity and energy generation were fairly clear, we were unable to compare our models with those having a discontinuity at the surface of the core, as such models do not exist for electron scattering opacity.

TABLE IV

$L \propto M^{\gamma}\mu^{\delta}$

Model	Opacity	γ	δ
Mixed	Electron scattering	3·0	4·78
Unmixed	Electron scattering	3·0	5·4
Mixed	Kramers'	5·0	7·78
Unmixed	Kramers'	5·0	9·9

As in Paper I we can integrate a law of energy generation through the convective core, and, by comparing the energy generation at the core surface and just beyond with the mean generation in the core, we can estimate the importance of energy production outside the core. In Model VI we find a rapid increase of energy production as we enter the zone of increasing hydrogen content just outside the core, and in this model shell burning of hydrogen outside the core is very important. In both Models IV and V the energy production

is small at the core surface, and continues to drop in the transition zone ; energy production outside the core is possibly important in Model V but not in Model IV. In Models II and III there is again an increase of energy production as the transition zone is entered, because the change in composition is almost discontinuous, but this is soon balanced by the decrease further out.

Finally, with the knowledge that but for Model VI most of the energy is produced in the core, we can estimate the increase of central temperature which we have neglected previously. Assuming that all the energy of Model V is produced in the core, we find that the central temperature will have increased by about one-fifth. This is of the same order as the increase found in (**14**). It is likely to be an overestimate as some energy is produced outside the core. Such a change does not cause much alteration in the evolutionary tracks discussed in the following section, especially when one considers the uncertainties discussed above.

6. *Conclusions and comparisons.*—Using the results shown in Table II the positions of the sequence (relative to an arbitrary starting point) can be plotted in the H.R. diagram. The results can be compared with those of (**14**) and at first sight it appears that the replacement of a discontinuity of composition by a zone of variable composition has made a clear difference to the models. However there appears to be an error in the results of (**14**). Equation (3.10) in (**14**) (equivalent to our equation (5.1)),

$$\ln \frac{P_c r_s}{G\rho_c M_s} = \ln Q - u + \int_0^u \frac{Q}{S}\, du + \int_u^\infty \frac{N}{S}\, du, \tag{6.1}$$

must be handled carefully if the range of integration of the second integral contains a point of discontinuity of ρ. At such a point N ($= 1 - P/\rho(d\rho/dP)$) is momentarily infinite and this leads to a finite contribution to the integral.

In fact

$$\ln \frac{P_c r_s}{G\rho_c M_s} = \ln \frac{\mu Q}{\mu_c} - u + \int_0^u \frac{Q}{S}\, du + \int_u^\infty \frac{N}{S}\, du \tag{6.2}$$

where now N can be considered finite everywhere.

We have taken Roy's solutions in homology variables and have recalculated their physical properties by using equations (5.1) to (5.6) of the last section. This involves the assumption of constant central temperature so that the results are not exactly equivalent to those found by Roy. The results of these calculations are shown in Table V. It can be seen that the introduction of the factor $\ln(\mu/\mu_c)$ has virtually removed the apparent differences between the models of (**14**) and the present paper. Fig. 4 shows the tracks of the two sets of models in the H.R. diagram, and it can be seen that they only differ for the last two, and most uncertain, models of the sequence. Thus it seems that, although the assumptions of (**14**) neglect the zone of variable composition and imply the convection of energy against the temperature gradient, they have very little effect on the properties of the star as a whole during the early stages of its evolution. Added to that the assumption of a discontinuity leads to much simpler mathematics.

Also shown in Fig. 4 is the evolutionary track for fully mixed stars. Corresponding models in the mixed and unmixed sequences have the same mean molecular weight. Finally we show the track followed by the models of Sandage and Schwarzschild (**15**); in these evolution to a Schönberg–Chandrasekhar

limiting isothermal core (**16**), is followed by gravitational contraction. These models also neglect the possible importance of a transition zone.

TABLE V

	I	II	III	IV	V	VI
r_e/r_{eI}	1·00	1·15	1·42	1·65	2·01	2·33
$-\delta M_{BOL}$	0·00	0·21	0·46	0·58	0·71	0·79
$-\delta \mathrm{Log}_{10} T_e$	0·000	0·008	0·029	0·049	0·080	0·105
ρ_e/ρ_{eI}	1·00	0·96	0·91	0·87	0·82	0·73
M_{core}/M_s	0·146	0·142	0·137	0·136	0·135	0·136
r_{core}/r_s	0·170	0·150	0·124	0·110	0·094	0·084
X_{core}	0·9900	0·7777	0·5138	0·3790	0·2300	0·1459
Mass burned/M_s	0·000	0·030	0·067	0·084	0·103	0·115

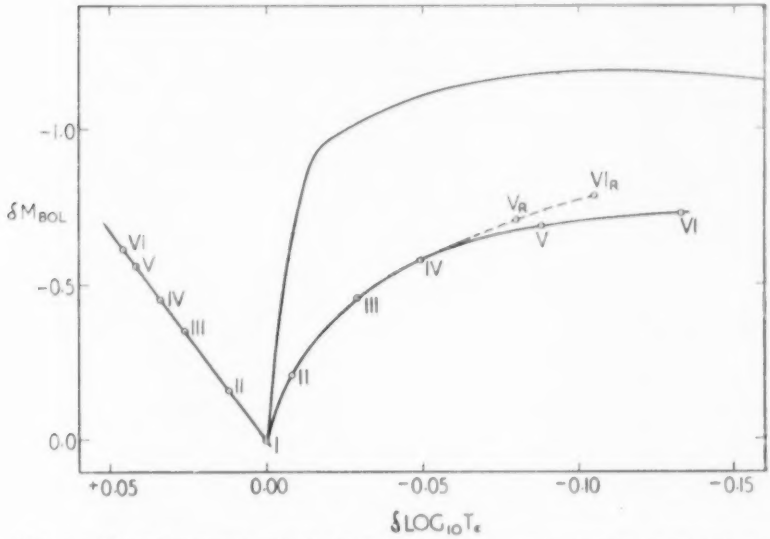

FIG. 4.—*The evolutionary tracks in the H.R. Diagram. The straight line to the left shows the evolutionary track of a well mixed star. The upper curve is the H.R. Diagram for the models of Sandage and Schwarzschild. The lower curve is the H.R. Diagram for the sequence of models of the present paper; the points* V_R *and* VI_R *show the deviations of models with a discontinuity in composition from the solid curve.*

Fig. 5 shows the instantaneous H.R. diagram for stars of different masses which started their evolution at the same time. Assuming that the central temperature is effectively constant for different masses, we can apply the homologies

$$L \propto M^5, \quad r \propto M, \quad T_e \propto M^{3/4}, \quad \text{Time} \propto (M/L).$$

In Fig. 5 the most massive star has completed the evolution from Model I to Model VI, while the lightest has, in the same time, scarcely started its evolution.

It will be seen that Fig. 5 is very similar to the one obtained for massive stars in Paper I and to that obtained by Sandage and Schwarzschild. In this case the "knee" in the diagram occurs at the point of 8 per cent burning of hydrogen. This is rather lower than the results obtained previously. The curve is in qualitative agreement with the lower part of the observational curve for globular clusters ((**1**) etc.); but it seems that almost any series of models that assumes

a low enough degree of mixing in stellar interiors will obtain such qualitative agreement. At the moment physics rather than observational astronomy must be used to differentiate between the theoretical results.

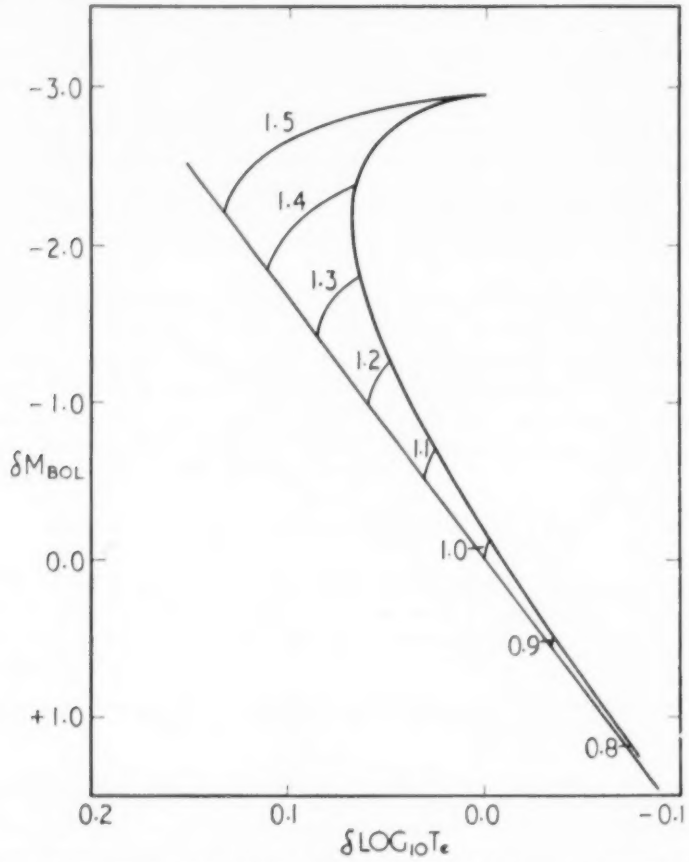

FIG. 5.—*Instantaneous H.R. Diagram for the stars of varying masses. The straight line at the left of the diagram is the original main sequence; the curve at the right is the locus for stars of varying masses after a time depending on the unit of mass and other parameters of the problem. The connecting curves are evolutionary tracks of individual stars whose masses (in arbitrary units) are shown at their starting points.*

This problem would have presented far more difficulties had Dr Roy not deposited detailed tables of the models of (**14**) with the Royal Astronomical Society. I am grateful to Dr Roy, and to the Royal Astronomical Society, for the loan of these tables.

Note added in proof—Since this paper was submitted, Roy has published a further note* in which the error in his equation [14, (3.10)] has been corrected by the introduction of the factor in μ/μ_e, and his evolutionary tracks then essentially agree with those found above.

A.E.R.E.,
Harwell, Didcot,
Berkshire :
1955 *November* 9.

* *M.N.*, **115**, 396, 1955.

References

(1) H. C. Arp, W. A. Baum and A. R. Sandage, *A.J.*, **58**, 4, 1953.
(2) C. M. Bondi and H. Bondi, *M.N.*, **109**, 62, 1949.
(3) H. Bondi, *M.N.*, **110**, 595, 1950.
(4) *British Association Mathematical Tables*, **2**, 1932.
(5) P. Epstein, *Ap. J.*, **112**, 207, 1950.
(6) J. G. Gardiner, *M.N.*, **111**, 94, 1951.
(7) R. Härm and M. Schwarzschild, *Ap. J.*, **121**, 445, 1955.
(8) R. Härm and M. Schwarzschild, *Ap. J. Supp.*, **1**, No. 10
(9) F. Hoyle and M. Schwarzschild, *Ap. J. Supp.*, **2**, No. 13.
(10) P. Ledoux, *Ap. J.*, **105**, 305, 1947.
(11) P. Naur and D. Osterbrock, *Ap. J.*, **117**, 306, 1953.
(12) E. J. Öpik, *Proc. Roy. Irish Acad.*, **53A**, 1, 1950–51.
(13) A. Reiz, *Ap. J.*, **120**, 342, 1954.
(14) A. E. Roy, *M.N.*, **112**, 484, 1952.
(15) A. R. Sandage and M. Schwarzschild, *Ap. J.*, **116**, 463, 1952.
(16) M. Schönberg and S. Chandrasekhar, *Ap. J.*, **96**, 161, 1942.
(17) R. J. Tayler, *Cambridge Doctoral Dissertation*, 1953.
(18) R. J. Tayler, *Ap. J.*, **120**, 332, 1954.
(19) R. J. Tayler, *A.J.*, **59**, 413, 1954.

MOTIONS IN THE SUN AT THE PHOTOSPHERIC LEVEL
VI. Large Scale Motions in the Equatorial Region

A. B. Hart

(Communicated by the Director, University Observatory, Oxford)

(Received 1955 November 4)

Summary

A series of line-of-sight velocity measurements, made on spectra of the Sun obtained at Oxford in 1953 May, is described. Spectra some 15 mm in height, taken with a solar image of 85 mm diameter, covered an arc of length 4×10^5 km in the surface extending inwards from the limb. Measurement was made of two plates, taken an hour apart at the East equatorial limb, each carrying four exposures obtained in rapid succession. Each of the eight spectra was measured at 140 points 0·10 mm apart, corresponding to an average spatial resolution of 4×10^3 km on the solar surface. The error to be attributed to a velocity measurement is carefully considered ; with the fine-grain plates used in the present investigation, a value $\pm 0{\cdot}09(0) \pm 0{\cdot}02(8)$ km sec^{-1} is found for the error of measurement of a single velocity.

An investigation of the equatorial velocity field is based on the 1120 measurements of velocity. Measurements from the four exposures on a plate were combined to give the best values of the velocity, thereby reducing the uncertainty of the velocity at any point on the surface to $\pm 0{\cdot}04(5) \pm 0{\cdot}01(4)$ km sec^{-1}. The residual velocities remaining after the limb effect and the component of solar rotation have been removed show a dispersion of $\pm 0{\cdot}16(1)$ km sec^{-1}. This dispersion exceeds the error of the velocity at a point on the surface by some eight times the uncertainty of the latter, thus providing conclusive proof of the existence of a velocity field. An irregular distribution of the velocity residuals over the solar surface is found ; correlographic analysis gives $2{\cdot}6 \times 10^4$ km as the average linear extent of a velocity fluctuation. The stability of the field is established from the similarity in the velocity distribution at the beginning and end of the period of observation. Finally, a suggestion is put forward for the possible origin of the field.

Introduction.—Measurements of the rotational velocity of the Sun, using Doppler displacements of spectral lines, have always shown much larger variations from one determination to another than could be explained by the random error of measurement (**2, 9, 16, 22, 24**). Whether these discrepancies, amounting to a few tenths of a kilometre per second, were the result of a variation of the photospheric circulation with time or were due to local variations in velocity was not, however, clear.

In a previous paper by the writer (**11**), measurements of velocity, made at intervals along arcs extending inwards up to $2{\cdot}5 \times 10^5$ km from the limb in the equatorial region, were described. A dispersion in velocity of $\pm 0{\cdot}17$ km sec^{-1} was found, which significantly exceeded the error of measurement, estimated as $\pm 0{\cdot}08 \pm 0{\cdot}02$ km sec^{-1} for a single velocity. Since it was also shown that scattering of light in the terrestrial atmosphere and by the telescope (**14**) could not produce spurious velocity differences of this size, as had once been suggested (**7, 8**), clear evidence was obtained for the existence of motions in the photosphere.

The linear scale of the velocity fluctuations was fairly large, varying from about $2{\cdot}5$ to $8{\cdot}5 \times 10^4$ km, and the observations indicated that the motion was quite stable, persisting perhaps for 3 hours. As a precise determination of the velocity field the investigation was, however, inconclusive for several reasons. The true velocity variation along an arc of surface was partially masked by the random velocities due to errors of measurement. Furthermore, even the value $\pm 0{\cdot}08$ km sec^{-1} was only achieved by measuring over such a length of solar surface that features extending less than 2×10^4 km could not be resolved. Finally, although some velocity sequences covered a length of $2{\cdot}5 \times 10^5$ km, most were restricted to about $1{\cdot}3 \times 10^5$ km near the limb, so that the general distribution of velocity, even in the equatorial region, was hardly established.

Attention in the present paper has, therefore, been focused on a detailed determination of the velocity variation along an arc of length 4×10^5 km, in the equatorial region, over a period of an hour. Satisfactory spatial resolution has been achieved by measuring velocities at 140 positions along the arc, corresponding to an average interval of 4×10^3 km between two successive positions. Spectra of moderate height covering the necessary length of arc in the solar surface have been obtained by reducing the size of the solar image. Errors in the measured velocities have been minimized in two ways. The actual accuracy of measurement was increased by using finer-grain plates. Secondly, both at the beginning and at the end of the period, repeated observations were made of the velocity field. Altogether the velocity at 1120 positions has been obtained.

In the sections which follow, an account is given of the observations made at Oxford in 1953 May, the measurement of the spectra obtained, and their reduction to velocities on the Sun. An analysis of the results is carried out in the last section and their physical implications are briefly considered.

Papers in this series " Motions in the Sun at the Photospheric Level " are referred to by their serial numbers.

1. *Observations.*—In its normal form the Oxford solar equipment consists of a vertical telescope of the Cassegrain type (**17**) with an equivalent focal length of 19·8 m, feeding a fixed horizontal Littrow spectroscope (**18**) whose slit lies in an E–W direction. The diameter of the image produced by the telescope is 180 mm, and in the wave-length region 5900 A the dispersion of the spectroscope is $1{\cdot}5$ A mm^{-1}. A guiding plate (**19**) placed in the beam in front of the spectroscope permits accurate focusing, and a precise determination of the position of the solar image on the spectroscope slit.

For the present set of observations, the size of the solar image was reduced by modifying the telescope. The hyperboloid and its carriage were removed and were replaced by a lens carried in vertical ways. The lens, supplied by Sir Howard Grubb, Parsons and Co., is a visually corrected achromatic doublet, 10 cm in diameter and of focal length 9·1 m. A parallel beam of light was fed to it in the usual way by the coelostat and secondary mirror. The converging beam from the lens was then deflected in a horizontal direction by the coudé mirror, the main paraboloidal mirror of the telescope, just below, being kept covered. An image of the Sun 85 mm in diameter was formed at the spectroscope slit. The telescope was thus used as a simple achromatic refractor.

The centre of the lens cell was moved laterally until a plumb-line from it intercepted the centre of the coudé mirror. By means of squaring-on screws and a sensitive level the lens cell was then made perpendicular to this vertical

axis. By moving the lens up and down in its ways, and observing the definition of the image in the eyepiece of the guiding device, the position of the lens for which the image lay precisely in the plane of the spectroscope slit could be detected. This position of best focus was sharply defined and remained unchanged throughout the fortnight when observations were made.

The spectroscope was adjusted so that the wave-length 5900 A was central on the plate. A diaphragm over the spectroscope slit limited its height to approximately 19 mm; about 15·5 mm of this was covered by the solar image, so guided that the slit intersected the limb close to the equator. While, say, the East limb was accurately maintained in position, four exposures were made on a plate. Each exposure lasted 10–20 seconds and all four were generally made within $3\frac{1}{2}$ minutes. The procedure was repeated at the same limb position at intervals of approximately an hour. Similar plates were obtained at the West equatorial limb. Ilford thin film panchromatic half-tone plates were used; they were developed in Parkhurst two-solution developer.

The first fortnight in 1953 May was a period of exceptionally good weather. During that time, six West limb plates and three East limb plates were obtained with seeing varying between 0 and 2 on a scale of 5 (**19**). Two East limb plates, separated by an interval of one hour, were selected as most suitable for measurement. Details of the exposures are given in the first two sections of Table I.

TABLE I

Spectrum	Date and U.T.	Exp. time sec	Sp. ht. mm	Slit width mm
E_{11}	1953 May 5·3625	11	15·42	0·04
E_{12}	5·3635	11	15·44	0·04
E_{13}	5·3643	11	15·41	0·04
E_{14}	5·3649	11	15·44	0·04
E_{21}	1953 May 5·4020	10·5	15·43	0·04
E_{22}	5·4027	10·5	15·43	0·04
E_{23}	5·4033	10·5	15·46	0·04
E_{24}	5·4044	10·5	15·39	0·04
Centre standard	1953 May 21·4558	16	18·76	0·04

1 mm on spectrum normal to the dispersion = 22″·49 on Sun.
1 mm on slit = 22″·33 on Sun.

When all the limb spectra had been obtained, the telescope was restored to its usual form. With the solar image focused 50 cm in front of the slit, so that local irregularities of velocity are smoothed out on the spectra, several exposures were made of the centre of the disk. The last row in Table I gives details of the spectrum selected as a standard for the velocity measures.

2. *Measurements*

2.1. *General method of measurement.*—Reliable values of velocity from Doppler displacements of solar lines are obtained when terrestrial atmospheric lines are used as standards of zero velocity (**16, 19**). Six unblended solar (Fe) lines, bracketed by six water-vapour lines of comparable strength, were measured in

all the spectra. Table II gives the wave-lengths recommended by the International Astronomical Union (**3, 10**) and the Rowland intensities of the lines (**23**).

TABLE II

Terrestrial lines		Solar lines			
Wave-length A	Rowland intensity	Wave-length A	Rowland intensity	Element	Vel. factor km sec^{-1} mm^{-1}
5901·468	6	5905·680	4	Fe I	74·69
5919·054	5	5916·257	3	Fe I	75·18
5919·644	7	5927·797	2	Fe I	75·74
5932·092	5	5929·682	2	Fe I	75·82
5946·006	3	5930·191	6	Fe I	75·85
5947·066	2	5934·665	5	Fe I	76·06

All the measurements were made on a modified Hilger photo-measuring micrometer. The plate is adjusted on the stage with the dispersion parallel to the run of the main measuring screw. A diaphragm in the eyepiece limits the height of spectrum visible and a single measuring wire, perpendicular to the dispersion, lies in the plane of the diaphragm. The stage carrying the plate can be moved by a second screw in a direction perpendicular to the dispersion, permitting measurement at various heights in the spectrum. From a series of fine scratches parallel to the dispersion, previously made at both ends of the spectrum at intervals of exactly 1 mm, the position on the solar image at which measurement is made can be determined.

Velocities corresponding to the measured line positions in a spectrum are accurately found, independently of asymmetry in the apparatus function of the spectroscope, by reference to a standard spectrum. Measurement of the centre spectrum (Table I) was made in the forward and reverse directions at 19 heights 1 mm apart, using a diaphragm height of 0·32 mm. The standard spectrum was then taken as the mean of the 38 readings for each of the 12 lines. It gives a velocity (calculated from the Hartmann dispersion formula) of $+0{\cdot}17(5)$ km sec^{-1} and corresponds to a point situated 0·05 mm to the East of the centre of the disk. Averaging measurements from different heights in the spectrum largely eliminates the effects of irregular silver grain distribution, as the low value, $\pm 0{\cdot}03(3)$ km sec^{-1}, for the root mean square error of this velocity shows.

2.2. *Preliminary measurements.*—Spatial resolution on the solar surface decreases but the consistency of measurement increases with the height of spectrum over which measurement is made. With a solar image 180 mm in diameter, a diaphragm height 0·75 mm and coarse-grain plates, an average value $\pm 0{\cdot}25$ km sec^{-1} for the root mean square error of a single solar line was obtained in the previous investigation ((**11**)—Paper IV).

In order to find the best spectrum height in the present conditions, diameter of the solar image 85 mm and fine-grain plates, a short series of preliminary measurements was made. Each spectrum on the selected pair of plates (Table I) and eight spectra on a similar pair of plates from the West limb were measured at 15 points, with a diaphragm height 0·32 mm (chosen to give about the same

spatial resolution as the earlier measurements). For 60 of these velocities the value of the root mean square error of a single solar line (Paper IV, Section 4.1) was calculated, the average value being $\pm 0{\cdot}14(0)\,\mathrm{km\,sec^{-1}}$. Remembering that the diaphragm height in the present case is less than one-half that used in the earlier measurements, it is clear that a factor of at least two in the accuracy has been obtained by the use of the finer-grain plates.

Attention in the final results is centred on the error attributed to the velocity at some point on the solar surface. As the velocity at any point is the mean from six lines and four independent exposures (Table I), the final errors should be smaller than the error of a single line-velocity by a factor of nearly $\sqrt{24}$. A diaphragm height of approximately 0·1 mm was therefore decided upon for the final measurements.

2.3. *Measurements of limb spectra.*—Definitive measurements were made of the eight spectra on the two East limb plates listed in Table I. Over the one or two millimetres of spectrum height nearest the limb, darkening towards the limb caused a noticeable decrease in density. As the consistency of measurement depends to some extent on the apparent contrast between the line and its adjacent continuum, the first point of measurement was taken a distance 1·34 mm in from the limb. (The limb appeared quite sharp on the spectrum owing to moderate seeing conditions and the use of contrasty plates; its position was estimated under low magnification with a cross-wire.) Each spectrum was measured direct and reversed at 140 points over a height of 0·13 mm at intervals of 0·10 mm, giving in all 1120 velocity measurements.

For any position on the solar image, let Δ_i be the difference between corresponding water-vapour line (wave-length λ_i) readings in the limb and the standard spectrum and let Δ_r, λ_r be the quantities for the solar lines. Then the dispersion of the limb spectrum is converted to that of the standard by the $\lambda_i - \Delta_i$ curve; in practice a straight line is taken through the centre of gravity of the six points λ_i, Δ_i. The difference, δ_r, between Δ_r and the value of the adopted $\lambda_i - \Delta_i$ curve at wave-length λ_r is the displacement of the limb line relative to the same line in the standard. The factor converting linear displacement to line-of-sight velocity can be calculated from the Hartmann dispersion and Doppler formulae; values corresponding to the dispersion of the standard are listed for the six solar lines in the last column of Table II. Multiplication of δ_r by the appropriate factor from this table gives line-velocities, u_r, relative to the standard spectrum. The spectrum-velocity, U, at the solar position considered, is the mean of the six line-velocities u_r.

The variation of line-of-sight velocity with position on the solar image is shown in Figs. 1 and 2. The four spectra E_{11}, E_{12}, E_{13}, E_{14} in Fig. 1 are those obtained at the beginning, E_{21}, E_{22}, E_{23}, E_{24} in Fig. 2, those obtained at the end of the interval of one hour (see Columns 1 and 2 in Table I). Let U_n be the velocity of the nth point of measurement occurring a distance h_n on the plate from the limb. n runs from 1 to 140 as the velocities were measured at 140 points on each spectrum. Abscissae are then the distances h_n along the E–W chord of the solar image defined by the spectroscope slit. For the purpose of presentation the velocity data have been smoothed in order to reduce the effects of random errors of measurement. Values of $\frac{1}{3}(U_{n-1} + U_n + U_{n+1})$ are therefore plotted in the figures as ordinates; the velocities are referred to an arbitrary origin, common to all the spectra.

2.4. *Accuracy of measurement.*—Errors due to measurement were investigated for a sample of 112 from the 1120 measured velocities. The calculations were made at corresponding heights in each spectrum, for 14 positions distributed at regular intervals over the spectrum height. In this way, any systematic variation of consistency with photographic density is taken into account (see Section 2.3). It is clear that the accuracy of measurement depends on the deviations of both atmospheric and solar lines forming the velocity. The discussion in the present section is outlined in Paper IV, Section 4.1, where the basic formulae are derived.

If s_s is the root mean square error of measurement of a single solar line-velocity u_r,

$$s_s^2 = \frac{1}{n-1}\sum_1^n (U-u_r)^2, \tag{1}$$

where $n=6$, since the spectrum-velocity is the mean of six line-velocities Let $\bar{s}_s$ be the average of the 112 values of s_s. The line-velocities are regarded as a random sample from a hypothetical infinite population of all possible measures. An estimate, σ_s, of the root mean square error of a single line-velocity in this population is

$$\sigma_s = [(n-1)/2]^{1/2}\Gamma\{(n-1)/2\}[\Gamma(n/2)]^{-1}\,.\,\bar{s}_s, \tag{2}$$

the standard error of this estimate being approximately $\sigma_s/[2(n-1)]^{1/2}$.

The deviations of the six water-vapour lines, at wave-lengths λ_i, from the $\lambda_i - \Delta_i$ curve (Section 2.3) contribute to the error of measurement in a way analogous to the solar line deviations. A "velocity-factor" can be attributed to the wave-lengths λ_i converting linear deviations to velocity deviations, v_i say, comparable with the solar $U-u_r$. The root mean square error of measurement of a single atmospheric line is then

$$s_a^2 = \frac{1}{n-1}\sum_1^n v_i^2, \qquad n=6, \tag{3}$$

the mean of the v_i-values being zero. $\bar{s}_a$, σ_a and $\sigma_a/[2(n-1)]^{1/2}$ can be calculated as in the solar case.

Fig. 3 (i) and (ii) shows the distribution of the 112 values of s for the solar and atmospheric lines, together with the predicted theoretical distribution (Paper IV, equation (15)). Comparison of the two sets of values of $\bar{s}$, σ and $\sigma/[2(n-1)]^{1/2}$ is made in Table III, columns 2, 3 and 4. Column 7 gives the displacement in microns on the plate to which the value of σ corresponds.

While dispersion of the solar lines about their mean appears as a random error of measurement, dispersion of the water-vapour lines about the $\lambda_i - \Delta_i$ curve introduces a common error into the individual line-velocities and their resultant spectrum-velocity. This systematic error, attributed to the centre of gravity of the six points λ_i, Δ_i, is the root mean square deviation, $\sigma_a/\sqrt{6}$, in Δ_i. Hence the root mean square error of measurement of a single line-velocity is

$$\pm\{\sigma_s^2+\sigma_a^2/6\}^{1/2} \quad \pm\{\sigma_s^2/[2(n-1)]+\sigma_a^2/[6\times 2(n-1)]\}^{1/2},$$

and the root mean square error of measurement of a spectrum-velocity is

$$\pm\{\sigma_s^2/6+\sigma_a^2/6\}^{1/2} \quad \pm\{\sigma_s^2/[6\times 2(n-1)]+\sigma_a^2/[6\times 2(n-1)]\}^{1/2}.$$

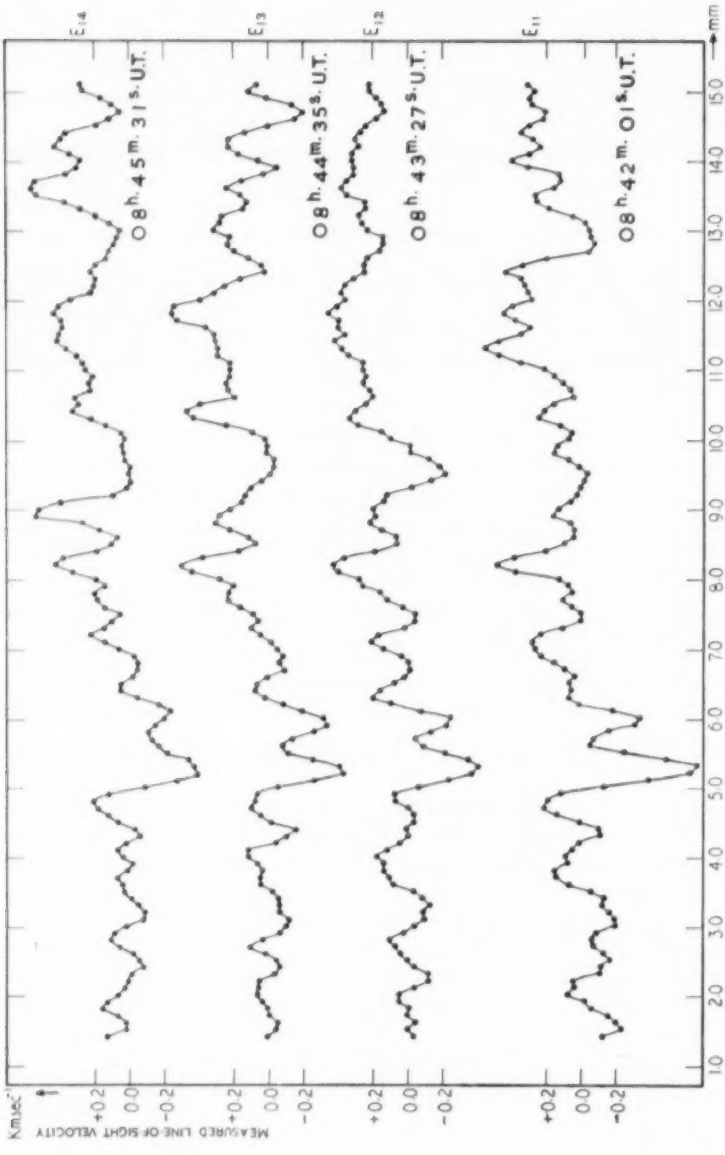

FIG. 1.—*Variation in line-of-sight velocity with position on the solar image; East equatorial limb; mean epoch* 1953 *May* $5^{d}08^{h}44^{m}$ *U.T.*
Abscissae: Distances from the limb along an E–W chord of the solar image.
Ordinates: Line-of-sight velocities referred to an arbitrary origin of velocity common to Figs. 1 *and* 2.

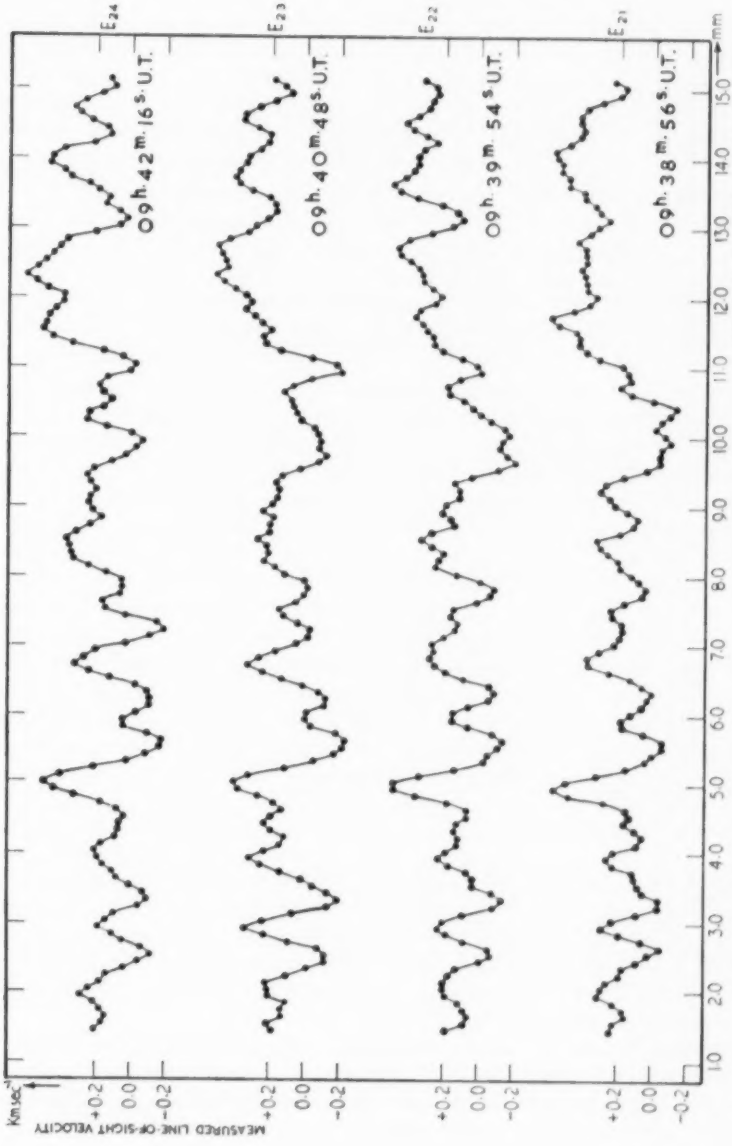

FIG. 2.—*Variation in line-of-sight velocity with position on the solar image; East equatorial limb; mean epoch* 1953 *May* $5^{d}\,09^{h}\,41^{m}$ *U.T.*
Abscissae: Distances from the limb along an E–W chord of the solar image.
Ordinates: Line-of-sight velocities referred to an arbitrary origin of velocity common to Figs. 1 *and* 2.

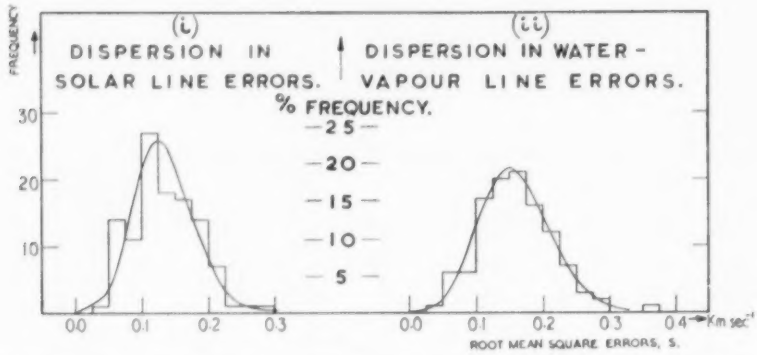

FIG. 3.—*Frequency histograms of the distribution of the root mean square errors of solar and water-vapour lines in a sample of 112 velocities.*
Abscissae: Root mean square error of measurement of a single line.
Ordinates: Actual and percentage frequencies of occurrence of a given error.
Observed distribution, irregular curve; theoretical distribution, smooth curve.

Values of $\sigma_{6a}=\sigma_a/\sqrt{6}$ and the corresponding root mean square error of the solar spectrum-velocity are listed in column 5 of Table III; standard errors, $\sigma_6/[2(n-1)]^{1/2}$, of the values σ_6, are given in column 6. Extracting the relevant values from Table III gives as the error of a single line-velocity

$$\pm 0{\cdot}15(7) \pm 0{\cdot}05(0)\,\mathrm{km\,sec^{-1}}$$

and for a spectrum-velocity

$$\pm 0{\cdot}09(0) \pm 0{\cdot}02(8)\,\mathrm{km\,sec^{-1}}.$$

TABLE III

	$\bar{s}$ km sec^{-1}	σ km sec^{-1}	$\sigma/\sqrt{2(n-1)}$ km sec^{-1}	$\sigma_6=\sigma/\sqrt{6}$ km sec^{-1}	$\sigma_6/\sqrt{2(n-1)}$ km sec^{-1}	$\sigma(\mu)$ microns
Solar	$\pm 0{\cdot}13(4)$	$\pm 0{\cdot}14(1)$	$\pm 0{\cdot}04(5)$	$\pm 0{\cdot}05(8)$	$\pm 0{\cdot}01(8)$	1·9
Water-vapour	$\pm 0{\cdot}16(0)$	$\pm 0{\cdot}16(8)$	$\pm 0{\cdot}05(3)$	$\pm 0{\cdot}06(9)$	$\pm 0{\cdot}02(2)$	2·2

Comparing the value $\bar{s}_a = \pm 0{\cdot}13(4)\,\mathrm{km\,sec^{-1}}$ with the value $\pm 0{\cdot}14(0)\,\mathrm{km\,sec^{-1}}$ obtained in the preliminary measurements, it is reassuring to find that reduction in the height of spectrum measured has not greatly changed the accuracy of measurement. The apparent gain in accuracy is illusory, the preliminary measurements having been made near the limb, where, as explained in Section 2.3, measurement error is highest.

Calculations of errors of measurement made in Paper IV only took account of the dispersion of the solar lines about their mean, so the values given there should be somewhat increased. Rather similar considerations apply to the error quoted in Section 2.1 for the measurement of the standard spectrum. Here, however, dispersion of the water-vapour lines contributes to the error in a more complicated manner; the value already derived can be regarded as a lower limit to the actual error.

3. *Solar velocities*

3.1. *Reduction to velocities on the Sun.*—The method of converting positions on the solar disk to positions on the Sun and measured velocities to line-of-sight velocities on the Sun is fully explained in Paper I (**19**).

For the standard centre spectrum the calculated velocity due to Earth's motion and solar rotation can be compared with the observed velocity found from the Hartmann formula (Section 2.1). A difference 0·07(1) km sec^{-1} exists. As common vertical motions of the photospheric matter amounting to as much as 0·15 km sec^{-1} may take place over several degrees of longitude (**20**), the observed velocity was adopted as the standard velocity V_2 to which all the limb velocities are referred. Possible error in the wave-lengths of the solar lines relative to the atmospheric ones (**1, 20**) and asymmetrical distortion of the line profiles by the horizontal apparatus function of the spectroscope (**5, 20**) may falsify this velocity, but in this case the amount is at least determinable.

Heliographic latitudes, B, and longitudes, L, were computed for positions on the limb plates at which measurement had been made. Corrections, V_1, were made to the measured velocities, V, for the effect of the observer's motion at the moment of observation, giving 1120 values of $V+V_1+V_2$, the velocity on the Sun.

3.2. *The velocity field.*—The four spectra on either plate (Table I) were measured at exactly the same 140 disk positions (see Figs. 1 and 2). Furthermore, the interval of $3\frac{1}{2}$ minutes between the first and fourth exposure is so short that the four sets of measurements refer to the same positions on the solar surface. At each of the 140 positions a mean velocity was, therefore, calculated. From the dispersion of the four measures at any given point, a value can be found for the root mean square deviation of a single velocity, which can be compared with the root mean square error of measurement given in Section 2.4. The deviations were calculated for the same 14 spectrum positions for which the measurement error had been calculated. The average of the 28 values for the two plates was $\pm$0·09(3) km sec^{-1}. This value falls within the estimated uncertainty, $\pm$0·02(8) km sec^{-1}, of the measurement error $\pm$0·09(0) km sec^{-1} for a single velocity. Hence it may be assumed that no significant changes in velocity occurred during $3\frac{1}{2}$ minutes, and taking mean velocities for each plate is justified. The values so found should represent, more accurately than those from individual spectra, the velocities actually occurring on the solar surface.

Interest in the present work centres mainly on the variation in velocity from point to point, so that it is convenient to remove from the velocities the limb effect and the component due to solar rotation. Accordingly, the residuals δV of the plate means $\overline{V+V_1+V_2}$ were calculated for the 280 solar positions from the equation

$$\delta V = \overline{V+V_1+V_2} - U\cos\gamma_1 - \Delta \qquad (4)$$

(Paper IV, equation (1)). U, Δ are the velocity of solar rotation and the limb effect at the point considered, γ_1 is the angle between the parallel of latitude at the point and the line-of-sight. Unfortunately, the variation of limb effect with position on the solar disk is poorly determined, interferometric measurements (**1**) disagreeing with values found from velocity measurements (**11**). However, in the present case no measurements were made very near the limb and the values found previously by the writer were used (Paper IV); at most the

correction amounted to 0·16(0) km sec^{-1}. Since the zone of latitude covered by the observations fell within the range $|B| \leqslant 4°{\cdot}0$, the linear rotational velocity U was taken as $U_0 \cos B$. For U_0, the equatorial velocity, 1·91 km sec^{-1} was adopted (Paper IV). Table IV(i) contains the 140 velocity residuals so calculated from the mean of spectra E_{11}, E_{12}, E_{13}, E_{14} (Table I) together with the heliographic latitudes and longitudes of the positions on the Sun where velocities were measured (Section 3.1). Similar information from spectra E_{21}, E_{22}, E_{23}, E_{24} is given in Table IV(ii). Columns headed E_1, E_2 contain the values of δV for E_{11}, ..., E_{14} and E_{21}, ..., E_{24} respectively. It should be emphasized that these values of the velocity residuals have not been smoothed.

The mean velocity residuals, $\bar{E}_1 = -0{\cdot}00(8)$ km sec^{-1} and $\bar{E}_2 = +0{\cdot}01(2)$ km sec^{-1}, were calculated for each plate. The small difference 0·02 km sec^{-1} between them is very satisfactory in showing that no spurious velocity difference exists between measurements on the two plates. That the mean of $\bar{E}_1 + \bar{E}_2$ is so closely zero is to some extent fortuitous, since it depends on the velocities adopted for U_0 and V_2 (cf. Section 3.1). From the point of view of having separated the velocity fluctuations from the systematic velocity, the position is entirely satisfactory.

The variation of residual velocity with heliographic longitude (tabulated in Table IV(i) and (ii)) is plotted in the lower half of Fig. 4. A given difference in longitude covers a varying length of arc on the surface, depending on the latitudes of the points on the arc. The linear distance between two points of observation can be calculated from the B and L entries in Table IV. (The observations being in the equatorial region, the linear distance corresponding to $1° L$ varies only very slightly; on the average $1° L \simeq 1{\cdot}232 \times 10^4$ km.) Precise linear intervals corresponding to the angular longitude ones are shown in Fig. 4.

Between the mean time of observation of the velocities E_1 and E_2 a period of nearly an hour elapsed. Inspection of Fig. 4 shows that many features of the velocity field have persisted for this time. For example, the features between $L = 236°$ and 240° are obvious in both E_1 and E_2 and the much smaller feature centred at 248°·8 is quite recognizable in both sequences. As entries in Table IV(i) and (ii) show that, at a common longitude, observations E_1 and E_2 were made at latitudes differing by not more than 0°·2, a mean velocity curve was constructed. At any longitude L where a velocity, E_1 say, had been measured, the value of E_2 was found by linear interpolation between two measured velocities; the mean, E, of these gave a point L, E on the mean curve. A similar procedure gave velocities at longitudes of observation of E_2. Successive points on the mean curve were joined by straight lines; this is the curve E shown in the upper part of Fig. 4. It can be regarded as the quasi-steady velocity field for the period of observation.

4. *The solar velocity field*

4.1. *Analysis of the velocity field.*—The root mean square deviation of a single velocity, as calculated directly from the residual velocities given in Table IV, is $\pm 0{\cdot}16(1)$ km sec^{-1}. Since each velocity E_1 or E_2 in the table is the mean of four values, the root mean square error of measurement to be attributed to a single velocity E_1 or E_2 is $\pm 0{\cdot}09(0) \pm 0{\cdot}02(8)/\sqrt{4}$ km sec^{-1} (Sections 2.4 and 3.2), i.e. a value $\pm 0{\cdot}04(5) \pm 0{\cdot}01(4)$ km sec^{-1}. The dispersion of the

TABLE VI (i)

L	B	E_1 km sec^{-1}	L	B	E_1 km sec^{-1}	L	B	E_1 km sec^{-1}
°	°		°	°		°	°	
222·9	−4·0	+0·10	239·1	−2·4	−0·37	249·4	−0·5	+0·01
223·5	4·0	− ·02	239·3	2·4	− ·17	249·6	0·4	− ·01
224·0	4·0	− ·06	239·6	2·4	·00	249·8	0·4	+ ·06
224·5	4·0	− ·05	239·8	2·3	+ ·02	250·0	0·3	− ·01
225·0	3·9	·00	240·1	2·3	+ ·10	250·1	0·3	+ ·06
225·5	3·9	+ ·07	240·3	2·2	+ ·07	250·3	0·2	+ ·17
226·0	3·9	+ ·09	240·6	2·2	− ·05	250·5	0·2	+ ·20
226·4	3·8	+ ·08	240·8	2·2	− ·08	250·7	0·2	+ ·19
226·9	3·8	+ ·11	241·0	2·1	− ·04	250·9	0·1	+ ·16
227·3	3·8	− ·03	241·3	2·1	+ ·03	251·1	−0·1	+ ·04
227·7	3·8	+ ·01	241·5	2·0	·00	251·3	0·0	+ ·20
228·1	3·7	− ·07	241·8	2·0	+ ·15	251·4	0·0	+ ·34
228·5	3·7	− ·06	242·0	2·0	+ ·17	251·6	+0·1	+ ·19
228·9	3·7	+ ·03	242·2	1·9	+ ·01	251·8	0·1	+ ·08
229·3	3·6	+ ·07	242·4	1·9	− ·09	252·0	0·1	+ ·04
229·7	3·6	+ ·14	242·7	1·8	− ·02	252·2	0·2	+ ·07
230·0	3·6	+ ·05	242·9	1·8	− ·02	252·4	0·2	·00
230·4	3·6	− ·09	243·1	1·8	+ ·10	252·5	0·3	− ·06
230·7	3·5	− ·07	243·3	1·7	+ ·17	252·7	0·3	·00
231·1	3·5	− ·06	243·5	1·7	− ·02	252·9	0·4	− ·10
231·4	3·5	− ·02	243·8	1·6	+ ·12	253·1	0·4	− ·19
231·7	3·4	− ·04	244·0	1·6	+ ·30	253·3	0·5	− ·19
232·1	3·4	− ·02	244·2	1·6	+ ·47	253·4	0·5	− ·14
232·4	3·3	+ ·13	244·4	1·5	+ ·33	253·6	0·6	− ·21
232·7	3·3	+ ·23	244·6	1·5	+ ·04	253·8	0·6	− ·07
233·0	3·3	+ ·08	244·9	1·4	− ·11	254·0	0·6	− ·10
233·2	3·2	+ ·10	245·1	1·4	·00	254·1	0·7	− ·10
233·5	3·2	+ ·17	245·3	1·3	+ ·01	254·3	0·7	− ·04
233·8	3·2	+ ·20	245·5	1·3	+ ·10	254·5	0·8	·00
234·1	3·1	+ ·05	245·7	1·3	+ ·19	254·7	0·8	+ ·12
234·4	3·1	− ·06	245·9	1·2	+ ·22	254·8	0·9	− ·02
234·7	3·0	− ·04	246·1	1·2	+ ·03	255·0	0·9	− ·15
235·0	3·0	+ ·06	246·3	1·1	− ·07	255·2	1·0	− ·07
235·3	3·0	+ ·16	246·6	1·1	− ·09	255·3	1·0	− ·07
235·6	2·9	+ ·12	246·8	1·0	− ·18	255·5	1·1	− ·02
235·9	2·9	+ ·21	247·0	1·0	− ·24	255·7	1·1	− ·03
236·2	2·9	+ ·21	247·2	1·0	− ·21	255·9	1·2	− ·06
236·5	2·8	− ·03	247·4	0·9	− ·13	256·0	1·2	+ ·01
236·7	2·8	− ·34	247·6	0·9	− ·15	256·2	1·2	− ·10
237·0	2·8	− ·42	247·8	0·8	− ·05	256·4	1·3	− ·35
237·2	2·7	− ·52	248·0	0·8	− ·15	256·5	1·3	− ·29
237·5	2·7	− ·39	248·2	0·7	− ·13	256·7	1·4	− ·25
237·8	2·6	− ·11	248·4	0·7	+ ·04	256·9	1·4	− ·20
238·0	2·6	− ·07	248·6	0·6	+ ·17	257·0	1·5	− ·12
238·3	2·6	− ·10	248·8	0·6	+ ·21	257·2	1·5	− ·09
238·6	2·5	− ·11	249·0	0·6	+ ·08	257·4	+1·6	− ·20
238·8	−2·5	− ·29	249·2	−0·5	− ·01			

TABLE IV (ii)

L	B	E_2 km sec^{-1}	L	B	E_2 km sec^{-1}	L	B	E_2 km sec^{-1}
222°·5	−4°·0	+0·19	238°·6	−2°·4	−0·06	248°·8	−0°·5	+0·05
223·0	4·0	+ ·17	238·8	2·4	− ·07	249·0	0·4	− ·18
223·5	4·0	+ ·11	239·1	2·4	− ·13	249·2	0·4	− ·35
224·0	3·9	+ ·11	239·3	2·3	− ·19	249·4	0·3	− ·27
224·5	3·9	+ ·03	239·5	2·3	− ·10	249·6	0·3	− ·14
225·0	3·9	+ ·19	239·8	2·2	+ ·05	249·8	0·2	− ·04
225·4	3·9	+ ·18	240·1	2·2	+ ·17	250·0	0·2	+ ·08
225·9	3·8	+ ·26	240·3	2·2	+ ·21	250·1	0·1	+ ·10
226·3	3·8	+ ·17	240·5	2·1	+ ·31	250·3	0·1	+ ·06
226·7	3·8	+ ·12	240·8	2·1	+ ·10	250·5	−0·1	+ ·12
227·1	3·8	+ ·08	241·0	2·0	·00	250·7	0·0	+ ·20
227·5	3·7	− ·03	241·3	2·0	+ ·03	250·9	0·0	+ ·14
227·9	3·7	− ·18	241·5	2·0	− ·15	251·1	+0·1	− ·01
228·3	3·7	− ·07	241·7	1·9	− ·14	251·3	0·1	+ ·01
228·7	3·6	− ·01	241·9	1·9	+ ·08	251·5	0·2	+ ·09
229·1	3·6	+ ·24	242·2	1·8	+ ·11	251·7	0·2	+ ·16
229·5	3·6	+ ·25	242·4	1·8	− ·06	251·8	0·3	+ ·15
229·8	3·5	+ ·26	242·6	1·7	− ·13	252·0	0·3	+ ·17
230·2	3·5	+ ·07	242·8	1·7	− ·14	252·2	0·3	+ ·09
230·5	3·5	− ·10	243·1	1·7	− ·13	252·4	0·4	+ ·11
230·9	3·4	− ·23	243·3	1·6	− ·03	252·6	0·4	+ ·18
231·2	3·4	− ·05	243·5	1·6	+ ·12	252·7	0·5	+ ·09
231·5	3·4	+ ·06	243·7	1·5	+ ·14	252·9	0·5	+ ·02
231·8	3·3	+ ·01	243·9	1·5	+ ·05	253·1	0·6	− ·19
232·1	3·3	+ ·09	244·1	1·5	+ ·13	253·3	0·6	− ·18
232·4	3·3	+ ·21	244·3	1·4	+ ·22	253·4	0·7	− ·17
232·8	3·2	+ ·31	244·6	1·4	+ ·15	253·6	0·7	− ·15
233·1	3·2	+ ·22	244·8	1·3	− ·12	253·8	0·8	− ·05
233·4	3·2	+ ·10	245·0	1·3	− ·01	254·0	0·8	·00
233·7	3·1	+ ·06	245·2	1·2	+ ·09	254·1	0·8	+ ·04
234·0	3·1	+ ·13	245·4	1·2	+ ·03	254·3	0·9	+ ·13
234·2	3·0	+ ·19	245·6	1·1	·00	254·5	0·9	+ ·04
234·5	3·0	+ ·09	245·8	1·1	+ ·02	254·6	1·0	+ ·03
234·8	3·0	+ ·02	246·0	1·1	·00	254·8	1·0	+ ·12
235·1	2·9	+ ·18	246·2	1·0	+ ·04	255·0	1·1	+ ·03
235·4	2·9	+ ·38	246·4	1·0	− ·17	255·1	1·1	− ·09
235·7	2·9	+ ·47	246·6	0·9	− ·33	255·3	1·2	− ·17
236·0	2·8	+ ·51	246·8	0·9	− ·26	255·5	1·2	− ·06
236·2	2·8	+ ·36	247·0	0·8	− ·24	255·6	1·3	·00
236·5	2·7	+ ·08	247·3	0·8	− ·33	255·8	1·3	− ·01
236·8	2·7	− ·07	247·5	0·8	− ·36	256·0	1·3	− ·07
237·0	2·7	− ·12	247·7	0·7	− ·18	256·1	1·4	− ·13
237·3	2·6	− ·15	247·9	0·7	− ·16	256·3	1·4	− ·23
237·6	2·6	− ·28	248·1	0·6	− ·21	256·5	1·5	− ·31
237·8	2·5	− ·16	248·3	0·6	− ·16	256·6	1·5	− ·19
238·1	2·5	+ ·06	248·5	0·5	− ·21	256·8	+1·6	− ·07
238·3	−2·5	+ ·12	248·6	−0·5	− ·12			

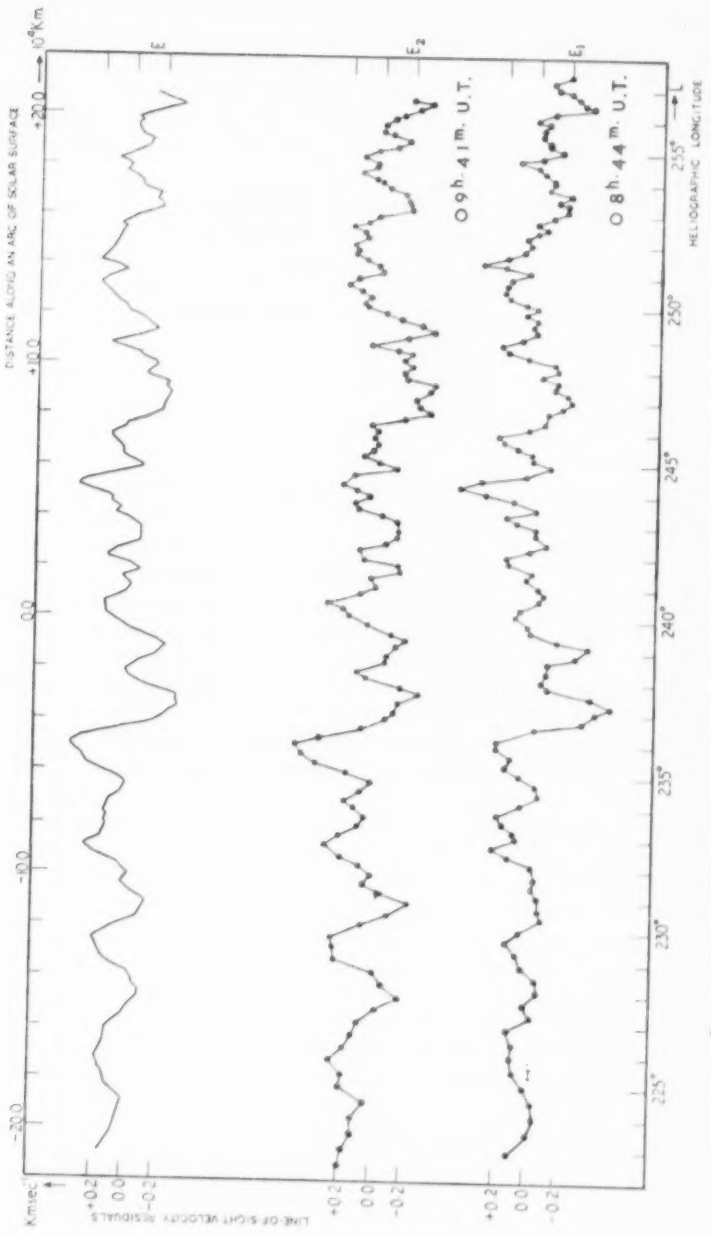

FIG. 4.—*Line-of-sight components of the velocity field for* 1953 *May* $5^d\ 08^h\ 44^m$ *to* $09^h\ 41^m$ *U.T.*
Abscissae: Heliographic longitude; linear distance on the solar surface.
Ordinates: Residual velocities.
E_1, E_2 are each the mean of 4 independent sets of velocity measurements. E_3, the mean of E_1 and E_2, is the quasi-steady velocity field for the period of observation.

velocities from point to point thus exceeds the error of measurement by some eight times its estimated uncertainty. Any suggestion that the velocity dispersion is a spurious effect due to errors of measurement can, therefore, be totally rejected; the variations in velocity shown in Fig. 4 essentially represent the motion occurring in the Sun. Moreover, the observational procedure has so reduced the absolute value of the uncertainty of a single velocity ($\pm 0{\cdot}04(5)$ km sec^{-1}), that the curves E_1 and E_2 actually depict the motion with a considerable degree of precision.

The linear scale of the velocity fluctuations is now required. This was found from a correlogram analysis of the mean curve E (Section 3.2, Fig. 4) since it may be taken as the steady field occurring during the period of observation. Values of E to 0·01 km sec^{-1} were tabulated at each 0°·1 interval of longitude over the 34° of longitude covered by the curve. Serial correlation coefficients r_k, defined by

$$r_k = \frac{\sum_{j=1}^{n-k} E_j E_{j+k}}{\left(\sum_{j=1}^{n-k} E_j^2\right)^{1/2} \left(\sum_{j=1}^{n-k} E_{j+k}^2\right)^{1/2}} \qquad (4)$$

(**13**), were calculated for $k = 1, 2, 3, \ldots, 30, 32, 34, 36$, where k is the order of the correlation coefficient and $n = 340$ is the total number of tabulated values. (This simple expression for the coefficient can be used when the mean residual, $\bar{E}$, is approximately zero, cf. Section 3.2.) Values of r_k are plotted in Fig. 5 against the longitude interval $k/10°$, corresponding to the order of correlation k. The correlogram is formed by joining successive points; $r_0 = 1$ by definition. Apart from this trivial initial maximum, the correlation coefficients have a maximum at a longitude interval 2°·1. This then gives, using the mean conversion factor

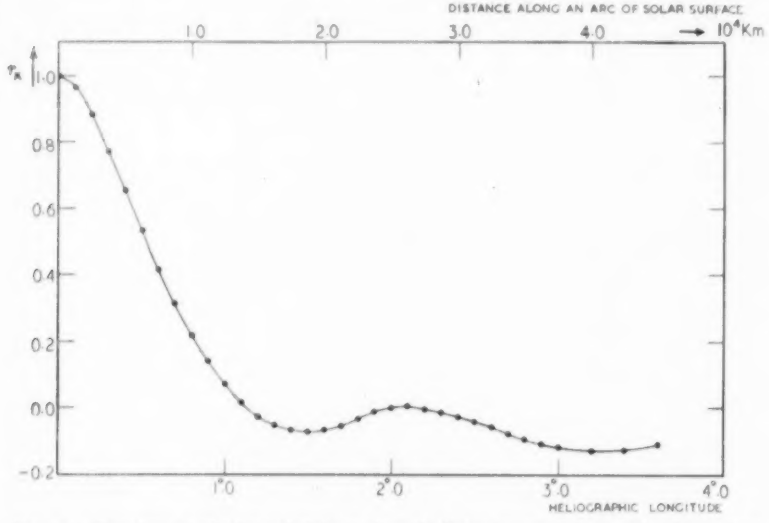

FIG. 5.—*Correlogram of solar velocities to show the linear extent of the velocity fluctuations.*
Abscissae: Longitude intervals; linear distance intervals.
Ordinates: Values of the correlation for the displacement interval of the corresponding abscissa.

$1^\circ L = 1{\cdot}232 \times 10^4$ km (Section 3.2), a distance $2{\cdot}6 \times 10^4$ km as the average linear extent of a velocity fluctuation. No great significance attaches to the value, however, as the curve E shows clearly that the field is extremely irregular. The broadness of the maximum displayed by the correlogram and the very small value, $+0{\cdot}001$, of the correlation coefficient at maximum reflect this absence of a single well-defined size of the motion element.

Questions concerning the duration of the field remain to be discussed. The general similarity of curves E_1 and E_2 in Fig. 4 is quite marked; one wishes to know whether it is a chance resemblance or whether it denotes the persistence of the field over the hour's interval between the observations. The correlation coefficient (**27a**) between the two curves E_1 and E_2 (as calculated from the 208 pairs of points from which the mean curve E is constructed; cf. Section 3.2) is $+0{\cdot}607$. Application of Fisher's z-ζ test (**27b**) shows that the probability of this correlation arising by chance from an uncorrelated population is less than 1 in 10^{22}. Clear evidence of the stability of the velocity field is thus provided.

Some comparison can now be made of the present results with those obtained in the previous investigation. The picture of an irregular field, with velocity fluctuations of amplitudes up to $\pm 0{\cdot}5$ km sec^{-1} extending some tens of thousands of kilometres, is very similar in the two cases. A precise comparison between the spatial distribution of the motion is difficult to make because of the great difference in spatial resolution; the average value $2{\cdot}6 \times 10^4$ km found here for the extent of a velocity fluctuation lies close to the original limit of resolution, 2×10^4 km. Owing to this and the irregular nature of the phenomenon, general similarity of the larger-scale motions is all that can be expected. The earlier value obtained for the dispersion in velocity was $\pm 0{\cdot}17$ km sec^{-1}. The close agreement of that value with the present one, $\pm 0{\cdot}16$ km sec^{-1}, is entirely satisfactory. Perhaps the most pleasing feature is, however, the conclusive demonstration of the stability of the velocity field from the present work. This result, foreshadowed in the earlier investigation, is of particular importance in that it is the only information at present available concerning the time scale of the motion.

Refinements in observational technique and the accumulation of a large number of accurate velocity measures have thus led to a much clearer conception of the dynamic state of the equatorial region of the Sun. This information may help in the identification of the physical processes causing the motion.

4.2. *Origin of the velocity field.*—A simple calculation shows that the energy of the velocity fluctuations is not negligible compared with the flux of radiant energy near the surface of the Sun. The energy density of black-body radiation is given by $4\sigma T^4/c$, where σ is Stefan's constant, T the absolute temperature and c the velocity of light; the kinetic energy per unit volume, on the other hand, is $\rho v^2/2$, where ρ is the density of the material and v its velocity. Taking $T = 5{\cdot}6 \times 10^3$ deg. K, $\rho = 1{\cdot}2 \times 10^{-7}$ g cm^{-3}, for $\tau = 0{\cdot}3$ at 5485 A (**21**), and $v = 0{\cdot}16$ km sec^{-1} (Section 4.1), values of 7·4 and 15·4 erg cm^{-3} are obtained for the radiation density and kinetic energy density, respectively. While the precise ratio of the two quantities is obviously somewhat uncertain, owing to the sensitivity of the radiation density to the assumed value of T, it is clear

that for any likely values of T and v the quantities are comparable in magnitude. It is interesting to see whether the magnetic energy density, $\mu H^2/8\pi$, makes any significant contribution. If the magnetic permeability μ is unity (**6**) and H, the magnetic field, is 1 gauss (**4**), the density is $0{\cdot}04\,\mathrm{erg\,cm^{-3}}$; a value $10\,\mathrm{erg\,cm^{-3}}$ would require a field of some 16 gauss. It would therefore appear that outside the zone associated with a sunspot (**4**), the energy resides mainly in the radiation and velocity fields.

The question arises of what mechanism is capable of producing such a large quantity of kinetic energy. The irregularity and large linear scale of the phenomenon (Section 4.1) rule out the obvious answer of convective instability. It appears more likely that the internal and gravitational energy of the gas are being converted into kinetic energy according to a suggestion made by Margules (**15**). Two contiguous columns of gas, of height h say, having a temperature difference ΔT between their bases are in unstable equilibrium and they tend to change to the stable configuration of the less dense gas on top, with the release of kinetic energy. If $\bar{c}$ is the average velocity developed, T the mean temperature of the two columns and g the acceleration due to gravity, it can be shown (**12**) that $\bar{c}^2 \simeq gh\Delta T/T$. For $\bar{c} = 0{\cdot}16\,\mathrm{km\,sec^{-1}}$, $g = 2{\cdot}74 \times 10^4\,\mathrm{cm\,sec^{-2}}$, $h = 300\,\mathrm{km}$ and $T = 5{\cdot}6 \times 10^3\,\mathrm{deg.\,K}$, $\Delta T \simeq 7\,\mathrm{deg.\,K}$; for $\bar{c} = 0{\cdot}5\,\mathrm{km\,sec^{-1}}$, $\Delta T \simeq 70\,\mathrm{deg.\,K}$. Thus the mechanism appears at least to be a possible one.

The problem of identifying the origin of temperature differences having the necessary linear extent remains. From an analysis of limb-darkening observations, it has been shown (**21**) that the observable region of the photosphere consists of two layers. Above optical depth $\tau = 1$ (at λ 5485 A) is a thermally stable layer of small temperature gradient in which the large-scale motions, considered in the present investigation, may take place; immediately below, granulation occurs in the form of convection cells in a narrow layer of steep temperature gradient (**20**). Beneath this again and as the ionization of hydrogen becomes important, Unsöld's hydrogen convection zone is encountered (**25, 26**). Variations in temperature will occur over the upper surface of this hydrogen convection zone owing to the differences in temperature between the ascending and descending material in the convection cells. These inequalities in temperature will be transmitted to the layers vertically above, though radiative transfer in a lateral direction will tend to reduce them somewhat. The linear extent of the observed motions may, therefore, give some indication of the size of the cells and hence of the thickness of the hydrogen convection zone.

Acknowledgments.—I wish to express my thanks to Professor H. H. Plaskett for suggesting the observational technique employed in the paper and to Dr M. G. Adam for help in making many of the observations. To both I am indebted for helpful discussions throughout the course of the work.

University Observatory,
Oxford:

1955 *October* 31.

References

(1) M. G. Adam, *M.N.*, **108**, 446, 1948; Comm. Univ. Obs., Oxford, No. 26.
(2) W. S. Adams, *Papers of the Mt. Wilson Observatory*, **1**, Part 1, 1911.
(3) H. D. Babcock, *Trans. I.A.U.*, **3**, 93, 1928.
(4) H. W. Babcock and H. D. Babcock, *Ap. J.*, **121**, 349, 1955.

(5) R. J. Bray, *M.N.*, **114**, 540, 1954 ; Comm. Univ. Obs., Oxford, No. 45.
(6) T. G. Cowling, *Solar Electrodynamics*, in *The Sun*, p. 532, ed. by G. P. Kuiper, Univ. of Chicago Press, Chicago, 1953.
(7) R. E. DeLury, *Ap. J.*, **44**, 177, 1916.
(8) R. E. DeLury, *Journ. Roy. Astr. Soc. Can.*, **33**, 345, 1939.
(9) J. Evershed and T. Royds, *M.N.*, **73**, 554, 1913.
(10) A. Fowler, *Trans. I.A.U.*, **4**, 60, 1932.
(11) A. B. Hart, *M.N.*, **114**, 17, 1954 ; Comm. Univ. Obs., Oxford, No. 43.
(12) B. Haurwitz, *Dynamical Meteorology*, pp. 247–251, McGraw-Hill Book Co. Inc., New York and London, 1941.
(13) M. G. Kendall, *The Advanced Theory of Statistics*, Vol. II, 3rd edn., pp. 402, 404, Griffin, London, 1951.
(14) T. D. Kinman, *M.N.*, **112**, 425, 1952 ; Comm. Univ. Obs., Oxford, No. 35.
(15) M. Margules, *Über die Energie der Stürme*, in *Jahrbuch der K. K. Central-Anstalt fur Meteorologie und Erdmagnetismus*, Vienna, 1903.
(16) H. H. Plaskett, *Ap. J.*, **43**, 145, 1916.
(17) H. H. Plaskett, *M.N.*, **99**, 219, 1939 ; Comm. Univ. Obs., Oxford, No. 14.
(18) H. H. Plaskett, *M.N.*, **112**, 177, 1952 ; Comm. Univ. Obs., Oxford, No. 33.
(19) H. H. Plaskett, *M.N.*, **112**, 414, 1952 ; Comm. Univ. Obs., Oxford, No. 34.
(20) H. H. Plaskett, *M.N.*, **114**, 251, 1954 ; Comm. Univ. Obs., Oxford, No. 44.
(21) H. H. Plaskett, *Physical Conditions in the Solar Photosphere*, in *Vistas in Astronomy*, Vol. I, p. 637, ed. by A. Beer, Pergamon Press, London and New York, 1955.
(22) J. S. Plaskett, *Ap. J.*, **42**, 373, 1915.
(23) C. E. St. John *et al.*, *Papers of the Mt. Wilson Observatory*, **3**, 1928.
(24) F. Schlesinger, *Publ. Allegheny Observatory*, **3**, 99, 1916.
(25) A. Unsöld, *Zs. für Astrophys.*, **1**, 138, 1930.
(26) E. Vitense, *Zs. für Astrophys.*, **32**, 135, 1953.
(27a) G. U. Yule and M. G. Kendall, *An Introduction to the Theory of Statistics*, 14th edn., p. 232, Griffin, London, 1950.
(27b) —— ibid. p. 497.

A STUDY OF THE OUTER SOLAR CORONA FROM A HIGH ALTITUDE AIRCRAFT AT THE ECLIPSE OF 1954 JUNE 30

II. Electron densities in the outer corona and zodiacal light regions

D. E. Blackwell

(Received 1955 December 29)

Summary

Data on the brightness and polarization of the solar corona given in a previous paper are analysed to separate the F and K components and to give the electron density in the outer corona and inner zodiacal light regions. The electron density is supposed to be a continuous function of distance from the Sun with a sharp cut-off at a variable position corresponding to a sudden decrease of ionization. Let p_θ^F be the polarization of the F component at elongation θ. The following results are demonstrated. (1) If no cut-off is assumed and $p_{35°}^F=0$, then $p_\theta^F<0$ for $\theta>35°$. But if $p_{35°}^F$ is sufficiently large and positive, $p_\theta^F>0$ for all θ. (2) If a cut-off is imposed just inside the orbit of the earth and $p_{35°}^F=0$, then $p_\theta^F>0$ for $\theta>35°$. The relation between the zodiacal light and the corona is discussed. It is shown that there is probably a sharp change of electron density gradient near a position $30R\odot$. from the Sun.

---

1. *Introduction.*—It is now well established (**1, 2, 3**) that the light of the solar corona is due to the scattering of sunlight by free electrons and by dust particles surrounding the Sun. The observed corona can therefore be considered as the superposition of two components, an electron (K) corona and a dust (F) corona. The brightness of the K component decreases with increasing elongation because both the electron density and the flux of sunlight on the electron cloud diminish with increasing distance from the Sun. The brightness of the F component also diminishes with increasing elongation; it is determined by the distribution of particles around the Sun, and by their average phase functions (which give the angular distribution of scattered light).

The chief problem of the solar physicist is to separate the two components and calculate the electron density as a function of distance from the Sun. The separation is most easily made for the outer parts of the corona by making use of the observed polarization, because the K component should be strongly polarized and the F component weakly polarized. In a previous paper (**4**) data are given for the brightness of the solar corona in the equatorial regions at sunspot minimum to an elongation, θ, of $13°{\cdot}5$ and for the polarization to an elongation of $5°$, all at a wavelength of 6400 A. In Fig. 4 these polarization data are shown combined with the data obtained from zodiacal light studies by Behr and Seidentopf (**5**) which begin at elongation $35°$. It is the purpose of this paper to analyse these data to give the electron density as a function of distance from the Sun.

The polarization curve falls with increasing distance from the Sun, passes through a minimum at an elongation of about $6°$ and then rises to high values again. Because of severe technical difficulties no values for the polarization are available for the region $5°<\theta<35°$, but if we are to satisfy both the corona and the zodiacal light measures the rise in polarization must be very steep. There

are good theoretical and observational (**6**) reasons for supposing that in the neighbourhood of the Sun ($\theta < 1°$) the polarization of the F component is very small in comparison with the polarization of the K component. The gradually diminishing polarization with increasing distance from the Sun in this region is due to the increasing predominance of the F corona over the K corona. It may be conjectured that the rise in observed polarization beyond $\theta = 6°$ is due to the onset of polarization in the F component. However, it is unlikely that the F component is appreciably polarized at such small elongations. For very small particles the polarization is given by Rayleigh theory of scattering, independently of the refractive index of the particle material, at elongation θ, as

$$p = \frac{1 - \cos^2\theta}{1 + \cos^2\theta}$$

For $\theta = 5°$ (the limit of the present observations), $p = +0{\cdot}46$ per cent. For very large transparent drops the polarization is readily calculated by combining the reflected ray with the refracted ray, taking account of their phase difference. This has been done by Bricard (**7**) for water drops with the result that for $\theta = 5°$ the polarization is $+0{\cdot}40$ per cent. Polarization values for intermediate sizes can be calculated by the Mie theory of scattering, but they vary very rapidly between wide limits as the drop size is altered * and it is very difficult to obtain a realistic average, but the effective value is unlikely to be as high as the Rayleigh limit. The two extreme values quoted may be assumed representative of the maximum likely polarization for all materials at this elongation but it cannot be stated definitely whether the polarization will be positive or negative. These values are much smaller than the observed values for the corona (2·7 per cent at an elongation of 5°). A more satisfactory explanation for the minimum at $\theta \sim 6°$ is therefore that the ratio of the K component to the F component has passed through a minimum and that as the elongation increases this ratio is increasing.

2. *Electron densities in the equatorial regions of the outer corona.*†—The procedure for the calculation of the electron density over the range of distance from the Sun where the polarization has been measured is simple in principle. At a particular distance from the Sun let the observed degree of polarization be p_0 and the degree of polarization of the electron corona only p_k. At the same distance the contribution to the total intensity of the electron component is K and of the dust component is F. Then, assuming that the polarization of the F component is negligible in comparison with the observed polarization we have

$$p_0/p_k = K/(K + F) \qquad (1)$$

Now we proceed by successive approximations. We first assume plausible values for p_k as a function of distance and so calculate K as a function of distance. This brightness distribution corresponds to a unique variation of polarization with distance which can be calculated by van de Hulst's approximate method (**3**). If the initial guess was correct the calculated and assumed polarization values will be identical. If they are not, the assumed values must be changed until there is agreement.

Having now decided upon the true polarization of the electron corona we can, in principle, pass to the electron density distribution by solving an integral

* See, for example, the values obtainable from the tables of Gumprecht *et al.* (**8**).

† The problem of the electron density in the polar regions is treated in a later section.

equation. If $N(r)$ is the electron density at distance r from the Sun and $HK(x)$ the intensity of the electron corona at a distance x in the projected image, where all distances are measured in terms of the solar radius as unit and H is the mean surface brightness of the Sun, then we have, following van de Hulst (**3**),

$$K(x)=D\int_x^\infty N(r)\left\{\left(2-\frac{x^2}{r^2}\right)A(r)+\frac{x^2}{r^2}B(r)\right\}\frac{r\,dr}{\sqrt{r^2-x^2}}. \qquad (2)$$

A and B are complicated functions of r, which, for all distances from the Sun beyond $6R_\odot$, approximate to $1/2r^2$ and zero respectively. At this stage, however, it is necessary to draw attention to a fundamental difficulty. The brightness and polarization of the electron corona at distance x on the projected image depend upon the electron density at distances far beyond $x=r$. Supposing the model developed later in this paper to be correct, we find that about one quarter of the

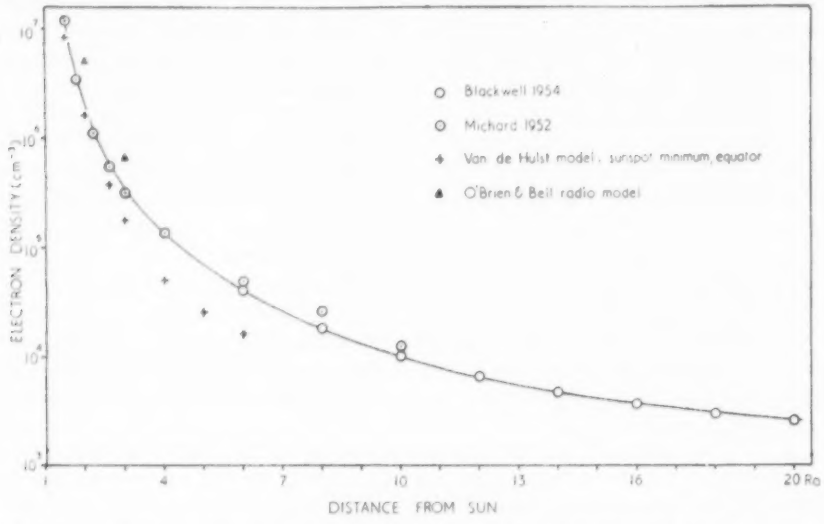

FIG. 1.—*Variation of electron density with distance from the Sun in the region of the ecliptic and solar equator.*

total brightness observed at a distance of $20R_\odot$ from the Sun in the image comes from parts of the corona which are more than $40R_\odot$ from the Sun. This limits the information obtainable about the corona at any specified distance from observations which extend only to this distance in the projected image. If no information is available beyond $x=r_0$ this difficulty can be met (but not surmounted) only by representing the electron density by an explicit function of distance and assuming that this function does represent the electron density well at distances of up to $r=3r_0$. Fortunately, the observations of the inner zodiacal light by Behr and Siedentopf (**5**) provide sufficient information about the electron density in these regions to allow the reduction of the outer corona observations to be carried through with reasonable accuracy. The interpretation of the zodiacal light observations will be considered in a later section and we here only assume that at the distance of $128R_\odot$* the electron density† is of the order of 10^3 electrons cm^{-3} and that the

* 1 A.U. $=213R_\odot$.

† This value is justified in Section 6.

electron density for the outer corona and the zodiacal light join in the way shown in Fig. 2.

This curve shows that there is a rapid change of gradient of electron density at about $25R_\odot$, and if this is neglected erroneous results will be obtained in interpreting the polarization measurements in the outer corona. Using the extra data provided by the zodiacal light observations the calculations have been

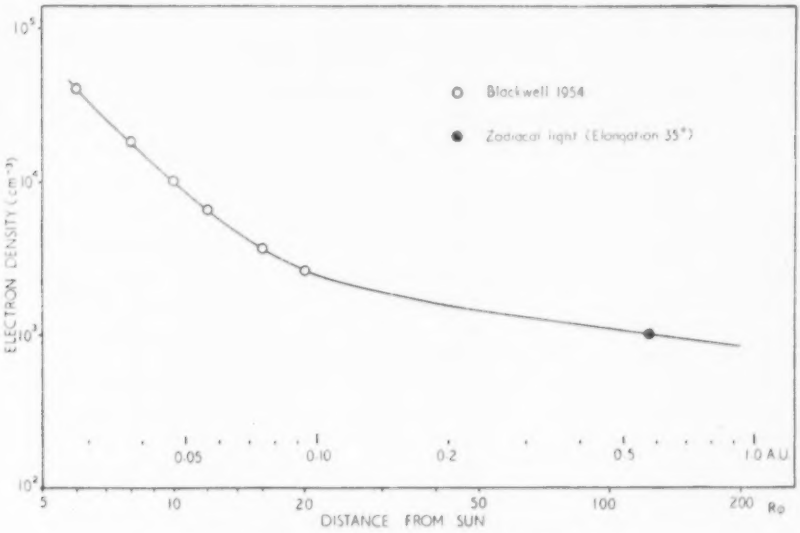

FIG. 2.—*Electron densities in corona and zodiacal light.*

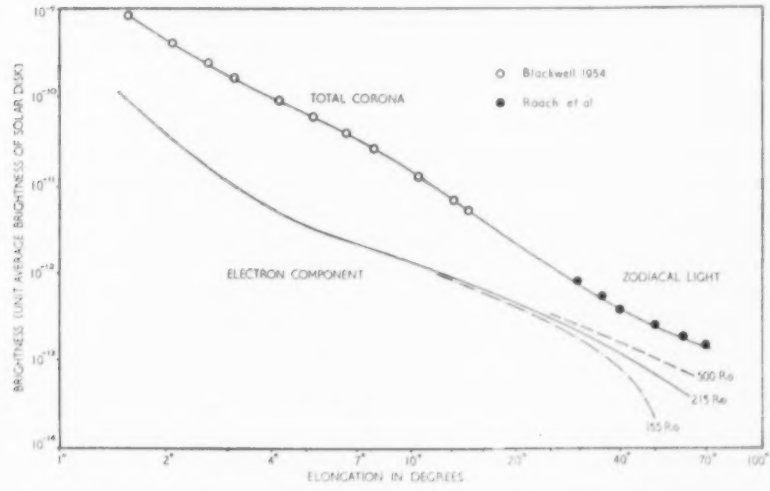

FIG. 3.—*The observed brightness of the solar corona and zodiacal light, and the computed intensity of the K component for three positions of cut-off of electron density at* $500R_\odot$, $215R_\odot$ *and* $165R_\odot$. *The coronal observations are those of Blackwell* (**4**) *and the zodiacal light observations are those of Roach* et al. (**9**).

completed by van de Hulst's approximate method with the results shown in part of Fig. 1. Results of calculation for the range of observation are given in Table 1. This table separates the observed corona into its components K and F and also gives the polarization of the K corona alone. The K component and

TABLE I

K and F components of the solar corona and electron densities

(*Unit of brightness is* $10^{-13} \times B\odot$)

$R/R\odot$	p_0	p_K	$\frac{p_0}{p_K} = \frac{K}{K+F}$	$K+F$	K	F	N
6	$0{\cdot}071_2$	0·61	0·117	851	99·6	752	$3{\cdot}98 \times 10^4$
7	$0{\cdot}060_4$	0·60	0·105	575	60·4	514	
8	$0{\cdot}053_2$	0·58	0·092	407	37·4	370	1·80
9	$0{\cdot}048_0$	0·57	0·084	295	24·8	270	
10	$0{\cdot}043_5$	0·56	0·078	234	18·3	216	1·02
11	$0{\cdot}040_0$	0·54	0·074	191	14·1	177	
12	$0{\cdot}037_0$	0·53	0·070	159	11·1	148	0·66
13	$0{\cdot}034_1$	0·52	0·066	133	8·78	124	
14	$0{\cdot}032_4$	0·51	0·064	115	7·35	108	0·48
15	$0{\cdot}030_8$	0·50	0·062	100	6·20	93·8	
16	$0{\cdot}029_7$	0·49	0·061	87·1	5·31	81·8	0·37
17	$0{\cdot}028_8$	0·48	0·060	77·6	4·65	72·9	
18	$0{\cdot}028_3$	0·47	0·060	69·2	4·15	65·0	0·30
19	$0{\cdot}027_9$	0·46	0·061	62·4	3·80	58·6	
20	$0{\cdot}027_5$	0·45	0·061	57·5	3·51	54·0	0·26

the sum $K+F$ are plotted in Fig. 3, in which the part as far as 5° relates to the present discussion. We have assumed in the computations that at 5° elongation the polarization of the F component is zero. We have already shown that at this elongation $|p^F| \pm 0{\cdot}40$ per cent, and the maximum error in electron density introduced by the forced assumption $p^F = 0$ is only ± 15 per cent. The assumption of zero polarization is made because the sign of the actual polarization is unknown. The probable error in the measurement of polarization at this elongation is of the order of ± 10 per cent, giving a total uncertainty in electron density of 18 per cent.

3. *Electron densities in the zodiacal light region.*—To continue this analysis into the zodiacal light region we need accurate values of the intensity and polarization of the zodiacal light at the wavelength already used for the coronal observations (6300A). The best measurements of polarization are those of Behr and Siedentopf (**5**) which we use even though they were made at a wavelength of 5400A. We also use those measurements of the total brightness of the zodiacal light by Roach *et al.* which have been made at the wavelength 6300A (**9**). The observations of total intensity have been plotted in Fig. 3 with a plausible interpolation curve linking them to the present measurements of the outer corona.

The observations of Behr and Siedentopf start at an elongation of 35°. Some previous discussions of intensity and polarization data at greater elongations (for example Siedentopf, Behr and Elsasser (**10**)) have assumed that the polarization of the F component—here denoted by p_0^F—is very small for all elongations,

although van de Hulst (**11**) has considered the possibility of appreciable polarization of the F component. In this discussion we make no assumptions about p_θ^F except that

$$p_{35^\circ}^F = 0.$$

This is not a drastic assumption. From the work of van de Hulst (**11**) and Bricard (**7**) it seems likely that $|p_{35^\circ}^F| \geqslant 5$ per cent. This value is much less than the 23 per cent polarization of the zodiacal light at this elongation, but even if $p_{35^\circ}^F$ is as much as $+15$ per cent the calculated electron density is only halved. The consequences of assuming $p_{35^\circ}^F \neq 0$ are discussed later.

An elongation of 35° corresponds to a distance of closest approach to the Sun of $R_{35^\circ} = 213 \sin 35^\circ = 123 R_\odot$. We now make the further assumption that if n_e is the electron density at this distance from the Sun then

$$\frac{d \log n_e}{d \log r} = \text{const.}$$

for all distances beyond $123 R_\odot$ that make an appreciable contribution to the intensity. This expression is the gradient of the graph in Fig. 2. In the graph, the electron density at $20 R_\odot$ has been calculated to be $0{\cdot}26 \times 10^4\,\text{cm}^{-3}$, and the electron density at $128 R_\odot$ is shown later to be of the order of $10^3\,\text{cm}^{-3}$. The gradient of electron density between these two points is small, and the only reasonable way of joining them without supposing a minimum in the electron density curve is shown. We are assuming that the curve continues beyond the point $r = 123 R_\odot$ as it approached it. In addition, we shall later consider the case in which a sharp cut-off of electron density is imposed at an arbitrary distance from the Sun.*

The brightness of the K corona can now be calculated from equation (2), and the polarization of K corona using equations 3, 4, 5, following

$$p_k(x) = \frac{K_t(x) - K_r(x)}{K_t(x) + K_r(x)} \tag{3}$$

$$K_t(x) = D \int N(r) \frac{dr}{r\sqrt{r^2 - x^2}} \tag{4}$$

$$K_t(x) - K_r(x) = D \int N(r) \frac{x^2}{r^3\sqrt{r^2 - x^2}}. \tag{5}$$

In these equations, which have been adapted from van de Hulst, K_t and K_r represent the transverse and radial components of the polarized light.

We first consider the case in which $d \log n_e / d \log r$ is a constant between $r = 123 R_\odot$ and $500 R_\odot$, and has the value corresponding to interpolation between $40 R_\odot$ and $123 R_\odot$ (see Fig. 2). The extrapolation involved is no greater than the range of interpolation and the electron density for distances greater than $500 R_\odot$ does not affect the computations. Indeed, the electron density at $500 R_\odot$ has only a very small weight in the computations. This density distribution gives the value

$$p_{35^\circ}^K = 0{\cdot}56$$

By observations

$$p_{35^\circ}^{K+F} = 0{\cdot}23.$$

* This does not imply a sudden reduction in space density of interplanetary gas, but only a sudden diminution of ionization.

Hence

$$\frac{K}{K+F}=0{\cdot}41$$

corresponding to an electron density at $r=123R\odot$ of

$$n_e=1{\cdot}08\times10^3\,\mathrm{cm}^{-3}.$$

The brightness of the K corona alone corresponding to this distribution is shown in Fig. 3 and the computed polarization of the sum of the two components, making the initial assumption that at all elongations $p_\theta^F=0$ (i.e. supposing only dilution of the K component by the F component) is shown in Fig. 4. The observations of Behr and Siedentopf are also plotted. Even assuming $p_\theta^F=0$ the calculated polarizations are too high and to obtain agreement with observation using this model it is necessary to assume negative values for p_θ^F. In Fig. 5 is shown the negative polarization that has to be assumed. From elongation $\theta=35°$ the negative value increases steadily.

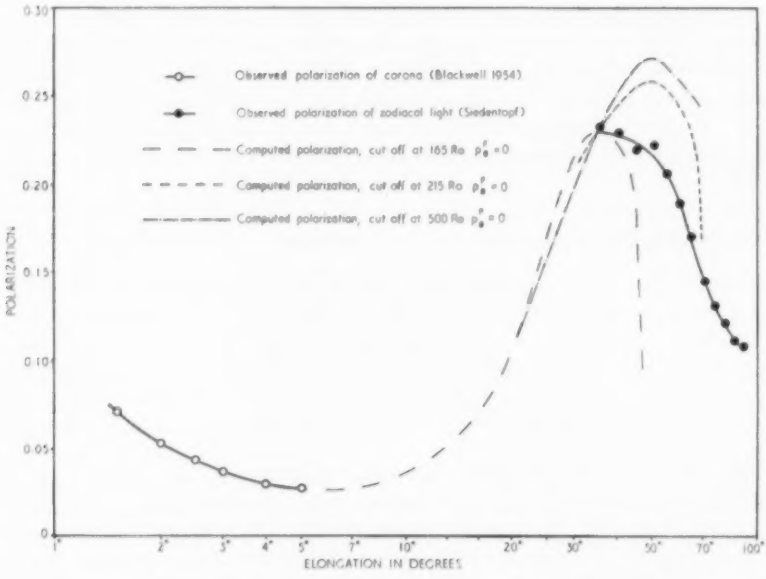

FIG. 4.—*Observed and calculated polarization in the solar corona and zodiacal light. In the coronal region the points represent the model of Blackwell* (**4**). *In the zodiacal light region the points represent the data of Behr and Siedentopf* (**4**). *The broken lines give the calculated polarization of the zodiacal light for positions of cut-off of electron density at* $500R\odot$, $215R\odot$ *and* $165R\odot$ *assuming* $p_\theta^F=0$ *for all values of* θ.

A negative polarization is not impossible but in the absence of any proof to the contrary it is desirable to try to find a model which needs only a positive value for p_θ^F. If it is supposed that $p_{35°}^F=0$ this can be achieved only by imposing a sudden cut-off on the electron density distribution.

Now let us suppose a sudden cut-off at $165R\odot$ (0·78 A.U.). This gives

$$p^K_{35°} = 0{\cdot}75$$

$$\frac{K}{K+F} = 0{\cdot}307$$

and

$$n_e = 1{\cdot}20 \times 10^3 \text{ cm}^{-3} \text{ (at } r = 123R\odot).$$

The brightness of this model K corona is shown in Fig. 3 and the computed polarization for $p^F_{35°} = 0$ is shown in Fig. 4. The polarization of the F corona that must be assumed to account for the observed polarization is shown in Fig. 5, together with another curve for a K corona with a cut-off at $215R\odot$. If a cut-off at $165R\odot$ is assumed, the F corona has a positive polarization, but a cut-off at $215R\odot$ still requires a negative value for p^F_0 for $\theta > 35°$.

We have so far assumed that $p^F_{35°} = 0$, and we should now investigate how far these conclusions are changed by assuming another value for $p^F_{35°}$.

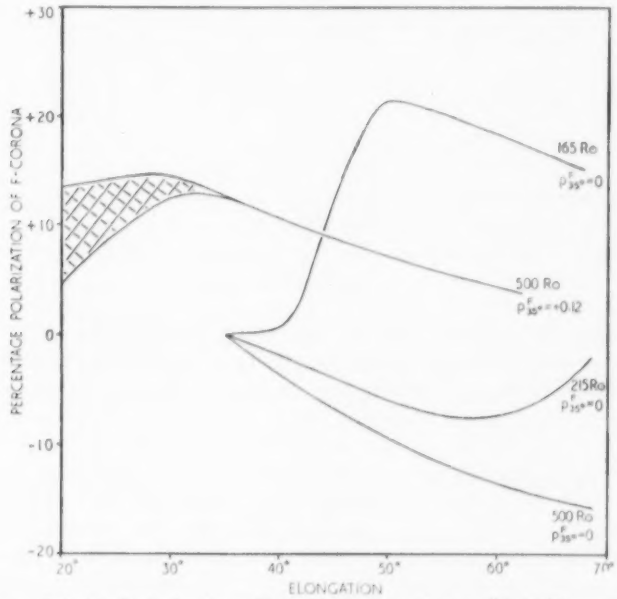

FIG. 5.—*Calculated polarization of F component for various models of K component.*

We now suppose $p^F_{35°} = 0{\cdot}12$ and no cut-off in electron density giving

$$p^K_{35°} = 0{\cdot}57$$

and

$$n_e = 0{\cdot}66 \times 10^3 \text{ cm}^{-3} \text{ (at } r = 123R\odot).$$

Even this extreme value for the F corona polarization alters the computed electron density very little. If plausible values of the polarization of the sum of the components are interpolated between the observations of the corona and the zodiacal light over the range $20° < \theta < 35°$ (a computed interpolation is given in Fig. 4) p^F_θ can be calculated for this range. The results are shown in Fig. 5. Here maximum and minimum interpolated values for p^{F+K}_θ have been assumed,

and the corresponding maximum and minimum values for p_θ^F have been shown. It will be seen that p_θ^F shows a maximum for elongations in the neighbourhood of 30°–35° and that even at $\theta = 20°$ the polarization cannot very well be less than 5 per cent and may be as much as 14 per cent. Both of these results conflict with the expectations of theory. In particular the results of Bricard make it likely that $|p_{20°}^F| > 3$ per cent. The ratio of the electron component to the combined components is plotted in Fig. 6 for two models.

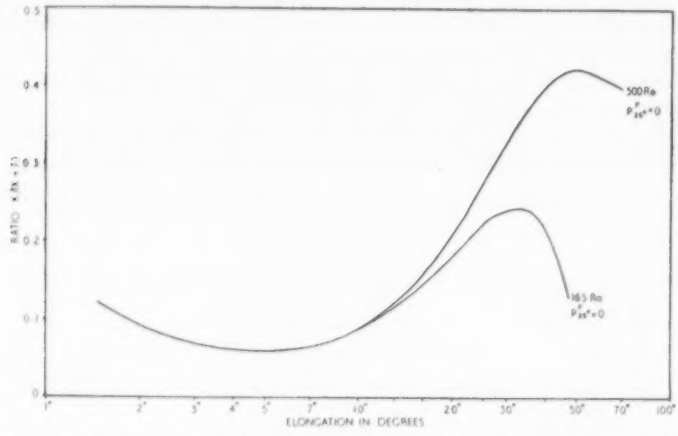

FIG. 6.—*Ratio $K/(K+F)$ for models of K components having cut-off at 500$R\odot$ and 165$R\odot$, and $p_{35°}^F = 0$.*

4. ***Summary of conclusions about electron densities in the zodiacal light region.***—We emphasize that this analysis depends upon the assumption that the intensity and polarization of the zodiacal light are accurately known. If the assumption that $p_{35°}^F = 0$ is made and no cut-off is imposed upon the electron density, then $p_\theta^F < 0$ for $\theta > 35°$. But if $p_{35°}^F$ is taken to be sufficiently high and there is no cut-off then $p_\theta^F > 0$ for all values of θ. However, p_θ^F is then also unreasonably high for $\theta \sim 20°$. If a cut-off is imposed just inside the orbit of the Earth and $p_{35°}^F = 0$, then $p_\theta^F > 0$ for $\theta > 35°$. An analysis of the data for the extreme cases of no cut-off and a cut-off at 165$R\odot$, both with $p_{35°}^F = 0$ is given in Table II.

5. *The form of the electron density curve.*—We should at this stage consider whether the derived electron density curve is a reasonable one.

It has been demonstrated that under certain conditions the observed data may be compatible only with a sharp reduction of electron density near the position of the Earth's orbit. Öpik (**12**), however, has considered theoretically the problem of the ionization of an interplanetary gas and concluded that the ionization is complete to distances far beyond the orbit of Jupiter.

It is disturbing that at distances beyond about 30$R\odot$ the density of the interplanetary gas seems to decrease so slowly with increasing distance from the Sun. An increased gradient can be obtained only by supposing that $p_{35°}^F \sim 0{\cdot}19$ but this assumption leads to an unlikely form for p_θ^F (see Fig. 5 where derived values of p_θ^F are plotted for $p_{35°}^F = 0{\cdot}12$). The derivation of the form of p_θ^F is the outstanding problem of the zodiacal light. At the present moment we have

to choose between a negative value for p_0^F over most of the range of elongation, and a cut-off of electron density near the orbit of the Earth. The first assumption is the more likely.

TABLE II

Models of the outer corona and inner zodiacal light regions

(*Unit of brightness* $10^{-12}\times$ *average intensity of solar disk*)

Elongation	$K+F$	No cut-off			Cut-off at $165R_\odot$ (0·78 A.U.)		
		K	$K/(K+F)$	p_0^{K+F}	K	$K/(K+F)$	p_0^{K+F}
8°	24·0	1·70	0·071	0·032			
10°	14·1	1·23	0·087	0·039			
13°	7·08	0·851	0·120	0·054			
16°	3·98	0·617	0·155	0·072			
20°	2·21	0·457	0·21	0·10	0·398	0·18	0·12
25°	1·15	0·331	0·29	0·16	0·257	0·22	0·17
30°	0·75	0·246	0·33	0·19	0·178	0·24	0·21
35°	0·49	0·186	0·38	0·23	0·118	0·24	0·23
40°	0·39	0·155	0·40	0·25	0·083	0·21	0·22

6. *Comparison with other data.*—The electron density data are plotted in Fig. 1. On this diagram there are also shown the data of van de Hulst's model for the minimum corona (**3**), the results of Michard's computations from his observations of the eclipse of 1952 February 25 (**13**) and the coronal model of O'Brien and Bell (**14**) deduced from radio observation over the period July 1951 to July 1952. The agreement with Michard's data is within the limits of experimental error, but the electron densities of van de Hulst are probably too low. On the basis of Fig. 1 it is suggested that the electron density values of Table III. are more representative of sunspot minimum than the model of van de Hulst.

TABLE III

Suggested electron densities in the equatorial regions at sunspot minimum

$R/R_\odot$	N
3·0	$3·39\times10^5$
3·5	2·09
4·0	1·35
4·5	0·96
5·0	0·69

The larger electron densities obtained by O'Brien may only be due to the difference in phase of the solar cycle. As Allen (**15**) has pointed out the radio results are not strictly comparable with the optical results because the former are a measure of $[\overline{n_e^2}]^{1/2}$. In Fig. 2 the corona data are related to the datum obtained from zodiacal light observations at an elongation of 35°. There is naturally good agreement with Siedentopf's electron densities (**5, 10**) in the region near $123R$ because practically the same data have been used, but in the absence of

observational data about the polarization of the *F* component at great elongations it is unjustifiable to draw conclusions about the electron densities at greater distances. Storey (**16**) has derived the electron density of 400 cm^{-3} for regions near to the Earth's orbit. This value is of the same order of magnitude as those shown here.

7. *Connection between corona and zodiacal light.*—It has often been discussed whether or not the zodiacal light is continuous with the solar corona. The solar physicist is chiefly concerned with the electron component and he wishes to know whether or not the electron component of the zodiacal light can be considered to be part of the solar corona. The *F* component is only an unwanted diluent of this component and for this reason it is impossible to decide this question simply by an examination of total brightness, because except very close to the Sun and perhaps at elongation 40°–50° the total brightness is dominated by the *F* corona. Any arguments based on total intensity are therefore very misleading. But there is no *a priori* reason to expect a smooth gradation of electron density

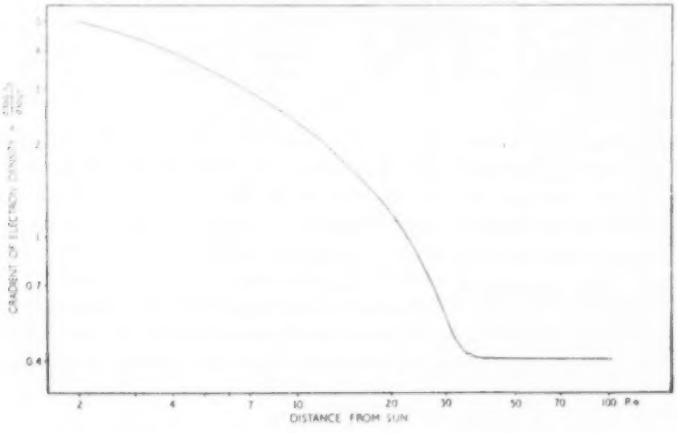

FIG. 7.—*Gradient of electron density in the region of the ecliptic and solar equator.*

between corona and zodiacal light. Looking at the electron densities of Fig. 2 it is evident that there is no discontinuity in electron density, although there is a rapid change in density gradient near $30R_\odot$. In Fig. 7 the gradient has been plotted as a function of distance and there is clearly a discontinuity at this point, although it should be realized that the part from $20R_\odot$ onwards has been derived from an interpolated curve. Even bearing in mind the fact that the electron density curve is not well defined in this region, it is difficult to avoid the conclusion that there is a sharp change of gradient here. We do not suggest at this stage, however, that this discontinuity represents a real difference in origin between the corona and the zodiacal light.

8. *Electron density in the polar region of the corona.*—The polarization data here are very uncertain because the polarization is low. Supposing (from paper I) that at $6R_\odot$ the polarization is 0·006, the calculated electron density is of the order of $1{\cdot}5 \times 10^3$ cm^{-3}. This value for the electron density is an order of magnitude only, but it is not incompatible with the value that would be expected from an

extrapolation of van de Hulst's model for the polar region at sunspot minimum ($10^3\,cm^{-3}$). On the other hand it is considerably less than the value found from a reasonable extrapolation of Michard's model ($8{\cdot}5 \times 10^3\,cm^{-3}$), and we suggest that this difference is due to the difference of phase of the solar cycle between the two eclipses. There can certainly be no doubt that the electron density in the polar regions at sunspot minimum is very low in comparison with densities in the equatorial regions. All available electron densities are shown plotted in Fig. 8. Van de Hulst's model for sunspot minimum in the polar regions may be taken to be a good guide to the electron density and we suggest the addition of the following data (Table IV).

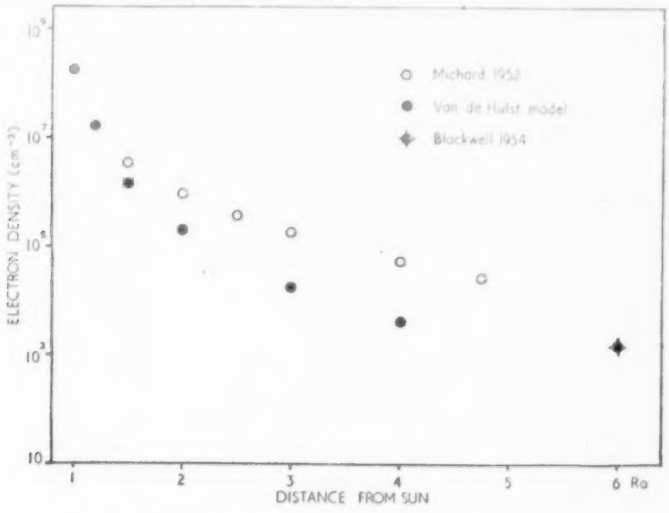

FIG. 8.—*Electron densities in the polar regions at sunspot minimum.*

TABLE IV

Electron densities in the polar regions at sunspot minimum

$R/R_\odot$	N
5	$2{\cdot}3 \times 10^3$
6	$1{\cdot}5$

9. ***Further observational work.***—It is now possible to make a reliable interpolation between the intensity of the corona and the intensity of the zodiacal light, but there is still a wide gap between the two polarization curves, the closing of which will greatly help their interpretation. The practical difficulty in bridging this gap from the sunward side lies in the fact that the quantity to be measured on the photographic plate to deduce the polarization of the corona is made small by the presence of the sky background. Thus in the work described in Paper I it was necessary to measure a polarization of 0·63 per cent on the plate in order to deduce a polarization of the corona of 2·8 per cent at an elongation of 5°. This

work was done at an altitude of 30 000 ft. Using a likely polarization curve interpolated between the outer corona and the zodiacal light we can now calculate the height at which observations should be made to give polarization data of the same accuracy as before at various distances from the Sun. The distances and corresponding heights are given in Table V. It can be seen from this table that, using this technique, it will not be possible to push the measures of polarization much beyond $40R_\odot$ from the Sun.

TABLE V

Heights at which the difference between the polarization of the sky alone and the combined sky and corona is 0·0063

Elongation	Height of Observer	Distance from Sun	Height of Observer
5°·0	30 000 ft.	15°·0	68 000 ft.
7°·5	53 000 ft.	20°·0	73 000 ft.
10°·0	62 000 ft.	25°·0	76 000 ft.

It is even more desirable that the zodiacal light data should be extended back towards the Sun. In the region $20° < \theta < 30°$ the polarization is probably of the order of 20 per cent and the uncertainty in interpretation introduced by the assumption $p_\theta^F = 0$ is a minimum. It is hoped to present some data for this region in a later paper.

Acknowledgment.—The author is much indebted to Professor R. O. Redman for discussion of these problems.

The Observatories,
Cambridge:
1955 *December.*

References

(1) Allen, C. W., *M.N.*, **106,** 137, 1946.
(2) Blackwell, D. E., *M.N.*, **112,** 652, 1952.
(3) van de Hulst, H. C., *B.A.N.*, **11,** 135, 1950.
(4) Blackwell, D. E., *M.N.*, **115,** 629, 1955.
(5) Behr, A., and Siedentopf, H., *Zeit. f. Astrophys.*, **32,** 19, 1953.
(6) Öhman, Y., *Stockholm Observatory Annals*, **15,** No. 2, 1947.
(7) Bricard, J., *Journ. de Phys. et le Rad.*, **4,** Ser. 8, 57, 1943.
(8) Gumprecht, R. O., Neng-Lun Sung, Jin H. Chin and Sliepcevich, C. M., *J.O.S.A.*, **42,** 226, 1952.
(9) Roach, F. E., Petit, H. B., Tandberg-Hanssen, E. and Davis, D. N., *Ap. J.*, **119,** 253, 1054.
(10) Siedentopf, H., Behr, A. and Elsasser, H., *Nature*, **171,** 1066, 1953.
(11) van de Hulst, H. C., *Les Particles solides dans les astres. Institut d'Astrophysique Cointe-Liège (Belgique)*, 1955, p. 88.
(12) Öpik, E. J., *Zeit. f. Astrophysik*, **35,** 43, 1954.
(13) Michard, R., *Ann. d'Astrophys.*, **17,** 429, 1954.
(14) O'Brien, P. A., and Bell, C. J., *Nature*, **173,** 219, 1954.
(15) Allen, C. W., *Rep. Prog. Phys.*, **17,** 135, 1954.
(16) Storey, L. R. D., *Phil. Trans. Roy. Soc.*, **246A,** 113, 19

Note added in proof.—This paper inadvertently omits reference to Öhman's discussion (*Stockholm Observatory Annals*, **18,** No. 8, 1955) of his observations of negative polarization in the *F* component of the corona (**6**).

CORONAL PHOTOMETRY AT THE ECLIPSE OF 1954 JUNE 30

C. W. Allen

(Received 1955 November 24)

Summary

The paper describes the occulting disk method of coronal photography and photometry used at the solar eclipse of 1954 June 30. Although the eclipse was obscured by thin cloud it has been possible to measure the coronal brightness, colour and ellipticity in the range 1.2 to 12 radii.

---

1. *Introduction.*—Eclipses of the Sun provide the only opportunities for making those optical observations of the Sun's outer corona which are required for studying the physics of the solar corona and interplanetary particles. Some of the more serious difficulties for photometric observations have been

(*a*) to allow for the light scattered from the brilliant inner corona,

(*b*) to allow for sky light, and

(*c*) to cope with the great range of relative intensity from the inner to the outer corona.

The apparatus and observations of the University of London Observatory eclipse expedition of 1954 June were designed to determine or eliminate these effects as well as possible. The eclipse was observed from the island of Syd Koster, Sweden.

The observations were made by photographic photometry in two colours. The novel feature of the apparatus was an occulting disk, a little larger than the camera aperture, driven at the diurnal rate about 15 feet in front of the equatorially mounted camera. The disk prevents any light from the precise direction of the camera axis from passing into the camera. The effective camera aperture was thus zero for the axis (for the umbral region in the centre of the plate), but increased outward (in the penumbra) and became full aperture at about a quarter of the full radius of the field. Very little light from the bright inner corona reached the camera lens and hence scattering within the optical system was reduced to a minimum. At the same time the change in effective aperture counterbalanced to some extent the change in surface brightness of the corona.

The eclipse of June 30 was observed through thin cloud and therefore the photometric results cannot be as accurate as was hoped. Nevertheless it has been possible to determine from the photographs the distribution of coronal brightness from 1·1 to 12 solar radii and to give some estimate of the colour and ellipticity of the corona in this range. Because of cloud absorption it was necessary to utilize the inner corona to obtain absolute intensity calibration. The corona was of extreme minimum type.

2. *Equipment.*—Two cameras A and B were attached to the ends of the declination axis of a weight driven polar axis mounting as shown in Fig. 1. Each

camera was provided with interchangeable gelatine filters F; Wratten 47 for blue, and Wratten 27 for red. The stops S used in the lenses were considerably smaller than full size with the result that there was no vignetting over the field of the plate. Each lens was enclosed with a hood H to prevent general sky light from reaching it, but of course not obscuring the outer corona field.

The trolley mechanism T driving the disks was mounted on the top of a 14-ft. wooden tower. Its motor was operated by lead storage batteries and the speed controlled by means of a rheostat. The occulting disks D were blackened on the under surface.

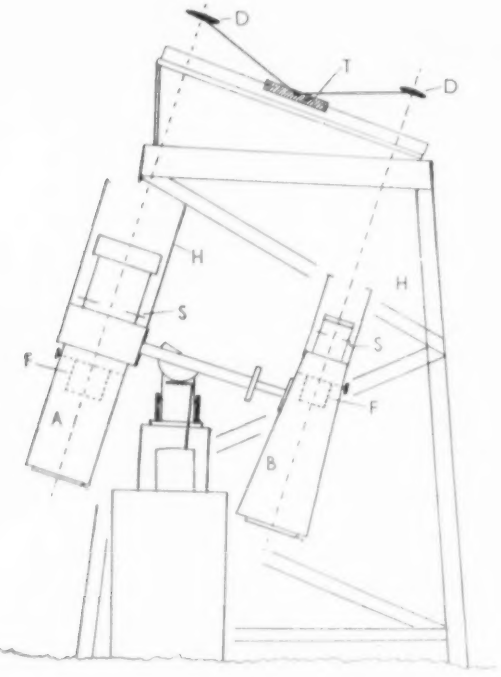

FIG. 1.—*Sketch of arrangement of cameras A and B and occulting disks D. T=trolley, H=hood, S=stop, F=filter.*

The dimensions of the optical systems for cameras A and B are given in Table I, where "umbra" and "penumbra" refer to the out-of-focus shadow of the disk on the photographic plate.

The reason for having two cameras was that it seemed important to obtain photographs with the umbral radius both greater than and smaller than the solar radius. In the former case (camera A) the inner corona is lost completely but the intensity variations of the outer corona are well compensated by the disk shadow. If on the other hand the whole inner corona is to appear, the umbral radius must be smaller than the solar radius. In that case the compensation is not as good and photographs have a large intensity range. For the camera B the umbral shadow was only slightly smaller than the solar disk and the intensity

range was satisfactory (not more than 20 : 1). A more realistic and informative photograph of the corona is obtained if the inner corona is just visible and it would now appear that the ideal arrangement is to have the umbra about the same size as the solar image.

TABLE I

Optical dimensions

	Camera A	Camera B
Focal length of camera lens	67·4 cm	75·5 cm
Diameter of stop	8·54 cm	6·54 cm
Aperture (seen from outside)	9·71 cm	6·80 cm
Disk diameter	14·50 cm	10·70 cm
Distance, disk to aperture	447 cm	433 cm
Plate size (square)	15·9 cm	15·9 cm
Field diamter (to 15·0 cm)	12°·7	11°·4
Radius of Sun (on plate)	3·08 mm	3·45 mm
Radius of umbra (on plate)	3·62 mm	3·40 mm
Radius of penumbra (on plate)	18·25 mm	15·2 mm
Distance, disk to dec. axis	455 cm	

The duplication of the cameras introduced some difficulties that were not entirely overcome at this eclipse. Relative to the cameras the disk system rotates around the camera axis at sin(solar dec.) times the diurnal rate and in consequence it is not possible to have each disk moving precisely with its camera. It was thought that this effect could be tolerated during the 154 seconds of totality, but during the adjustment period before totality an allowance had to be made for the misalignment of the Sun, disk and camera. This could be done approximately on rehearsal days by observing the somewhat obscured solar image on a ground glass screen, but in the partial eclipse phase this procedure became very inaccurate. As a result the disks are not well centred on the Sun in the eclipse photographs and this gives rise to asymmetry of the photometry. It has not been difficult to allow for this effect, but it has prevented any opportunity of observing the real asymmetry of the coronal radiation.

3. *Eclipse photographs.*—Twelve plates were exposed during the 154 seconds of totality. Half of these were blue-sensitive plates Kodak II-O exposed through the blue Wratten 47 filter giving an effective wave-length of about 4500 A. The others were panchromatic Kodak P300 plates exposed through the red Wratten 27 filter and giving an effective wave-length of about 6200 A. Plates were exposed simultaneously on both cameras and the same exposure time given to the blue and red plates. The three groups of four plates (blue and red in cameras A and B) had exposure times of 8 sec., 2 sec., and 20 sec. in this order. Transparency was improving during totality.

The plates were developed in pairs (blue and red) in a Dobson tank (1) for 5 minutes with Kodak D76 fine-grain low-contrast developer. The usual contrast of coronal images was reduced in this case by both the occulting disk and the cloud absorption. Consequently the coronal pictures had a rather dull appearance but at least they gave the intended result of showing (in the longer exposures) the complete inner and outer corona on one picture.

4. *Photometric standardization.*—It was not convenient to expose the intensity calibration marks on to the same plates as the coronal photographs. Instead these were put on to plates from the same batch and developed in similar conditions.

The characteristic curve for the plates was obtained with the help of a tube photometer having 12 tubes and entrance holes ranging in diameter from 0·39 to 4·99 mm. The same filters were used in the photometer as with the eclipse plates.

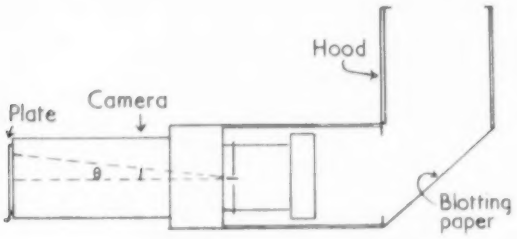

FIG. 2.—*Arrangement for absolute intensity standardization.*

Absolute intensity standardization was provided by exposing the eclipse camera A to sunlit white blotting paper. The arrangement is shown in Fig. 2. The blotting paper was shaded from general sky illumination by a hood and set with its normal about 45° from the direction of the Sun and the camera. Rough tests with an exposure-meter showed that the intensity of scattered light from the paper was almost independent of the viewing angle and hence the surface brightness of the illuminated paper could readily be computed in terms of the Sun's mean surface brightness and the albedo of the paper. The albedo could have been determined by laboratory photometry if justified by eclipse success, but for our purpose we assume the albedo to be 0·7. The surface brightness of illuminated white paper is about 10 times greater than the inner corona and about 10^4 times greater than the eclipse sky. To make plate densities comparable it was therefore desirable to reduce the lens diameter by nearly 100 when used with illuminated paper. The diameter of the stop actually used was 2·4 mm as compared with 85 mm for the corona.

Tests were also made to determine the variation of intensity of light reaching the plate with position on the plate. Geometrical considerations indicate a variation of intensity proportional to $\cos^4\theta$ (θ from Fig. 2) which is almost negligible. To test this, some plates were exposed on an evenly bright twilight sky (during a rehearsal). Photometry revealed that the variation of intensity was much greater, being approximately proportional to $\cos^{30}\theta$ and that the eclipse photographs required correction for this effect. The effect itself is possibly associated with the method of plate development.

5. *Photometric measurements.*—Only the four 20-second exposure plates obtained towards the end of totality were measured.

All plates were photometered with a new Hilger microphotometer. Runs were made through the centre of the Moon's shadow in four directions: (i) equatorial, 4° N of E to 4° S of W, (ii) polar, actually in the N–S line, (iii) and (iv) at 45° to the N–S line. No attempt was made to discriminate

between intensities on either side of the Sun, these being averaged in all cases. Likewise the two 45° runs were averaged.

The blue photographic plates with blue filter were about twice as sensitive to sunlight as the red with red filter. Photographic densities were converted into intensities from a calibration curve in the usual way. The intensity scales of the curves were chosen to make the exposures on sunlit white blotting paper give the same intensity for both blue and red plates. Any difference of blue and red intensity measurement thus represents a departure from solar colour. No distinguishable departure from solar colour was found in any part of the corona. For intensity measurements the blue and red intensities have been averaged.

The sky was far more intense than the outer corona. To correct for sky light it was assumed that the light in the outer part of the field (over 20 radii from the Sun) was entirely due to the sky. The sky brightness was then evaluated using the $\cos^{30}\theta$ distribution mentioned in Section 4, but also taking unevenness of sky illumination into account as far as possible. The estimated sky intensity was subtracted from the measured intensity to give the coronal values. The reliability of this procedure may best be judged by the agreement of measurements in Fig. 4.

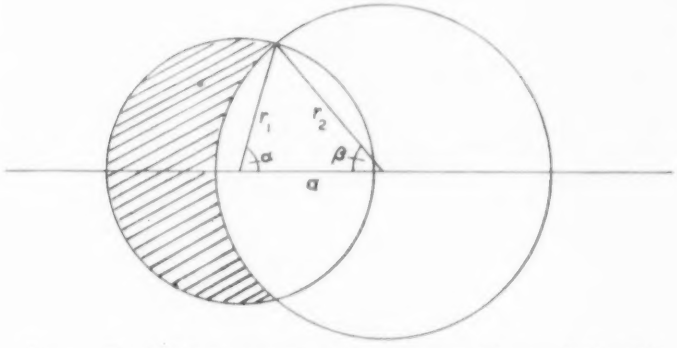

FIG. 3.—*The shaded area represents effective aperture of lens occulted by disk.*

Within the penumbral region of the disk shadow the measured intensities required adjustment for the variation of effective aperture; see Fig. 3. To compute this we note that the common area of two intersecting circles of radii r_1 and r_2 and with centres separated by a is

$$c = r_1^2\alpha + r_2^2\beta - \tfrac{1}{2}(2a^2r_1^2 + 2a^2r_2^2 + 2r_1^2r_2^2 - a^4 - r_1^4 - r_2^4)^{1/2}$$

where

$$\cos\alpha = (a^2 + r_1^2 - r_2^2)/(2ar_1)$$

$$\cos\beta = (a^2 - r_1^2 + r_2^2)/(2ar_2)$$

Identifying r_1 with the radius of the lens aperture, r_2 with that of the disk, and a with ψd where ψ is the angular distance between the relevant point in the sky and the line joining the centres of the aperture and the disk (which should be lined on to the centre of the Sun but was not precisely so in this eclipse) and d is the disk-to-aperture distance, we may compute the effective aperture $(\pi r_1^2 - c)$ as a function of ψ. Measured intensities were then increased in the ratio of full/effective aperture.

Because of errors in alignment ψ was not precisely the same as the angular distance ρ from the centre of the Sun. In order to estimate the misalignment the corrections were made for several assumed differences between ψ and ρ. The value that gave a symmetrical coronal intensity distribution was chosen as the correct one. However it was found that the results, averaged on both sides of the Sun, were not at all sensitive to any ambiguity in estimating the difference of ψ and ρ.

6. *Distribution of coronal brightness.*—The coronal measurements of surface intensity are shown in Fig. 4, where the data for the equatorial, 45°, and polar directions have been separated to avoid superposition. The differences between the curves are too small to show in the diagram, but appear in Table II, where they are compared with data from van de Hulst's model corona (**2**). The sky intensity on the same scale as the corona (with absorption) is shown in Fig. 4.

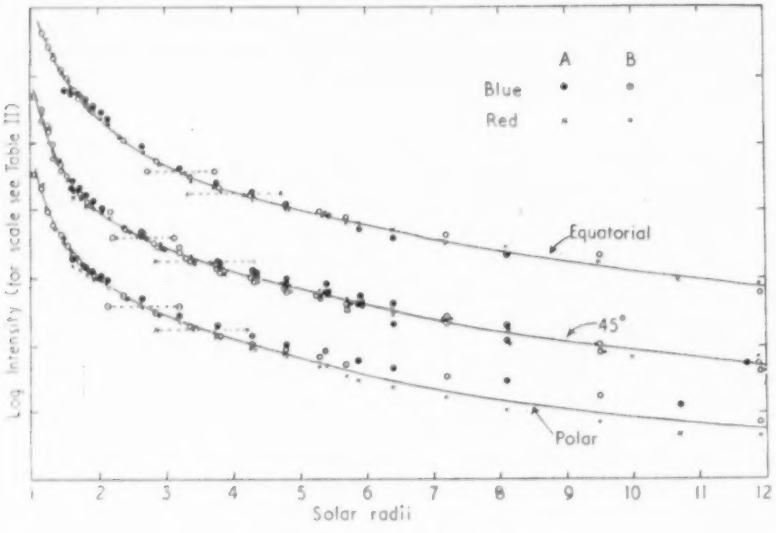

FIG. 4.—*Coronal surface intensity.*

O – – – – – – O *Blue sky intensity on same scale.*
X – – – – – – X *Red sky intensity on same scale.*

Since clouds absorbed light from the corona by an amount that could not be determined directly, some assumption had to be made to give the results on an absolute scale. For this purpose the intensity of the inner corona was fitted to van de Hulst's model for sunspot minimum (sp-min). It is then found that there is good agreement between the observations and the model over the whole range of radial distance.

The coronal colour may be estimated by comparing the blue and red intensities in Fig. 4. As no systematic difference is found over most of the corona it is concluded that the colour is the same as the Sun. This was known already for the inner corona (**3**) but the diffraction theory (**4, 5**) predicted a small reddening for larger radii. No such reddening is detectable in the data. The polar data

appear to indicate the outer regions (6 to 12 radii) to be bluish but the blue plate microphotograms in the polar direction were rather irregular and this effect is almost certainly due to inaccuracy. When interpreting these observations it

TABLE II

Logarithm of coronal surface intensity in terms of the mean solar intensity

Radius	Observations			Model (van de Hulst, sp-min)		
	Equatorial	45°	Polar	Equatorial	Polar	F
$R_\odot$						
1·1		$\bar{7}$·7	$\bar{7}$·6	$\bar{6}$·01	$\bar{7}$·75	$\bar{7}$·06
1·2	$\bar{7}$·65	$\bar{7}$·31	$\bar{7}$·18	$\bar{7}$·65	$\bar{7}$·29	$\bar{8}$·86
1·2	$\bar{7}$·36	$\bar{7}$·01	$\bar{8}$·91	$\bar{7}$·37	$\bar{8}$·96	$\bar{8}$·70
1·4	$\bar{7}$·16	$\bar{8}$·76	$\bar{8}$·70	$\bar{7}$·14	$\bar{8}$·73	$\bar{8}$·55
1·5	$\bar{8}$·99	$\bar{8}$·55	$\bar{8}$·52	$\bar{8}$·95	$\bar{8}$·56	$\bar{8}$·43
1·6	$\bar{8}$·82	$\bar{8}$·40	$\bar{8}$·38	$\bar{8}$·78	$\bar{8}$·42	$\bar{8}$·32
1·8	$\bar{8}$·61	$\bar{8}$·15	$\bar{8}$·15	$\bar{8}$·50	$\bar{8}$·20	$\bar{8}$·14
2·0	$\bar{8}$·41	$\bar{9}$·99	$\bar{9}$·99	$\bar{8}$·27	$\bar{8}$·04	$\bar{8}$·00
2·5	$\bar{9}$·98	$\bar{9}$·68	$\bar{9}$·69	$\bar{9}$·86	$\bar{9}$·74	$\bar{9}$·72
3	$\bar{9}$·66	$\bar{9}$·44	$\bar{9}$·47	$\bar{9}$·60	$\bar{9}$·52	$\bar{9}$·51
4	$\bar{9}$·29	$\bar{9}$·11	$\bar{9}$·11	$\bar{9}$·25	$\bar{9}$·20	$\bar{9}$·20
5	$\bar{9}$·00	$\bar{10}$·87	$\bar{10}$·83	$\bar{10}$·99	$\bar{10}$·95	$\bar{10}$·95
6	$\bar{10}$·77	$\bar{10}$·62	$\bar{10}$·58	$\bar{10}$·78	$\bar{10}$·75	$\bar{10}$·75
8	$\bar{10}$·40	$\bar{10}$·24	$\bar{10}$·20	$\bar{10}$·47	$\bar{10}$·44	$\bar{10}$·44
10	$\bar{10}$·11	$\bar{11}$·96	$\bar{11}$·93	$\bar{10}$·23	$\bar{10}$·20	$\bar{10}$·20
12	$\bar{11}$·9	$\bar{11}$·7	$\bar{11}$·8			

should be remembered that the sky background was considerably more intense for the blue than the red light and hence some systematic differences might have appeared. All we can conclude from the present observations is that there is no severe change of colour in the outer corona as far as 10 radii.

The ellipticity of the corona may be determined by comparing the equatorial and polar intensity. The equatorial/polar intensity ratio of 2·9 in the inner corona is typical for sunspot minimum. For the outer corona beyond 3 radii the intensity ratio remains about 1·5 as compared with the van de Hulst model of 1·1. This may mean either that the intensity of the diffraction F corona is less than supposed or that it is somewhat elliptical as close to the Sun as 5 or 10 radii.

7. *Absorption and sky brightness.*—The sky brightness determined by comparison of plate density of the coronal sky with the exposures made with sunlit paper are

$$\text{Sky (in blue)} = 1{\cdot}9 \times 10^{-9} \text{ mean solar intensity}$$

$$\text{Sky (in red)} = 0{\cdot}9 \times 10^{-9} \text{ mean solar intensity}$$

These agree very closely with the corresponding measurements at the 1940 eclipse ($1{\cdot}9 \times 10^{-9}$ and $1{\cdot}1 \times 10^{-9}$) (**6**) despite the fact that one eclipse was clear and the other somewhat cloudy.

By comparing the coronal brightness given in Table II with values determined by absolute photometry with the sunlit paper, the absorption towards the end of totality was found to be about three quarters of a magnitude. It is evident that the absorption was greater during the early stages of totality.

8. *Conclusions.*—The various intensity measurements in the outer corona cannot be applied to physical arguments until the two components K-corona (electron scatter) and F-corona (particle diffraction) can be segregated. This can be done by measurements of Fraunhofer intensities or polarization and it is hoped that such measurements will be available in due course for the present eclipse. In the meantime it is advisable not to attempt any re-analysis but merely to look for tendencies that appear in the present data.

The observations agree well enough with van de Hulst's model (**2**) to ensure that only minor ammendments to that model will be needed. The departures from the model that appear to be detectable are (*a*) no reddening of the outer corona is found, (*b*) the outer corona is more elliptical than expected, and (*c*) the outer corona is fainter than expected. These results suggest an F-corona somewhat fainter than the values used in the model.

The University of London Observatory eclipse expedition to Syd Koster, Sweden was made possible by a grant from the Joint Permanent Eclipse Committee. Much assistance was given the author both in setting up the equipment and making the exposures by the Observatory's Chief Technician, Mr. C. R. Spratt. The London expedition shared a site selected by Professor R. O. Redman of Cambridge from whom much assistance was obtained. Willing help from the residents of Syd Koster and the Swedish astronomers was also much appreciated.

University of London Observatory,
Mill Hill Park,
London, N.W.7:
1955 *November* 23.

Addendum on Eclipse of 1955 *June* 20

An attempt to repeat the measurements, but with only a single camera and disk, was made at the eclipse of 1955 June 20 in Ceylon. However, the eclipse was obscured by heavy cloud. It has now been decided that if the same principle is to be applied at future eclipses the disk should be placed *inside* the camera since it is probably easier and safer to allow for the light scattered in the lens than to erect and align the travelling disk.

References

(1) Dobson, Griffith and Harrison, *Photographic Photometry*, p. 77, 1926.
(2) H. C. van de Hulst, *B.A.N.*, **11**, 135, 1950.
(3) W. Grotrian, *Z. Ap.*, **3**, 199, 1931.
(4) H. C. van de Hulst, *Ap. J.*, **105**, 471, 1947.
(5) D. E. Blackwell, *M.N.*, **112**, 652, 1952.
(6) C. W. Allen, *M.N.*, **107**, 426, 1947.

AN ATTEMPT TO DETECT DEUTERIUM IN THE SOLAR ATMOSPHERE

*T. D. Kinman**

(Communicated by the Director, University Observatory, Oxford)

(Received 1955 November 26)

Summary

A search is made for the λ 6561·023 deuterium line in eight centre and limb spectra of the Sun using an interferometer with a resolving power of $1{\cdot}2 \times 10^5$. Near this wave-length there are two atmospheric water vapour lines at λ 6560·562 and λ 6561·097, the former of which is shown to be blended with a weak solar line at λ 6560·596. An analysis of the line λ 6561·097 for centre, East and West limbs yields equivalent widths of the deuterium line of $0{\cdot}0 \pm 1{\cdot}1$, $0{\cdot}03 \pm 0{\cdot}5$, $0{\cdot}09 \pm 0{\cdot}7$ mA respectively. There is, therefore, no evidence for deuterium on the Sun. The observational errors, however, are such that a weak line of equivalent width 1·1 mA (corresponding to $^2H/^1H = 4 \times 10^{-5}$) might remain undetected. de Jager's claim to have detected a line of 6 mA was based on a single centre spectrum from which sufficient photometric accuracy could not be obtained.

Introduction.—The solar abundances of deuterium, lithium and beryllium are of particular interest because these elements are rapidly destroyed by thermonuclear reactions at the temperature of the solar interior. Greenstein, Richardson and Tandberg–Hanssen (**8, 9**) have observed that the solar abundance ratio Be/Li is about 30 times the meteoric value; this is taken as evidence that mixing may occur between the photosphere and the depth where the Li but not the Be abundance is much reduced (about 0·5 solar radii) but no deeper. It is important therefore to try to detect deuterium in the Sun since Salpeter (**23**) calculates that it should have a mean life of 5×10^9 years at a depth of only 0·14 solar radii (100 000 km) and so should be absent on the mixing hypothesis.

The atomic spectrum of terrestrial hydrogen, which contains 0·015 per cent ^2H (**10, 25**), shows the deuterium lines as faint satellites to the blue of the hydrogen lines; the separation is proportional to the wave-length of the hydrogen line and equals 1·785 A at Hα. The first suggestion that deuterium could be detected on the Sun was made in 1931 by Menzel (**13**) who showed that an unidentified line of intensity -3 is listed in Rowland's Revision close to the predicted wave-length of the deuterium satellite to Hβ. The region, however, is heavily blended with solar lines and he could find no other coincidences of unidentified with deuterium lines. The deuterium line which should be most intense in the visible solar spectrum is the 2^2P^0-3^2D transition (λ6561·023) in the wing of Hα and lies close to two atmospheric lines. Although Claas (**2**), from an inspection of the single

* Radcliffe Travelling Fellow in Astronomy.

spectrum of the Utrecht Atlas (**4**), finds no evidence for a depression greater than 2 mA at this wave-length, de Jager (**3, 4**) claims that this spectrum shows a depression of 6 mA corresponding to his predicted profile of the deuterium line. However, to detect so weak a line in the presence of the water vapour lines clearly requires more than one spectrum and for this purpose new observations have been obtained with high resolving power using an interferometer. It is possible to allow for the effect of the water vapour lines (which are formed by exponential absorption and have symmetrical profiles) and so derive the true wing of Hα from the observed profile; the deuterium line, if present, should then appear as a dip in this continuum. Although such a dip is likely to be very weak, a comparison between spectra of the solar centre and limb (where the solar lines will be shifted by solar rotation) and between spectra obtained on days of different atmospheric water vapour content should distinguish between a weak solar line at λ 6561·023 and the random errors of observation.

1. *Observations and photometry*

1.1. *Method of observation.*—Spectra of the violet wing of Hα were obtained using a Fabry–Perot etalon placed behind the Oxford 19·8 m. telescope (**19**) and spectroscope (**20**) using Treanor's method of circular channels (**28**). In the arrangement of this method for line profile measurement suggested by Dr M. G. Adam, the etalon is adjusted to give a broad central heterochromatic fringe and then tilted slightly so that the line falls on to this fringe; in this way the difficulties of photometry around a narrow circular channel are avoided.

The apparatus is identical with that used by Hindmarsh (**11**). A 1·5 mm interferometer spacer was used in conjunction with a slit width of 0·20 mm; in this case the order-to-order scattered light (which increases with slit width and spacer distance) corresponds to only about 2·5 per cent. The general scattered light in the primary spectroscope (**20**) with the small slit height used (3·2 mm) is calculated to be only 0·06 per cent. By mounting the interferometer with its wedge angle perpendicular to the dispersion, the ghost images were thrown vertically clear of the central fringe; thus a line height of about 3 mm was available for photometry. Spectra of the Cd line (λ 6438) which were taken by Hindmarsh shortly after the present observations showed a resolving power of $1{\cdot}2 \times 10^5$ with the 1·5 mm spacer.

Fifteen spectra were taken of the centre of the disk, and seven of the East limb and five of the West limb of the Sun. The limb spectra were taken with the slit along the E–W line and the slit centre at the point inside the limb corresponded to $\cos\theta = 0{\cdot}233$. To calibrate the plates the etalon was removed and a spectrum of the centre of the disk was taken through a calibrated step-wedge (**1**) mounted just in front of the spectroscope slit. A similar spectrum without the wedge was taken for the correction for non-uniform illumination of the slit. Diaphragms in the focal plane of the camera allowed either three limb or three centre interference spectra to be taken on each plate in addition to the two calibration spectra. The exposure times for all spectra on each plate were made equal by adjusting the slit width for the calibration spectra and by using neutral tint filters. The backed Ilford Rapid Process Panchromatic plates used were stored for 24 h after exposure to equalize the fading of the latent image on all exposures before brush development in Parkhurst developer.

Three plates which were judged to have the most suitable photographic density were selected for measurement:

1. Three spectra of the centre of the disk ($\cos\theta = 1{\cdot}0$) on 1954 Oct. 28 at 10^h08^m, 10^h13^m and 10^h20^m U.T.
2. Three spectra of the East limb ($\cos\theta = 0{\cdot}234$) on 1954 Oct. 30 at 9^h47^m, 9^h58^m and 10^h08^m U.T.
3. Two spectra of the West limb ($\cos\theta = 0{\cdot}233$) on 1954 Nov. 9 at 10^h05^m and 10^h16^m U.T.

1.2. *Microphotometry of the plates.*—Microphotometer (**18**) tracings of the central heterochromatic fringe were made parallel to the dispersion with high magnification ($\times 48{\cdot}2$) using a photometer slit 0·25 mm high and 0·057 mm wide. In order to reduce the effects of plate grain, these tracings were made at five heights, 0·25 mm apart, in each spectrum. A low-magnification tracing ($\times 6{\cdot}98$) of the whole of each spectrum parallel to the dispersion was also made; this was used to find the dispersion curve across the central fringe (see Section 2.1 below).

To find the characteristic curve for each plate, tracings were made parallel to the dispersion through each of the seven steps of the wedge. A tracing perpendicular to the dispersion of the spectrum without the step wedge gave the correction for non-uniform illumination along the slit. Seven points in both the lines and continuum in each step were measured so that forty-nine points were available to give a well determined characteristic curve for each plate. No wave-length dependence of the curves was found over the wave-length range used ($\lambda\lambda 6562{\cdot}8$–$74{\cdot}2$), so these curves were also applicable to the measured region of the interference spectra ($\lambda\lambda 6558$–62).

2. *Reduction of the microphotometer tracings*

2.1. *Determination of wave-lengths.*—Treanor (**28**) has shown that in the central heterochromatic fringe the dispersion along the radius z from the monochromatic centre is:

$$d\lambda/dz = -\lambda z/F^2 \qquad (1)$$

where F is the camera focal length. If p is the distance between monochromatic and heterochromatic centres and h is the distance from the heterochromatic centre along the same radius, then $z = (p + h)$ which on substituting in (1) and integrating gives:

$$\ln\left(\frac{\lambda}{\lambda_0}\right) = -\left(\frac{ph}{F^2} + \frac{h^2}{2F^2}\right) \qquad (2)$$

where λ_0 is the wave-length at the heterochromatic centre. With sufficient accuracy this may be written:

$$\lambda = \lambda_0\left(1 - \frac{ph}{F^2} - \frac{h^2}{2F^2}\right). \qquad (3)$$

In the low-magnification tracings the heterochromatic centre can be found from the outer heterochromatic fringes so that the distances (h) of lines from this centre in tracing units may be found. Four lines of known wave-length (shown with an asterisk in Table I) may then be used to find the unknowns p and λ_0 in eqn. (3) by least squares; the resulting dispersion curve gives the wave-length at h tracing units from the heterochromatic centre in the low-magnification tracing.

As the position of this centre is not known in the high-magnification tracings, the low-magnification dispersion curve must be written in terms of distances (h^*) measured from the Ti II line (λ6559·580) for which a corresponding distance (H^*) can be measured on the high-magnification tracings. The ratio (H^*/h^*) of high to low magnification is known, so that the high-magnification dispersion curve may be found. This curve, however, refers to the dispersion along a diameter through the heterochromatic centre, while the tracings refer to a set of chordal lines. True dispersion curves may be found by plotting a curve of errors for each tracing (derived from the four lines of known wave-length) and by using this to correct the radial dispersion curve; any error in the assumed value of (H^*/h^*) is also corrected by this procedure. In this way the wave-length may be found for each point measured on a high-magnification tracing.

2.2. *Determination of the mean profile* $I(\lambda)$. $g(\lambda)$.—Table I gives details of the identified lines in the region covered by the tracing and also of the deuterium line. The first and second columns give the element and the Rowland number in the disk from Rowland's Revision (**22**), while the last three columns give the wave-lengths for the three plates from Rowland's Revision corrected according to I.A.U. recommendations (**27**) and also corrected for solar rotation and Earth's motion.

TABLE I

Identified lines and the deuterium line

Element	Rowland number	Corrected wave-length		
		Centre	East limb	West limb
Atm. wv.*	—1N	6558·154	6558·154	6558·154
Ti II*	0	6559·567	6559·535	6559·602
Atm. wv.	1Nd ?	6560·562	6560·562	6560·562
^{2}H		6561·010	6560·978	6561·045
Atm. wv.*	—2	6561·097	6561·097	6561·097
^{1}H (Hα)	40	6562·799	6562·767	6562·834
Atm. wv.	—2	6563·525	6563·525	6563·525
Atm. wv.	—1	6564·067	6564·067	6564·067
Atm. wv.*	0	6564·212	6564·212	6564·212

(* used to determine wave-lengths)

The high-magnification tracings were measured from $\lambda\lambda$6558·8–6561·8 and converted to intensities by means of the characteristic curve. In the vicinity of the deuterium line ($\lambda\lambda$6560·2–6561·6) the measures were made at each tenth of a tracing square (approx. 0·013 A apart) on the *unsmoothed* tracings. In the region to the blue and red of this ($\lambda\lambda$6558·8–60·2 and $\lambda\lambda$6561·6–61·8) a smooth curve was drawn through the tracings and measures of this curve were made at every fifth of a tracing square. No smoothing was attempted in the central region in order that no distortion should be introduced or weak lines smoothed out. In the other regions, however, which are needed to find the continuous background it is advantageous to smooth out the plate grain. The scale in tracing units was converted to wave-lengths as described above so that for each of the five tracings in each spectrum the intensity in arbitrary units was known at each measured point.

This observed profile $O(\lambda)$ may be expressed as the product $I(\lambda) \cdot f(\lambda) \cdot g(\lambda)$, where $I(\lambda)$ is the profile of the continuous background (the wing of Hα), $g(\lambda)$ is the profile of any absorption lines that may be present and $f(\lambda)$ is the profile of the central heterochromatic fringe. At the three wave-length regions close to λ6559·0, λ6560·2 and λ6561·6 there are no absorption lines, so that here we may put $g(\lambda) = 1$. The factor $f(\lambda)$ may therefore be found for these wave-lengths by comparing the observed intensities with those of a standard profile of the Hα wing (**3**). The values of $f(\lambda)$ at intermediate wave-lengths may be found by fitting a power series interpolation formula. The central fringe was purposely made broad so that $f(\lambda)$ was a relatively slowly varying function and could always be represented with sufficient accuracy by either a quadratic or cubic equation. Since the tracings correspond to different cross-sections of the central fringe, $f(\lambda)$ had to be determined separately for each; the intensity in the Hα wing including superimposed absorption lines (i.e. $I(\lambda)g(\lambda)$) could then be derived at the measured points in each tracing. A profile was drawn and the intensity in the profile tabulated at 0·2A intervals; these intensities for the five tracings were then combined to give a mean profile in each spectrum. As the time interval between the first and last spectra on each plate did not exceed twenty minutes, little variation in the intensities of the atmospheric water vapour lines may be expected between different spectra on the same plate. No systematic difference between these spectra could be seen and so they were combined to give a mean profile.

The intensity at each point in a spectrum is the mean of five tracings; the r.m.s. deviation of a single tracing from this mean was calculated for about fifteen points in each plate and the average value of this r.m.s. deviation (σ_1) is given for each plate in the second column of Table II. The intensity at each point in the mean profile in each plate is the mean of two or three spectra; the r.m.s. deviation of a single spectrum from this mean was calculated for about fifteen points in each plate and the average value of this r.m.s. deviation (σ_2) is given for each plate

TABLE II

Average r.m.s. errors expressed as a percentage of the true continuum

Plate	σ_1	σ_2
Centre of disk (3 spectra)	0·73 per cent	0·54 per cent
East limb (3 spectra)	1·00 per cent	0·48 per cent
West limb (2 spectra)	0·90 per cent	0·42 per cent

in the third column of Table II. It is seen that σ_2 is significantly smaller than σ_1 as would be expected if the systematic differences between the spectra on the same plate are appreciably smaller than the random errors in each spectrum. Taking a mean profile from the spectra on each plate is therefore justified.

2.3 *Determination of the mean profile* $g(\lambda)$.—Our aim is to detect any depression in the Hα wing which remains when we have allowed for the water vapour lines (λ6560·562 and λ6561·097). To do this we must find $g(\lambda)$, the observed profile of these lines, then allow for the absorption profile of the water vapour lines and finally examine the nature of any residual absorption.

We obtain $g(\lambda)$ by dividing $I(\lambda)\,g(\lambda)$ obtained above by the standard Hα wing $I(\lambda)$; the resulting profile is thus independent of any assumption about the function $I(\lambda)$ except that both it and $f(\lambda)$ vary smoothly. The only additional assumption is that $g(\lambda)$ is unity (no absorption lines) in the three regions λ6559·0, λ6560·2 and λ6561·6. It is possible that faint absorption lines may be present although a search in these spectra gave no indication of them. The systematic error from this cause at either λ6560·2 or λ6561·6 is unlikely to exceed the average inter-spectrum scatter (σ_2) of 0·5 per cent and this would lead to a spurious difference in intensity between the red and blue wings of the water vapour line λ6561·097 of only 0·1 per cent, which is well within the random errors of these observations.

Fig. 1 shows the profile of $g(\lambda)$ obtained for the centre of the disk.

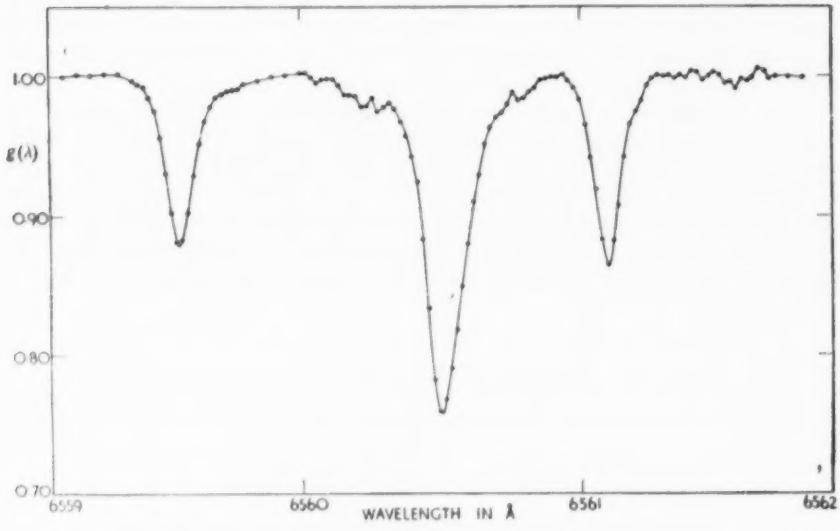

FIG. 1.—*The intensity profile* $g(\lambda)$ *for the centre of the solar disk.*

2.4. *Scattered light.*—For the purpose of detecting a weak line, only the distortion produced by the variation of the scattered light across the observed profile is important. Hindmarsh (**11**) has shown that the order-to-order scattered light for a 1·5 mm spacer is 2·25 per cent at the hetochromatic centre and varies as the inverse square of the distance from the adjacent order. Since the whole measured range of $g(\lambda)$ extends over only one fifth of the interorder distance near the heterochromatic centre, the variation of the scattered light across $g(\lambda)$ must be negligibly small.

3. *Discussion of the observed profile $g(\lambda)$*

In this profile the region of the deuterium line contains two blending lines (λ6560·562 and λ6561·097) which it is convenient to consider separately.

3.1. λ6560·562.—This line although identified as being due to atmospheric water vapour in Rowland's Revision, is listed as Nd? ("broad for its intensity"; "a double whose components are difficult to separate" (**21**)). The present observations confirm that the line is broad and also that its wave-length is variable; this suggests that the water vapour line is blended with a solar line. The components of this blend will be weak and therefore on the linear part of the curve of growth, so it may be assumed that the equivalent width (W_1) of the w.v. component is k_1 times that of (W_{wv}) of the w.v. line (λ6561·097) and that the equivalent width (W_2) of the solar component is k_2 times that (W_s) of the Ti II line (λ6559·580). The w.v. component is formed by exponential absorption, so that if $r_1(\lambda)$ and $r_2(\lambda)$ are the respective residual intensities at wave-length λ of the two components when unblended, the equivalent width (W_3) of the blend is given by

$$\int_{-\infty}^{+\infty} (1 - r_1(\lambda) r_2(\lambda)) d\lambda$$

which on expansion gives:

$$W_3 = k_1 W_{wv} + k_2 W_s - \int_{-\infty}^{+\infty} (1 - r_1(\lambda))(1 - r_2(\lambda)) d\lambda. \qquad (1)$$

If we assume that both components have a Gaussian profile of half-width σ, then eqn (1) becomes:—

$$W_3 = k_1 W_{wv} + k_2 W_s - \frac{0{\cdot}664 k_1 k_2 W_{wv} W_s}{\sigma} \qquad (2)$$

Since the third term (ϵ) on the right-hand side of eqn. (2) is small, it may be ignored in a first approximation (i.e. the equivalent width of the blend is taken to be the sum of the equivalent widths of its components), and with this equation of condition a least-squares solution for k_1 and k_2 is made. From these preliminary values of k_1 and k_2 and by taking $\sigma = 0{\cdot}13$A (the mean value for λ6561·097 and λ6559·580), the third term (ϵ) may be found; this term can now be included in the equation of condition and a final solution made for the factors k_1 and k_2 and hence for W_1 and W_2. Values of these equivalent widths for the three plates are given in Table IIIa; the last column gives the observed *minus* calculated residuals for the blend, which are seen to be satisfactorily small. The plate-to-plate variation of the atmospheric component is due to the variation in atmospheric water vapour while the solar component shows the centre-limb variation.

TABLE III

(a) Equivalent widths in mA

Plate	observed			calculated 6560·562				W_3 obs-calc
	W_s	W_3	W_{wv}	W_1	W_2	ϵ	W_3	
Centre	17·32	49·06	16·08	38·74	8·04	−1·47	45·31	+3·75
East	28·54	58·45	21·48	51·75	13·25	−3·23	61·77	−3·32
West	25·42	34·53	9·47	22·82	11·80	−1·27	33·35	+1·18

(b) Wave-lengths in A

Plate	Δ	Blend λ_{obs}	wv comp. λ_{calc}	solar comp. λ_{calc}	blend λ_{calc}	blend $\lambda_{obs}-\lambda_{calc}$
Centre	−0·013	6560·509	6560·499	6560·583	6560·514	−0·005
East	−0·045	·513	·499	·551	·510	+0·003
West	+0·022	·538	·499	·618	·540	−0·002

The shift of the solar lines (Δ) is known for each plate (Table IIIb, column one) so that knowing the intensities of the two components, their wave-lengths may be deduced It is assumed that the observed wave-length centre of gravity of the blend (λ_{wv+s}) is the sum of the centres of gravity of the components weighted according to their equivalent widths. For this purpose it is necessary to use the approximate values for which (W_1+W_2) equals W_3, and this gives for the equation of condition $\lambda_{wv}W_1-(\lambda_s+\Delta)W_2=\lambda_{wv+s}W_3$ for each plate. The least-squares solution for the wave-lengths of the water vapour component (λ_{wv}), the solar component (λ_s) and the resulting blend are given in columns four, five and six of Table IIIb; the observed *minus* calculated residuals for the wave-length of the blend are given in the last column.

The smallness of both the equivalent width and wave-length residuals in these approximate calculations confirms the hypothesis that λ6560·562 is a blend of an atmospheric water vapour with a solar line. The only line near to the solar component (λ6560·596) which is listed in the *Revised Multiplet Table* (**15**) is the $4p^3D_1$–$7d^3F_2$ transition of Si I observed by Kiess (**12**) in an arc spectrum at λ6560·68. While the coincidence in wave-length is within the error of the laboratory wave-length of 0·1A estimated by Kiess, much stronger lines of Si I of similar excitation potential are not found in the solar spectrum, so that the identification with Si I is highly unlikely.

The complexity of λ6560·562 and in particular the presence of a solar line make it unsuitable for further analysis to detect the deuterium line in its red wing.

3.2. λ6561·097.—This line is an overtone line of the P branch (λ6524 band) of the fundamental vibration spectrum of atmospheric water vapour (**7**) and lies in the region where the red wing of the deuterium line may be expected. Ideally the deuterium wing might be detected in the water vapour line by an analysis similar to that used for λ6560·562. Since, however, the equivalent width of the deuterium wing cannot exceed a few milliangstroms, the comparison water vapour line would need to be unblended to a much higher accuracy and it cannot be certain that any of the neighbouring water vapour lines (obtainable with a simultaneous exposure) have the required purity. The deuterium line will be stronger in the blue than the red wing of λ6561·097, however, so that it should be possible to detect the deuterium line by analysing the symmetry of the observed line, if the water vapour line can be taken to be symmetrical. The Doppler half-width of the water vapour line will be approximately 0·02A, while the intrumental half-width found by Hindmarsh is 0·051A, and consequently the observed half-width of 0·105A must be due to the combined influence of the interferometric profile and collisional broadening. Van de Hulst (**29**) has shown that asymmetry effects predicted by the Lenz formula are not found in the atmospheric oxygen vibration lines (e.g. Panofsky (**16**)), and Elsasser (**5**) considers that there should be little or

no asymmetry in water vapour lines resulting from non-electronic transitions. It is, therefore, legitimate for such a weak line (equivalent width 10–20 mA) to assume that its profile is symmetrical.

Let the observed profile $g(\lambda)$ of $\lambda 6561{\cdot}097$ be considered as a symmetrical water vapour line $\alpha(\lambda_0' + \Delta\lambda)$ superposed on a background $\beta(\lambda_0' + \Delta\lambda)$ so that:

$$g(\lambda_0' + \Delta\lambda) = \alpha(\lambda_0' + \Delta\lambda)\beta(\lambda_0' + \Delta\lambda)$$

and λ_0' is the wave-length centroid of $\alpha(\lambda_0' + \Delta\lambda)$. Now if λ_0 is the observed wave-length centroid of $g(\lambda_0 + \Delta\lambda)$, a function $s(\lambda_0 + \Delta\lambda)$ can be found which is

$$s(\lambda_0 + \Delta\lambda) = \tfrac{1}{2}\{g(\lambda_0 + \Delta\lambda) + g(\lambda_0 - \Delta\lambda)\}.$$

Since $\beta(\lambda_0' + \Delta\lambda)$ is very nearly unity, λ_0 and λ_0' will only differ by about 0.001 A, so that for these purposes it is permissible to put $\lambda_0 = \lambda_0'$ and obtain

$$s(\lambda_0 + \Delta\lambda) = \tfrac{1}{2}\alpha(\lambda_0 + \Delta\lambda)\{\beta(\lambda_0 + \Delta\lambda) + \beta(\lambda_0 - \Delta\lambda)\}.$$

The quotient $Q(\lambda_0 + \Delta\lambda)$ obtained by dividing $g(\lambda_0 + \Delta\lambda)$ by $s(\lambda_0 + \Delta\lambda)$ may be calculated from the observed profile for each wave-length; it equals

$$\frac{2\beta(\lambda_0 + \Delta\lambda)}{\beta(\lambda_0 + \Delta\lambda) + \beta(\lambda_0 - \Delta\lambda)}$$

and is seen to be a function of the unknown background only.

The deuterium line will be broad and shallow, because the combined Stark and Doppler effects will produce a broadening of its core comparable to that in Hα, so that for simplicity the deuterium wing may be considered as a straight line of slope m. The background profile containing this hypothetical line is shown in Fig. 2 and has the form: $\beta(\lambda_0 + \Delta\lambda) = 1{\cdot}0 + m(\lambda - \lambda_1)$ in the wave-length region $(\lambda < \lambda_1)$ which is being considered. For this background, $Q(\lambda_0 + \Delta\lambda)$ is a straight line equal to unity at λ_0 and of slope M where

$$M = \frac{m}{m(\lambda_0 - \lambda_1) + 1{\cdot}0} \simeq m \text{ to sufficient accuracy.}$$

Now M can be found by passing a straight line through the calculated points of $Q(\lambda_0 + \Delta\lambda)$ by least squares and so the slope m of the background may be found. These results are given in Table IV for the three plates: column one gives the plate, column two gives the slope m as a percentage of the continuous background per A, column three gives the r.m.s. error (σ_m) of this slope, while column four gives the maximum slope (m_{max}) corresponding to a depression which could lie within this error ($m_{max} = m + \sigma_m$). These background slopes are very small, vary at random from plate to plate and are well within their r.m.s. errors; they are

TABLE IV

Plate	m	σ_m	m_{max}	W (mA)	$\left(\frac{^2H}{^1H}\right)$	W_{max} (mA)	$\left(\frac{^2H}{^1H}\right)_{max}$
Centre	−0·06	± 1·10	+1·04	0·00	0·0	1·07	$4{\cdot}0 \times 10^{-5}$
East Limb	+0·06	± 0·94	+1·00	0·03	$0{\cdot}2 \times 10^{-5}$	0·55	$4{\cdot}4 \times 10^{-5}$
West Limb	+0·15	± 1·27	+1·42	0·09	$0{\cdot}7 \times 10^{-5}$	0·79	$6{\cdot}3 \times 10^{-5}$

(b) Wave-lengths in A

Plate	Δ	Blend λ_{obs}	wv comp. λ_{calc}	solar comp. λ_{calc}	blend λ_{calc}	blend λ_{obs}-λ_{calc}
Centre	−0·013	6560·509	6560·499	6560·583	6560·514	−0·005
East	−0·045	·513	·499	·551	·510	+0·003
West	+0·022	·538	·499	·618	·540	−0·002

The shift of the solar lines (Δ) is known for each plate (Table IIIb, column one) so that knowing the intensities of the two components, their wave-lengths may be deduced It is assumed that the observed wave-length centre of gravity of the blend (λ_{wv+s}) is the sum of the centres of gravity of the components weighted according to their equivalent widths. For this purpose it is necessary to use the approximate values for which (W_1+W_2) equals W_3, and this gives for the equation of condition $\lambda_{wv}W_1-(\lambda_s+\Delta)W_2=\lambda_{wv+s}W_3$ for each plate. The least-squares solution for the wave-lengths of the water vapour component (λ_{wv}), the solar component (λ_s) and the resulting blend are given in columns four, five and six of Table IIIb; the observed *minus* calculated residuals for the wave-length of the blend are given in the last column.

The smallness of both the equivalent width and wave-length residuals in these approximate calculations confirms the hypothesis that λ6560·562 is a blend of an atmospheric water vapour with a solar line. The only line near to the solar component (λ6560·596) which is listed in the *Revised Multiplet Table* (**15**) is the $4p^3D_1$–$7d^3F_2$ transition of Si I observed by Kiess (**12**) in an arc spectrum at λ6560·68. While the coincidence in wave-length is within the error of the laboratory wave-length of 0·1A estimated by Kiess, much stronger lines of Si I of similar excitation potential are not found in the solar spectrum, so that the identification with Si I is highly unlikely.

The complexity of λ6560·562 and in particular the presence of a solar line make it unsuitable for further analysis to detect the deuterium line in its red wing.

3.2. λ6561·097.—This line is an overtone line of the P branch (λ6524 band) of the fundamental vibration spectrum of atmospheric water vapour (**7**) and lies in the region where the red wing of the deuterium line may be expected. Ideally the deuterium wing might be detected in the water vapour line by an analysis similar to that used for λ6560·562. Since, however, the equivalent width of the deuterium wing cannot exceed a few milliangstroms, the comparison water vapour line would need to be unblended to a much higher accuracy and it cannot be certain that any of the neighbouring water vapour lines (obtainable with a simultaneous exposure) have the required purity. The deuterium line will be stronger in the blue than the red wing of λ6561·097, however, so that it should be possible to detect the deuterium line by analysing the symmetry of the observed line, if the water vapour line can be taken to be symmetrical. The Doppler half-width of the water vapour line will be approximately 0·02A, while the intrumental half-width found by Hindmarsh is 0·051A, and consequently the observed half-width of 0·105A must be due to the combined influence of the interferometric profile and collisional broadening. Van de Hulst (**29**) has shown that asymmetry effects predicted by the Lenz formula are not found in the atmospheric oxygen vibration lines (e.g. Panofsky (**16**)), and Elsasser (**5**) considers that there should be little or

no asymmetry in water vapour lines resulting from non-electronic transitions. It is, therefore, legitimate for such a weak line (equivalent width 10–20 mA) to assume that its profile is symmetrical.

Let the observed profile $g(\lambda)$ of $\lambda 6561{\cdot}097$ be considered as a symmetrical water vapour line $\alpha(\lambda_0' + \Delta\lambda)$ superposed on a background $\beta(\lambda_0' + \Delta\lambda)$ so that:

$$g(\lambda_0' + \Delta\lambda) = \alpha(\lambda_0' + \Delta\lambda)\beta(\lambda_0' + \Delta\lambda)$$

and λ_0' is the wave-length centroid of $\alpha(\lambda_0' + \Delta\lambda)$. Now if λ_0 is the observed wave-length centroid of $g(\lambda_0 + \Delta\lambda)$, a function $s(\lambda_0 + \Delta\lambda)$ can be found which is

$$s(\lambda_0 + \Delta\lambda) = \tfrac{1}{2}\{g(\lambda_0 + \Delta\lambda) + g(\lambda_0 - \Delta\lambda)\}.$$

Since $\beta(\lambda_0' + \Delta\lambda)$ is very nearly unity, λ_0 and λ_0' will only differ by about 0.001 A, so that for these purposes it is permissible to put $\lambda_0 = \lambda_0'$ and obtain

$$s(\lambda_0 + \Delta\lambda) = \tfrac{1}{2}\alpha(\lambda_0 + \Delta\lambda)\{\beta(\lambda_0 + \Delta\lambda) + \beta(\lambda_0 - \Delta\lambda)\}.$$

The quotient $Q(\lambda_0 + \Delta\lambda)$ obtained by dividing $g(\lambda_0 + \Delta\lambda)$ by $s(\lambda_0 + \Delta\lambda)$ may be calculated from the observed profile for each wave-length; it equals

$$\frac{2\beta(\lambda_0 + \Delta\lambda)}{\beta(\lambda_0 + \Delta\lambda) + \beta(\lambda_0 - \Delta\lambda)}$$

and is seen to be a function of the unknown background only.

The deuterium line will be broad and shallow, because the combined Stark and Doppler effects will produce a broadening of its core comparable to that in Hα, so that for simplicity the deuterium wing may be considered as a straight line of slope m. The background profile containing this hypothetical line is shown in Fig. 2 and has the form: $\beta(\lambda_0 + \Delta\lambda) = 1{\cdot}0 + m(\lambda - \lambda_1)$ in the wave-length region $(\lambda < \lambda_1)$ which is being considered. For this background, $Q(\lambda_0 + \Delta\lambda)$ is a straight line equal to unity at λ_0 and of slope M where

$$M = \frac{m}{m\,(\lambda_0 - \lambda_1) + 1{\cdot}0} \simeq m \text{ to sufficient accuracy.}$$

Now M can be found by passing a straight line through the calculated points of $Q(\lambda_0 + \Delta\lambda)$ by least squares and so the slope m of the background may be found. These results are given in Table IV for the three plates: column one gives the plate, column two gives the slope m as a percentage of the continuous background per A, column three gives the r.m.s. error (σ_m) of this slope, while column four gives the maximum slope (m_{max}) corresponding to a depression which could lie within this error ($m_{max} = m + \sigma_m$). These background slopes are very small, vary at random from plate to plate and are well within their r.m.s. errors; they are

TABLE IV

Plate	m	σ_m	m_{max}	W (mA)	$\left(\frac{^2H}{^1H}\right)$	W_{max} (mA)	$\left(\frac{^2H}{^1H}\right)_{max}$
Centre	−0·06	± 1·10	+1·04	0·00	0·0	1·07	$4{\cdot}0 \times 10^{-5}$
East Limb	+0·06	± 0·94	+1·00	0·03	$0{\cdot}2 \times 10^{-5}$	0·55	$4{\cdot}4 \times 10^{-5}$
West Limb	+0·15	± 1·27	+1·42	0·09	$0{\cdot}7 \times 10^{-5}$	0·79	$6{\cdot}3 \times 10^{-5}$

due doubtless to the small photometric errors in the observed profiles. There is therefore no evidence for a deuterium line in this wave-length region.

de Jager (**3, 4**) has computed the deuterium profiles which would be produced by different abundance ratios ($^2H/^1H$) and these may be interpolated to calculate abundances from the present observations. It is assumed that the straight line profiles derived above approximate to the de Jager profile which has the same equivalent width over the wave-length range observed; the equivalent width (W) of the *whole* deuterium line and the abundance ratio ($^2H/^1H$) which correspond to a given slope (m) of the background can then be found. Columns five and six of Table IV give W and $^2H/^1H$ for the mean values of the slopes derived for each plate, and columns seven and eight give the same quantities for the maximum depression which could be present and be just within the r.m.s. error. The mean abundance from the three plates is only $0{\cdot}3 \times 10^{-5}$ and lies well within the errors of observation. The deuterium line should be strongest in the centre spectrum and here the strongest line which could just remain undetected would have an equivalent width of 1·1 mA, corresponding to a maximum abundance ratio of 4×10^{-5}. We may compare our observed abundance ratio of $0{\cdot}4 \times 10^{-5}$ and the maximum observable value of 4×10^{-5} with de Jager's claim to have found a line of equivalent width 6 mA corresponding to an abundance ratio $14{\cdot}5 \times 10^{-5}$ from the inspection of a single spectrum.

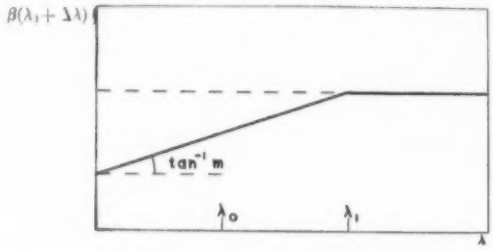

FIG. 2.—*Background profile* $\beta(\lambda_0 + \Delta\lambda)$ *containing the hypothetical deuterium line.*

Severny (**24**) claims to have found a 100 mA asymmetry between the red and blue wings of Hα which he attributes to deuterium. He assumes that his apparatus function is symmetrical because he observes that other strong solar lines including the D_2 sodium line are symmetrical; it is known, however, that D_2 is asymmetrical on account of a strong water vapour component in its violet wing. Previous photographic (**6, 26**) and photoelectric (**17**) observations of Hα give no evidence of any asymmetry and Severny's claim for a high deuterium abundance must be treated with reserve.

The deuterium line, if present, must be so weak that any attempt to detect it requires many independently reduced spectra; it is found from a series of such spectra of both solar centre and limb taken on days of different atmospheric water vapour content that no deuterium line is present. It is possible, however, that a line exists which is weaker than the limit set by photographic photometry, which corresponds to an abundance ratio ($^2H/^1H$) of 4×10^{-5}. Any attempt to detect such a so weak line will require a new photometric technique.

Acknowledgments.—This problem was suggested to me by Prof. H. H. Plaskett: I should like to express my sincere thanks for the generous help and encouragement which he has always given to me. I am grateful to Dr M. G. Adam (who suggested the use of the central heterochromatic fringe for profile determination) for her invaluable assistance in making the observations. I am also indebted both to her and Dr W. R. Hindmarsh for many helpful discussions. Thanks are due to Dr J. B. Sykes for his translation of the paper by Severny.

University Observatory,
Oxford:
1955 *November* 25.

References

(1) R. J. Bray, *M.N.*, **114,** 540, 1954; Comm. Univ. Obs. Oxf. No. 45.
(2) W. J. Claas, *Recherches Utrecht*, **12** (1), 36, 1951.
(3) C. de Jager, *Recherches Utrecht*, **13** (1), 1952.
(4) C. de Jager, Mem. in-8° Soc. Roy. Sci. Liège, Tome XIV, 460, 1954.
(5) W. M. Elsasser, *Ap. J.*, **87,** 497, 1938.
(6) D. S. Evans, *M.N.*, **100,** 156, 1940; Comm. Univ. Obs. Oxf. No. 17.
(7) K. Freudenburg and R. Mecke, *Zeits. Phys.*, **81,** 465, 1933.
(8) J. L. Greenstein and R. S. Richardson, *Ap. J.*, **113,** 536, 1951.
(9) J. L. Greenstein and E. Tandberg-Hanssen, *Ap.J.*, **119,** 113, 1954.
(10) N. F. Hall and T. O. Jones, *J. Amer. Chem. Soc.*, **58,** 1915, 1936.
(11) W. R. Hindmarsh, *M.N.*, **115,** 270, 1955; Comm. Univ. Obs. Oxford No. 47.
(12) C. C. Kiess, *Bur. St. Journ. Res.*, **21,** 185 (R.P. 1124), 1938.
(13) D. H. Menzel, *P.A.S.P.*, **44,** 41, 1932.
(14) M. Minnaert, G. F. W. Mulders and J. Houtgast, *Photometric Atlas of the Solar Spectrum*, Utrecht, 1940.
(15) C. E. Moore, *Revised Multiplet Table*, 1945.
(16) H. A. Panofsky, *Ap. J.*, **97,** 180, 1943.
(17) A. K. Pierce, *Ap.J.*, **120,** 233, 1954.
(18) H. H. Plaskett, *M.N.*, **95,** 160, 1934; Comm. Univ. Obs. Oxf. No. 4.
(19) H. H. Plaskett, *M.N.*, **99,** 289, 1939; Comm. Univ. Obs. Oxf. No. 14.
(20) H. H. Plaskett, *M.N.*, **112,** 177, 1952; Comm. Univ. Obs. Oxf. No. 33.
(21) H. A. Rowland, *Ap. J.*, **1,** 29, 1895.
(22) *Rowland Revision*, Publ. Carnegie Inst. Washington, 1928.
(23) E. E. Salpeter, *Phys. Rev.*, **97,** 1237, 1955.
(24) A. B. Severny, *Doklady Akademii Nauk SSSR*, **97,** 789, 1954.
(25) J. A. Swartout and M. Dole, *J. Amer. Chem. Soc.*, **61,** 2025, 1939.
(26) P. ten Bruggencate, H. Gollnow, S. Gunther and H. Strohmeier, *Z. f. Ap.*, **26,** 51, 1949.
(27) *Trans. I.A.U.*, Vol. IV, p. 60, 1932.
(28) P. J. Treanor, *M.N.*, **109,** 389, 1949; Comm. Univ. Obs. Oxf. No. 28.
(29) H. C. van de Hulst, *Ann. d'Ap.* **8,** 1, 1945.

ASTROMETRIC OBSERVATIONS OF EROS DURING THE 1954 OPPOSITION

J. v. B. Lourens

(Communicated by H. M. Astronomer at the Cape)
(Received 1955 November 8)

Summary

Table I gives the astrometric positions on the FK3 System for the equinox of 1950·0 of Eros on 45 occasions as observed at the Cape during the 1954 opposition.

At its opposition in 1954, Eros was too far south to be conveniently observed from any northern observatory. An effort was therefore made at the Cape to secure accurate observations of its position at approximately four day intervals from the end of January to the end of July. The observations were made with the 24-inch Victoria Refractor (scale 1 mm = 30″·64). The telescope was used west of the pier and the plates taken, as far as possible, when Eros was close to the meridian and thus at a relatively small zenith distance. Ilford Astronomical Zenith plates were used and in general four exposures were made on each plate. The exposure times varied from five minutes to one minute depending on the brightness of Eros, which even at its brightest ($11^m·7$) was nearly two magnitudes fainter than the reference stars. Stars were used for guiding so that on the longer exposures the images of Eros are slightly trailed.

The plates were measured with the Hilger Long-Screw Machine specially designed for astrometric work. Each plate was measured by two independent measurers, each measurer measuring both forward and reversed. The reference stars for reducing the plate measures were selected from the following catalogues:

Yale Zone Catalogues, $-22°$ to $-27°$ and $-27°$ to $-30°$, Epoch 1933.

Cape Zone Catalogues, $-30°$ to $-35°$ and $-35°$ to $-40°$, Epochs 1932 and 1936.

Cape Astrographic Zone Bright and Faint Star Catalogues, Epoch 1900.

To reduce the effect of uncertainties in the proper motions which are involved in bringing the catalogue places up to the epoch of the Eros plates, as many reference stars as could be found in the catalogues were used, though a few had to be rejected on account of poor distribution over the plate. Altogether 544 reference stars were used for the 45 plates, an average of 12 per plate, though the actual number on a single plate ranged from 7 to 16. Standard coordinates for these stars were computed for each plate, the unit for both the calculations and the measures being 0·0001 mm.

The ordinary linear plate constants were found by the Dyson–Christie method and were used both to reduce the measured position of Eros and to calculate the residuals (observed coordinate − computed coordinate) for the reference stars. These residuals are relatively large for those stars for which the proper motion is poorly determined. A second solution was therefore made for each plate

using the second set of measures and the observed positions of the reference stars deduced from the first set of measures and reductions. In a few cases where the distribution of the catalogue stars was poor, extra stars whose coordinates had been determined from the first set of measures were used for the reduction of the second set. The residuals from this second solution are small and presumably arise principally from the error of measurement.

The residuals obtained from the first solution were analysed to investigate the effect of the second and third order terms on the linear plate constants and to compute the necessary correction functions. This analysis indicated that the plates were very slightly tilted in the right ascension direction and that the cubic scale term is appreciable. There were insufficient data either to establish the existence or to evaluate the presence of a colour–magnitude effect; nor could such an effect be eliminated by the choice of reference stars of the same colour and magnitude as Eros. The mean photographic magnitude of the reference stars used is 9·7 and their mean colour index +0·47, though the means for the individual plates range from 8·7 to 10·6 and from −0·01 to +0·92. According to the ephemeris, the magnitude of Eros varied from 12·7 at the end of January to 11·7 at the time of opposition on May 14 and then to 13·8 by the end of July.

The positions finally deduced for Eros are given for each plate in the third and fourth columns of Table I. They are the mean places resulting from the two independent measures of all the exposures on the plate to which have been applied the plate corrections deduced from the analysis of the residuals of the reference stars and the systematic corrections needed to reduce the catalogue places of the reference stars to FK 3 system. The U.T. of the mid-time of the exposures is given in the second column of Table I and the estimated probable error of the given position, assumed to be the same in both coordinates, is given in the fifth column. This error includes both the errors of measurement and of the assumed positions of the reference stars. The sixth column gives the actual difference between the results obtained from the first and second set of measures.

These differences result mainly from the two measurements of the Eros images since the same reference stars were used for both solutions and the plates were centred on Eros. They indicate ±0″·035 in each coordinate as the probable error of the mean of the two sets of measures of the Eros images. The corresponding probable error for a star, as found from the differences of the two measures of each plate, averages ±0″·040 for all the plates, but varies with the exposure time and clearly shows the decrease in precision of measurement as the size of the image increases. The average value for plates with one minute exposure is ±0″·034, sufficiently close to that found for the much fainter Eros images to indicate that this is approaching the optimum precision that can be obtained from this series of plates.

The probable error of a single reference star as determined from the residuals of the first set of measures is ±0″·309 for all the plates, but there is a variation with the catalogue from which the assumed places were derived. Table II shows the average probable error corresponding to the different catalogues used. These probable errors indicate mainly the relative error of the proper motion contained in the positions of the reference stars at the epoch of the Eros plates. It will be noticed that the C.A.Z. proper motions, which were obtained by the differential measurement of two sets of photographic plates, are markedly

TABLE I

Serial No.	U.T. 1954	Equinox 1950·0 and FK3 system R.A. h m s	Dec. ° ′ ″	P.E. ″	Eros Measure (1st minus 2nd) s	″
1	Jan. 28·09473	14 23 03·120	−26 29 26·33	±0·14	−0·027	+0·28
2	Feb. 01·09651	14 33 26·917	−28 15 12·00	·16	−0·018	−0·10
3	,, 04·11390	14 41 09·706	−29 32 22·18	·12	−0·006	−0·03
4	,, 07·12328	14 48 44·051	−30 47 06·00	·18	+0·012	−0·08
5	,, 13·12817	15 03 25·581	−33 09 34·57	·11	−0·008	−0·19
6	,, 21·12000	15 21 56·320	−36 05 47·69	·09	−0·009	+0·07
7	,, 24·12140	15 28 30·719	−37 08 09·77	·09	−0·005	−0·19
8	,, 28·12279	15 36 53·026	−38 28 10·20	·09	−0·003	−0·20
9	Mar. 04·14594	15 44 46·705	−39 45 05·97	·11	−0·005	−0·10
10	,, 08·14227	15 52 01·527	−40 58 06·87	·09	−0·022	+0·02
11	,, 12·12631	15 58 34·925	−42 07 33·49	·08	+0·004	+0·04
12	,, 15·11101	16 03 00·683	−42 57 26·70	·09	+0·004	+0·03
13	,, 18·13822	16 07 02·165	−43 46 11·11	·09	+0·004	−0·04
14	,, 22·12285	16 11 33·380	−44 47 26·51	·09	+0·003	−0·05
15	,, 25·13726	16 14 19·372	−45 31 31·82	·06	−0·008	−0·15
16	,, 30·11283	16 17 32·234	−46 39 41·41	·06	−0·002	−0·08
17	Apr. 03·09728	16 18 46·103	−47 29 37·90	·05	−0·005	+0·13
18	,, 07·09913	16 18 42·142	−48 14 53·95	·07	+0·011	−0·01
19	,, 11·08384	16 17 17·262	−48 54 13·40	·08	+0·006	+0·07
20	,, 15·06658	16 14 30·195	−49 26 46·67	·06	+0·013	+0·04
21	,, 25·04015	16 01 43·495	−50 10 41·29	·08	−0·010	+0·12
22	,, 27·01518	15 58 18·978	−50 11 42·60	·06	−0·021	+0·04
23	May 06·96752	15 38 13·660	−49 30 39·03	·08	−0·002	−0·11
24	,, 10·91491	15 29 41·412	−48 52 10·27	·07	−0·003	0·00
25	,, 19·91364	15 11 22·956	−46 42 08·00	·06	−0·008	+0·14
26	,, 20·90058	15 09 34·563	−46 24 51·21	·08	+0·005	−0·02
27	,, 21·89763	15 07 48·166	−46 06 54·05	·09	+0·002	0·00
28	,, 24·88321	15 02 50·174	−45 10 31·90	·08	+0·011	+0·01
29	,, 30·87483	14 54 35·345	−43 08 50·37	·10	−0·008	−0·06
30	June 02·85517	14 51 24·579	−42 05 57·97	·07	−0·008	+0·03
31	,, 05·87999	14 48 49·215	−41 01 52·00	·10	−0·004	−0·03
32	,, 09·85420	14 46 23·405	−39 38 35·95	·11	+0·004	+0·03
33	,, 13·83832	14 44 59·990	−38 17 39·28	·10	+0·022	0·00
34	,, 17·82715	14 44 34·789	−37 00 20·78	·09	+0·002	+0·04
35	,, 18·82681	14 44 37·012	−36 41 39·55	·11	−0·004	−0·04
36	,, 21·84316	14 45 03·192	−35 47 06·77	·10	+0·002	−0·07
37	,, 27·79117	14 47 15·028	−34 08 12·18	·15	−0·010	−0·03
38	,, 30·80023	14 48 58·236	−33 22 44·67	·14	+0·005	+0·07
39	July 04·79085	14 51 49·539	−32 27 16·88	·18	−0·009	−0·04
40	,, 13·76928	15 00 18·703	−30 41 47·14	·18	−0·001	+0·04
41	,, 14·76410	15 01 24·312	−30 31 38·41	·13	−0·004	+0·06
42	,, 16·75410	15 03 40·373	−30 12 12·40	·13	+0·002	+0·06
43	,, 21·75299	15 09 48·982	−29 28 11·30	·12	−0·001	−0·04
44	,, 25·75385	15 15 09·147	−28 57 28·85	·10	+0·007	−0·32
45	,, 28·77408	15 19 24·478	−28 36 43·23	±0·13	−0·012	+0·09

superior as regards relative accidental errors to those in the Zone Catalogues which were obtained by comparing a photographic place with an earlier meridian place. Some information about the systematic errors of the proper motions will be obtained when the observed positions of Eros are compared with a definitive ephemeris.

TABLE II

Catalogue	No. of Plates	Mean P.E.	Δ Epoch years	Mean P.E. / ΔEpoch
		"		"
Yale −22° to −27°	1	±0·369	21	±0·0176
Yale −27° to −30°	5	0·357	21	170
Cape −30° to −35°	8	0·472	22	215
Cape −35° to −40°	9	0·306	18	170
CAZ −40° to −52°	22	±0·238	55	±0·0043

My best thanks are due to Mrs M. C. Coetzee, Mr W. A. Rasmussen and Mr T. W. Russo for their assistance in the measurements and the reductions and to Dr R. H. Stoy and Mr J. B. G. Turner for their help in securing the plates. It is hoped that a detailed account of these observations will be published in the *Annals* of the Cape Observatory.

The Cape Observatory:
1955 *October* 18.

A RADIO ECHO SURVEY OF SPORADIC METEOR RADIANTS

Gerald S. Hawkins

(Communicated by A. C. B. Lovell)

(Received 1955 November 25)

Summary

Radio echoes have been observed in two narrow-beam aerials over the period October 1949 to September 1951. An analysis of the hourly rate of echoes has given a measure of the radiant points of sporadic meteors. The radiants are found to be concentrated towards the plane of the ecliptic in the directions of the apex, Sun and antihelion points. The majority of meteors in space are moving in direct orbits about the Sun, and there is a dense complex of orbits in the region traversed by the Earth during the months May to August.

---

1. *Introduction.*—Both stream and sporadic meteor particles occur in the space surrounding the Earth. These particles evaporate on colliding with the atmosphere, generating heat, light and ionization. Stream meteors move in paths that are almost parallel, and their radiants lie in a small area on the celestial sphere, but sporadic meteors are dispersed so that the radiants are distributed over the entire sphere.

Although there was no observational evidence, for many years it was assumed that the motions of sporadic meteors in space were completely random. This

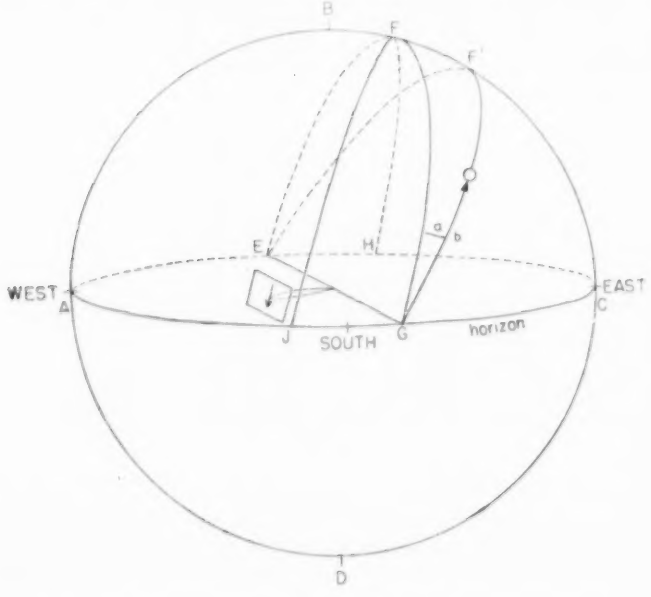

FIG. 1.—*The geometry of the radio echo reflection from a meteor trail.*

led to the erroneous idea that most meteors were interstellar in origin, as discussed by Lovell (1954). Subsequent observations have been made photographically (Whipple, 1954) but the number of sporadic radiants was insufficient and, of course, no daytime meteors could be included. This paper describes an investigation of the distribution of sporadic meteor radiants on a statistical basis, using the radio echo method of observation.

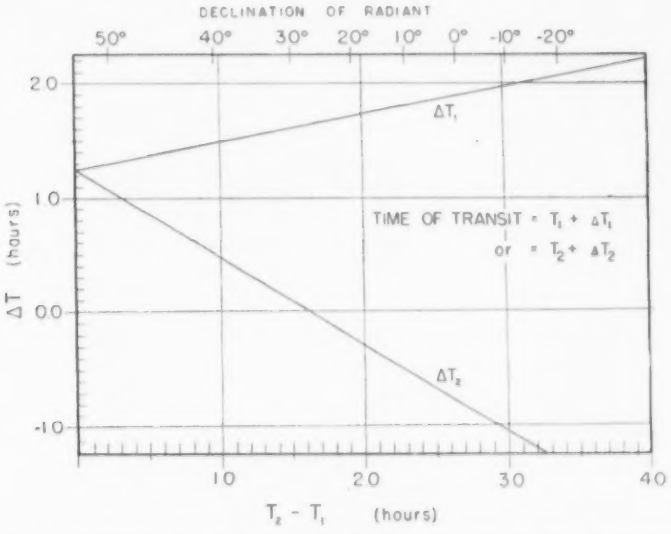

FIG. 2 *a.—Relation between time of transit of an active radiant and the time of appearance of echoes in each aerial.*

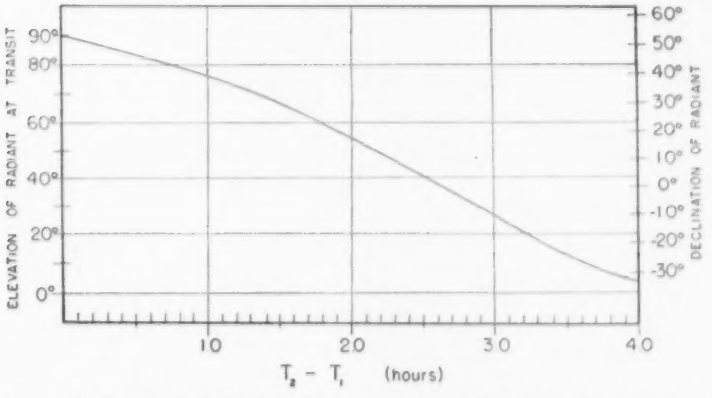

FIG. 2 *b.—Relation between declination of an active radiant and the time of appearance of echoes in each aerial.*

2. *Apparatus and method.*—The equipment, situated at Jodrell Bank, Cheshire, Long. 2° 18′ W, Lat. 53° 14′ N, was originally designed for the measurement of stream radiants and has been described by Aspinall, Clegg and Hawkins (1951).

Radio echoes were obtained when a meteor formed an ionized column, as shown in Fig. 1, in a plane perpendicular to a pencil beam aerial system. When the trail was projected on to the celestial sphere ABCD, the radiant point was somewhere on the great circle EFG. A similar aerial (not shown in the figure) detected echoes from radiants on the circle HFJ. Echoes were produced in each beam in turn as the celestial sphere rotated and carried a group of active radiants across these circles. In this way meteor activity in the northern hemisphere was sampled once in every 24 hour period. If echoes appeared at time T_1 in aerial 1 and at time T_2 in aerial 2 then the time of transit was a function of T_1 and T_2 as shown in Fig. 2*a*; the declination could be found from the time lag $T_2 - T_1$ as shown in Fig. 2*b*.

Because the aerial beam had a finite vertical width, echoes were obtained at an angle *a* above the centre of the beam from radiants on the great circle EF′G. The sector in which radiants could be observed was enlarged in a similar way by the horizontal beam width. If an element of area on the sphere supplied N radiants per hour from which N' echoes were actually detected, the sensitivity, S, of the equipment was defined as

$$S = N'/N. \tag{1}$$

The sensitivity depends on the position (a, b) of an element within the sector, where b is the angular distance from G, and for a narrow beam aerial we may write

$$S = f_1(a) \cdot f_2(b). \tag{2}$$

If we assume that N remains constant as a group of radiants crosses the sector, the function $f_1(a)$ is given by the range distribution of observed echoes, and

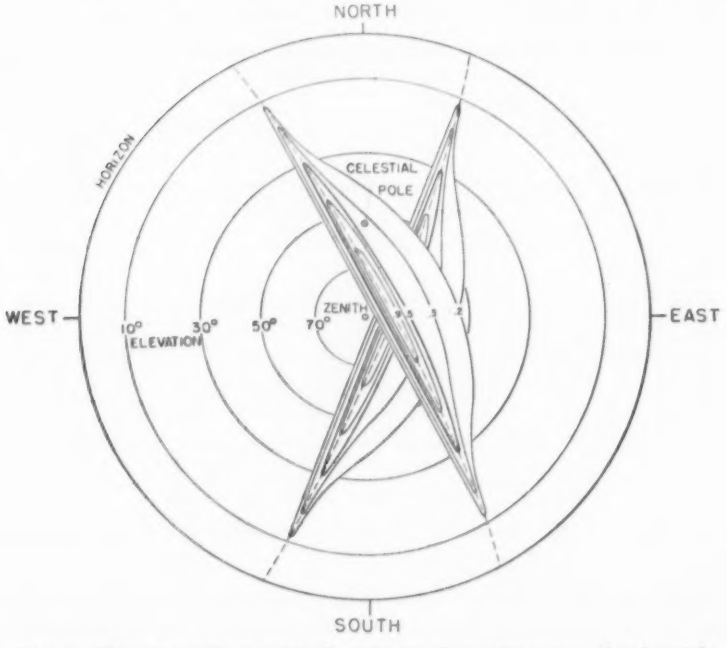

FIG. 3.—*Plan view of the celestial sphere showing the sensitive sectors of each aerial.*

$f_2(b)$ may be evaluated if we observe a stream radiant at different values of b with a moveable aerial. This has been done by Hawkins (1952), and normalized values of S for aerial 1 are plotted in Fig. 3, which is a plane projection of the celestial sphere centred on the zenith. These values are the same for aerial 2 except that the contours are displaced through a clockwise angle of 49°·2 about the zenith. The function $f_2(b)$ is approximately equal to $\sin b$. It should be noted that these radiant sensitivity contours, drawn on the celestial sphere, differ from those used by Clegg (1948) in which the aerial polar diagram was projected on to a layer 95 km above the Earth's surface. In the earlier method the time of passage of a radiant through the aerial beam was taken from the appearance of echoes at maximum range; in the present analysis only the rate of occurrence of echoes is taken into account.

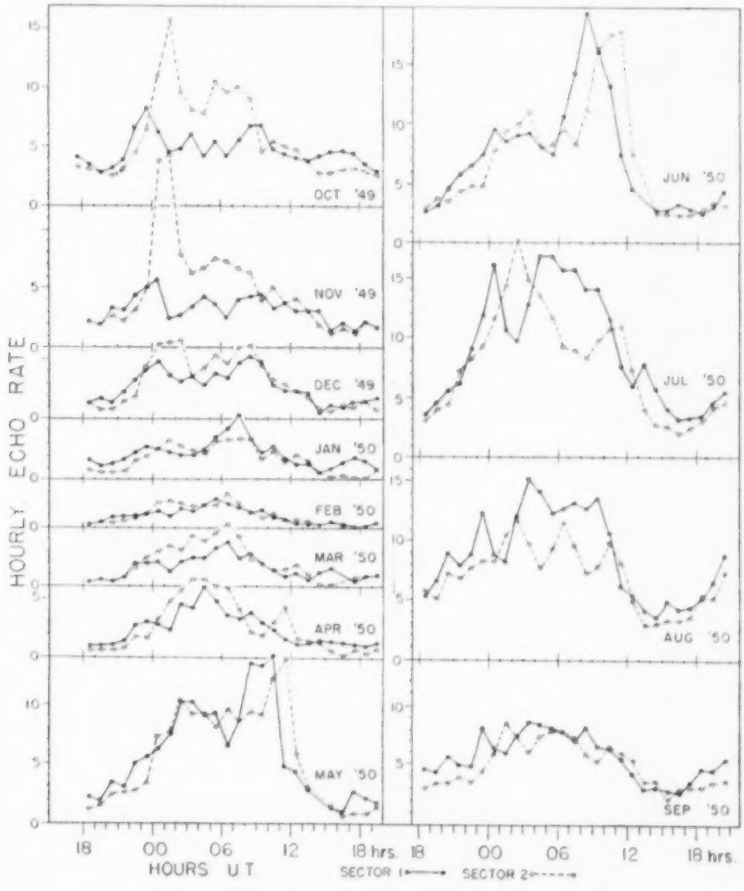

FIG. 4.—*Mean monthly diurnal rate curves for* 1949–50.

A meteor producing a trail of 10^{13} electrons/metre was just detectable with this equipment (Lovell and Clegg, 1948). Greenhow and Hawkins (1952) have shown that the visual magnitude of a meteor moving with velocity V m/sec,

and generating a trail with α electrons/metre is given by the formula

$$m_v = 70{\cdot}4 - 2{\cdot}5(\log_{10} V^3 + \log_{10} \frac{\tau}{p} + \log_{10} \alpha) \qquad (3)$$

where τ is the luminous efficiency and p is the number of electrons produced by one evaporating meteor atom. For Perseid meteors, with a velocity of 6×10^4 metres/sec, the equation has been evaluated observationally as

$$m_v = 40{\cdot}1 - 2{\cdot}5 \log_{10} \alpha \qquad (4)$$

and the limiting magnitude of the equipment with $\alpha = 10^{13}$ electrons/metre is $+7{\cdot}5$. It is not known how τ and p vary with the meteor velocity, and hence the limiting magnitudes for other velocities is uncertain.

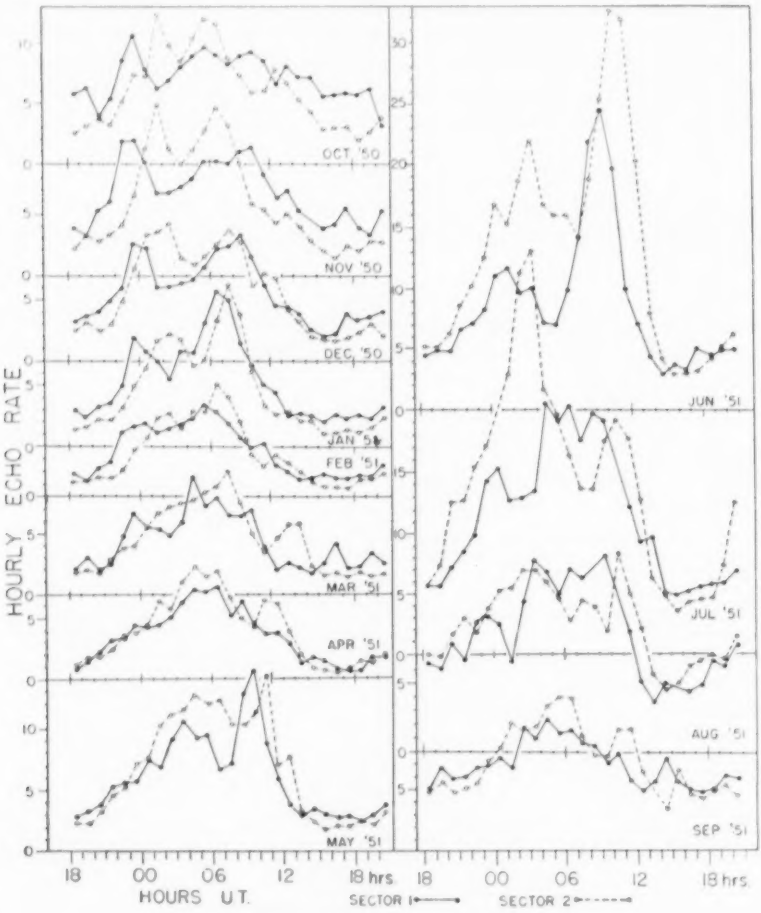

FIG. 5.—*Mean monthly diurnal rate curves for* 1950–51.

The receiver, transmitter, and other apparatus were checked at frequent intervals, and the overall sensitivity was maintained to within $\pm 3db$. Any records which were affected by interference, solar noise or apparatus defects were

rejected. There were no appreciable variations of sensitivity due to galactic noise. As a final check, measurements were repeated for a second year.

3. *Observational data.*—A continuous survey was maintained from 1949 October 1 to 1951 September 30. In this period 240 000 echoes were observed, and 5 per cent of these have been attributed to meteor streams (Hawkins and Almond, 1952 a and b). The few hours of the survey showing echoes from meteor

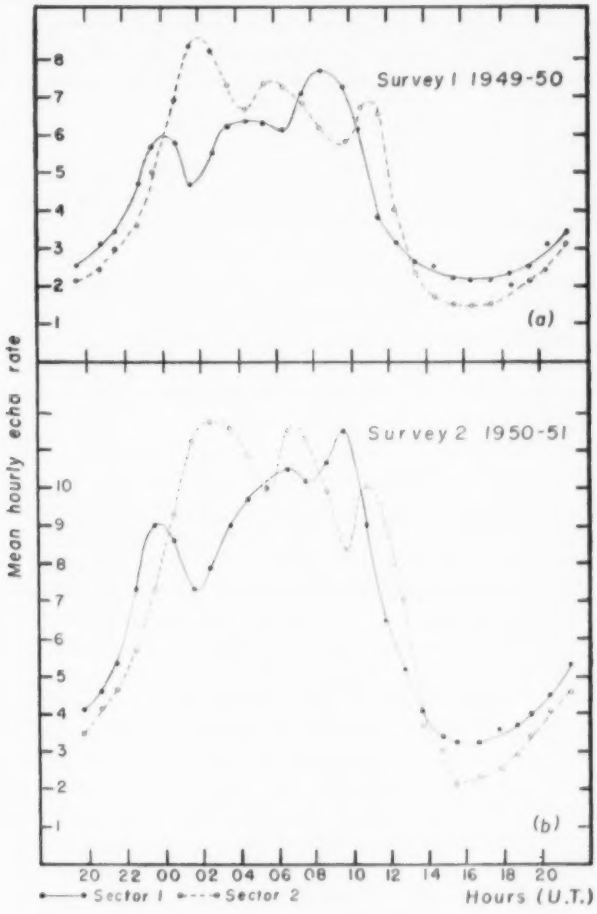

FIG. 6.—*Mean diurnal rate curves taken over a period of a year.*

streams have been rejected. The basis of the present analysis is the hourly rate of sporadic echoes detected in the sector of each aerial; the mean rate for a given hour of Universal Time has been taken over a month. Fig. 4 shows the diurnal variation of the hourly rate, plotted month by month, for the year 1949–50; Fig. 5 gives the variation for the year 1950–51. In this way the results have been subdivided into two surveys which cover two complete rotations of the Earth about the Sun. Fig. 6 shows the average of all the monthly curves throughout the year, with 6(*a*) corresponding to Fig. 4 and 6(*b*) corresponding to Fig. 5.

4. *Analysis.* (*a*) *The concentration of radiants in the plane of the ecliptic.*—The monthly curves in Fig. 4 and 5 show three concentrations of radiant points at 0130 U.T. in the winter night-time, at 1030 U.T. in the summer daytime and at 0600 U.T. throughout the year. These concentrations are shown more clearly in the yearly curves of Fig. 6, where the angle between the sectors has displaced the maxima and two intermediate minima by an average value of 2·35 hours, which, from Fig. 2*b*, corresponds to a mean radiant elevation of 45°·3 above the horizon. For radiants confined to the ecliptic, crossing a sector at an elevation θ, the hourly rate is given by the sensitivity contours of Fig. 3, and varies as $\sin\theta$. In this case a mean elevation $\bar{\theta}$ would be observed, given by the equation

$$\bar{\theta}\int_{\theta_1}^{\theta_2}\sin\theta\,d\theta=\int_{\theta_1}^{\theta_2}\theta\sin\theta\,d\theta \qquad (5)$$

where θ_1 and θ_2 are the minimum and maximum elevations of the ecliptic. For Jodrell Bank, $\theta_1=13^\circ 19'$, $\theta_2=60^\circ 13'$, which gives a value of $\bar{\theta}$ of 41°·1. This is in good agreement with the observed value, showing that there is a strong concentration of radiant points in the plane of the ecliptic. Between 14^h and 22^h the curves of the sectors are not displaced, indicating a high mean declination. This implies that when the meteors are observed in the hemisphere containing the antapex, there is a more uniform distribution of radiants. The sensitivity contours of sector 2 do not pass as close to the celestial pole as those of sector 1 (Fig. 3), hence the lower value of the evening minimum in sector 2 is further evidence for high declination radiants at this time.

(*b*) *Apparent distribution of radiants in ecliptic longitude.*—To obtain the mean distribution of radiants in ecliptic longitude, time shifts must be applied to allow for the angle between the sectors. With radiants at 45°·3 elevation, Fig. 2*a* shows that 1·8 hours must be added to the time scale of sector 1 and 0·55 hours subtracted from sector 2, so that both sectors are effectively aligned on the prime meridian of the observing station. Displacing the yearly diurnal rate curves in this way and taking the mean of both sectors, we can obtain the radiant density in a band at longitude λ, where λ is given by the time of transit. This band is approximately 6° wide, and its average position is perpendicular to the ecliptic with a variation of $\pm 23{\cdot}5^\circ$. If λ_s is the longitude of the Sun, the angle $(\lambda-\lambda_s)$ may be called the local longitude because the band is in this position at the same time each day. Fig. 7 shows the apparent distribution of radiants in local longitude, plotted in polar coordinates with the Earth at the origin. It was assumed that with equal sensitivities the same number of meteors would have been observed in survey I as in survey II, and the observed rates in survey I have therefore been multiplied by 1·52.

(*c*) *The distribution of meteor directions in space.*—Most radiants, and hence most meteor orbits, lie close to the plane of the ecliptic, and we may assume that the apparent distribution of orbital directions in this plane is given by Fig. 7. To obtain the heliocentric distribution of directions at a point on the Earth's orbit we must correct for the Earth's orbital motion in the following manner. If a meteor is moving with a velocity V relative to the Sun, then its apparent direction as seen by an observer moving with velocity V_E relative to the Sun, may be obtained by reducing the Earth to rest, and applying a velocity $-V_E$ to V. If N_ϵ radiants/sec are observed within a sector $d\epsilon$ on the ecliptic at an apparent

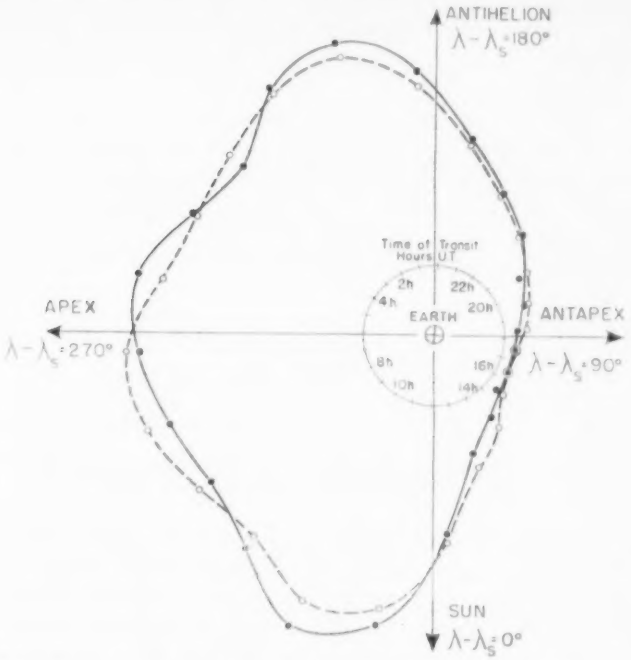

FIG. 7.—*Polar diagram drawn in the plane of the Earth's orbit which shows the apparent number of meteor radiants detected per unit angle, per second.*

elongation ϵ from the apex, then the true elongation ϵ_0 is given by the equation

$$\epsilon_0 = \epsilon + \sin^{-1}\left(\frac{V_E}{V}\sin\epsilon\right) \tag{6}$$

These radiants are located in a sector $d\epsilon$ which may be found by differentiating (6), inverting the differential and substituting for the apparent velocity V' by the cosine rule.

$$\frac{d\epsilon}{d\epsilon_0} = \frac{V}{V'}\sqrt{1 - \frac{V_E^2}{V^2}\sin^2\epsilon}. \tag{7}$$

An increase in the apparent velocity V' increases the number of intercepted meteors. If N_{ϵ_0} is the number of meteors/sec crossing the Earth's orbit at elongations between ϵ_0 and $\epsilon_0 + d\epsilon_0$, then

$$N_{\epsilon_0} = N_\epsilon \frac{d\epsilon}{d\epsilon_0}\cdot\frac{V}{V'} = \frac{N_\epsilon V^2\sqrt{1 - \frac{V_E^2}{V^2}\sin^2\epsilon}}{V^2 + V_E^2 + 2VV_E\cos\epsilon_0}. \tag{8}$$

By taking $V = 40$ km/sec, 2 km/sec below the parabolic limit, we can correct the apparent distribution for the Earth's motion by using equations (6), (7) and (8). The corrected direction distribution is shown in Fig. 8, where N_{ϵ_0} is plotted against ϵ_0. It represents, for any point in the Earth's orbit, the number of meteors which cross at an elongation ϵ_0 in unit time. The space density, or number of meteor paths per unit volume per radian is equal to N_0/V. Since V is assumed

to be constant, the form of Fig. 8 also gives the space density distribution. This analysis is a revision of previous work by the author (Hawkins, 1952) and quoted by Lovell (1954).

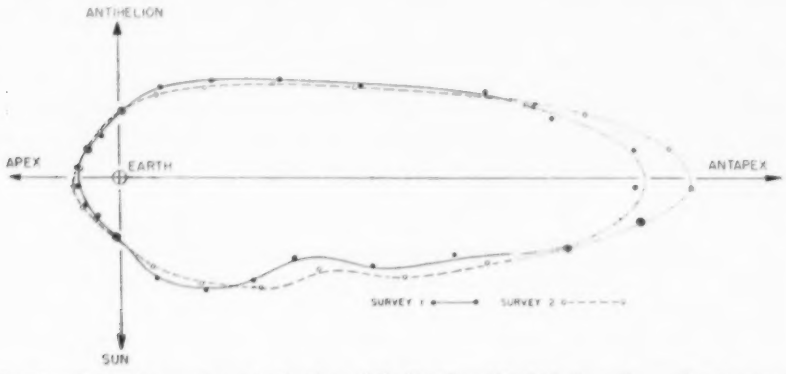

FIG. 8.—*Polar diagram drawn in the plane of the Earth's orbit which shows the number of meteors per unit angle which cross the Earth's orbit per second.*

(*d*) *The distribution of meteor debris along the Earth's orbit.*—The area under the diurnal curve is proportional to the total daily influx of sporadic meteors. Let us suppose that the space density of meteors is constant along the entire length of the Earth's orbit. The distribution of apparent radiants in local longitude is shown in Fig. 7 and may be written $f(\lambda-\lambda_s)$. Because of the concentration towards the ecliptic, the echo rate, N', at any instant is given by the equation

$$N' = N.f(\lambda-\lambda_s).\sin\theta. \qquad (9)$$

The elevation of the ecliptic, θ, changes with the time of day and season of the year. Fig. 9 shows the predicted hourly rates for a sector along the prime meridian of Jodrell Bank for each month. When Fig. 4 and 5 are compared with Fig. 9 it can be seen that the observed seasonal variation is greater than that expected from the gyrations of the ecliptic. It is evident, therefore, that meteors are not uniformly distributed along the Earth's orbit, and the ratio of the areas under the observed curves to those under the predicted diurnal curves gives the variation in space density from month to month. This ratio is plotted in Fig. 10. It shows that meteor orbits congregate in the space traversed by the Earth between April and August when the Sun's longitude is between 40° and 150°.

5. *Discussion.* (*a*) *Distortions produced by the ionosphere and other effects.*—There is no evidence for a difference in meteoric ionization between the night and daytime sky. The distribution of radiants in local longitude (Fig. 7) is symmetrical; the same number of sporadic meteors are detected by night as by day, and this would be expected astronomically. (See section (*b*) following.) Any enhancement of the ionization by the ambient electron density of the *E* region, or by sunlight, would have permitted the detection of smaller meteor particles and would have caused a noticeable day–night asymmetry.

There is, however, a systematic deviation in the average diurnal curves (Fig. 6). During the night, between 2000 U.T. and 0800 U.T., the rate in sector 1

increases and the rate in sector 2 decreases. For radiants near the ecliptic the sectors are almost identical, so that the discrepancy cannot be an astronomical effect. It represents a systematic change in sensitivity of 1 *db* between the two aerials.

(*b*) *Significance of the ecliptic distribution.*—The concentration of radiants towards the ecliptic indicates that meteor orbits are aligned with the plane of the Earth's orbit, and are therefore intimately connected with the solar system.

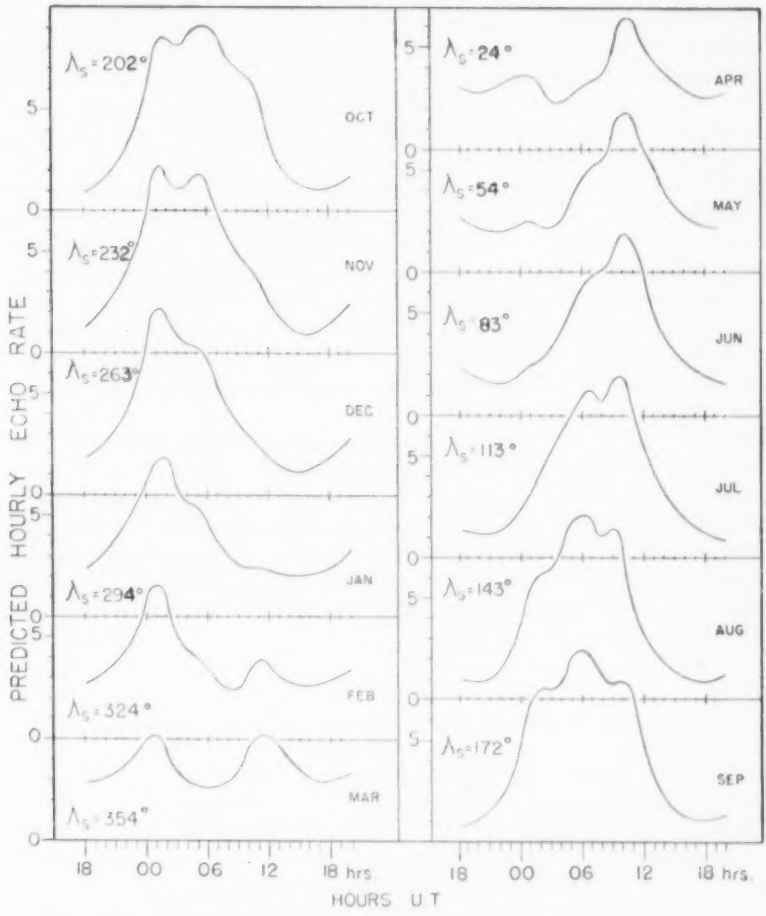

FIG. 9.—*Mean monthly diurnal curves predicted for a sector aligned with the North–South meridian. It has been assumed that the space density of meteors along the length of the Earth's orbit is constant, and that the distribution of directions is given by Fig.* 8.

It can be seen that the true and apparent longitude distributions (Fig. 7 and 8) exhibit a symmetry about the apex. This is a natural consequence of the fact that meteor orbits are conic sections, because, if the directions of perihelia are uniformly distributed, every night-time orbit has its counterpart in the daytime sky. Night-time meteors are approaching a perihelion point inside the Earth's

orbit, and daytime meteors are receding. The probability of meteors colliding destructively with Mercury, Venus, the Earth and particles in the zodiacal cloud is negligible for one perihelion passage. Hence we would expect, as shown by this survey, the same number of meteors incident from two hemispheres with poles directed towards and away from the Sun.

The maximum in the radiant distribution at the apex is caused by meteors which are swept up by the Earth. The side lobes, at elongations of 66° from the apex, close to the Sun and antihelion points give the most frequently observed sporadic meteor orbits if the mean velocity is known. We may assume that the heliocentric velocity is between 34 and 40 km/sec (Lovell 1954, page 234), and we may compute the series of orbits that correspond to an elongation of the radiant of 66°. These are given in Table I where it can be seen that the most frequently observed orbit is probably elliptical, with high eccenticity and with a semi-major axis comparable to the short period meteor streams.

(*c*) *The distribution of meteor directions in space.*—When the correction for the Earth's velocity is applied the results show a remarkable preponderance of direct moving meteors; orbits to the left of the line between the Sun and antihelion in Fig. 8 are retrograde. Points near the longitude of the antapex have been rejected because they do not represent orbits in the plane of the ecliptic. The distribution could imply that meteors move in almost circular orbits overtaking the Earth. If this is the case, a heliocentric velocity of 30 to 35 km/sec should be assumed in section 4 (*c*) instead of 40 km/sec, and this would further increase the number of directly moving meteors in space.

However, there are uncertainties in this part of the analysis that must be borne in mind. Large corrections, amounting to a factor of 42 for antapex meteors, have been applied, and the correction is critically dependent on the assumed heliocentric velocity. Furthermore, the distributions are for a limiting electron density of 10^{13}/metre in the meteor trail. The corresponding visual magnitude and mass of the meteor are undoubtedly functions of geocentric velocity, and hence of ϵ_0, so that the distribution when taken to a certain limiting mass would be different from that in Fig. 8.

TABLE I

The orbits that correspond to assumed heliocentric velocities between 34 and 40 km/sec

V km/sec	*a* Semi-major axis	*e* Eccentricity	*q* Perihelion distance	*A* Aphelion distance
40	5·16	0·982	0·09	10·23
38	2·69	0·958	0·11	5·27
36	1·86	0·927	0·14	3·58
34	1·44	0·886	0·16	2·71

(*d*) *Irregularities along the Earth's orbit.*—Fig. 10 shows the seasonal variation in the total meteor flux incident on the Earth, which increases by a factor of 4 between February and June. The fact that the maximum corresponds to the summer solstice might indicate that the measurements had been influenced by variations in the height of the meteor layer, in ionization levels in the E region

or by other effects dependent on solar radiation. However the annual variation of height (Jacchia) is small, and the ionosphere does not produce diurnal distortions (Section 5 *a*) so that seasonal effects would not be expected.

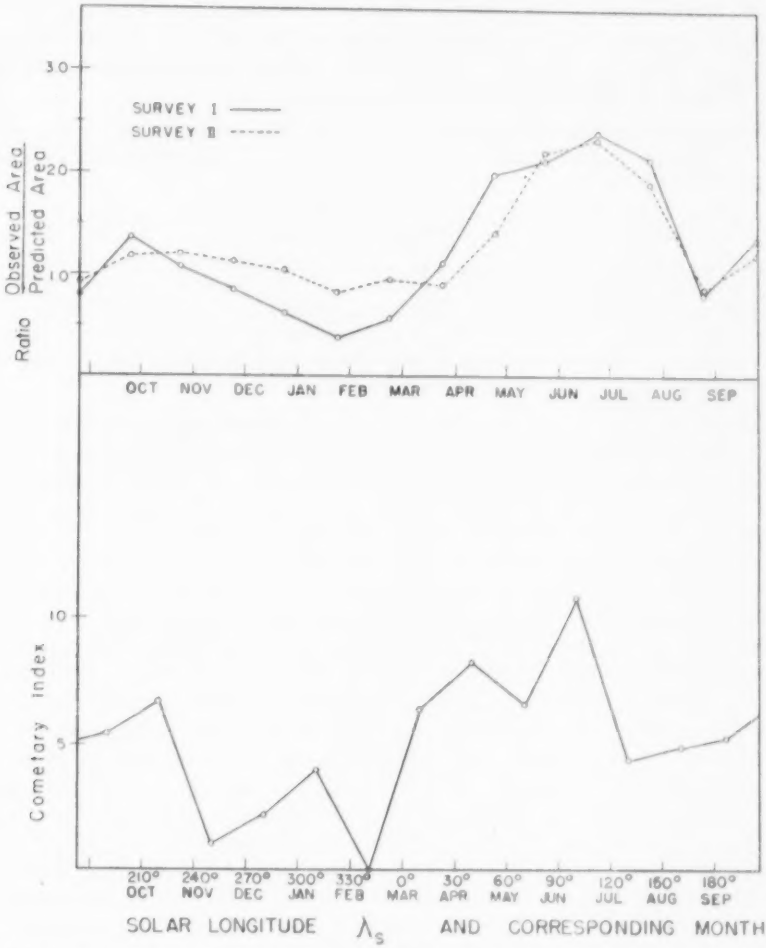

FIG. 10.—*Variation in the space density of meteors along the length of the Earth's orbit (top figure) compared with the cometary index (bottom figure).*

The variations in the density correlate significantly with the cometary index of Herschel and Hoffmeister (1948) which is plotted for comparison in Fig. 10. This index is proportional to the number of comets crossing the Earth's orbit and their closeness of approach. The correlation suggests that sporadic meteors and comets have a similar origin.

6. *Acknowledgments.*—The author wishes to thank A. Aspinall who participated in most of the observational programme and Dr J. G. Davies for his interest and advice. The survey was undertaken at the Jodrell Bank

Experimental Station, University of Manchester, under the direction of Professor A. C. B. Lovell, whose advice and encouragement during the work has been greatly appreciated. The author is indebted to the Department of Scientific and Industrial Research for the award of a maintenance grant during the period of the observations. The analysis has been completed at Harvard College Observatory under United States Air Force Contract No. AF19(122)–458, subcontract No. 57. During this period the author wishes to thank Professor F. L. Whipple for his interest in the investigation.

Jodrell Bank Experimental Station,
University of Manchester:
1955*November* 24.

Harvard College Observatory,
Cambridge, Mass., U.S.A.

References

Aspinall, A., Clegg, J. A., and Hawkins, G. S., 1951, *Phil. Mag.*, **42**, 504.
Clegg, J. A., 1948, *Phil. Mag.*, **39**, 577.
Greenhow, J. S. and Hawkins, G. S., 1952, *Nature*, **170**, 355.
Hawkins, G. S., 1952, Ph.D. Thesis, University of Manchester, England.
Hawkins, G. S., and Almond, M., 1952 a, Jodrell Bank Annals, **1**, 2; 1952 b, *M.N.*, **112**, 219.
Hoffmeister, C., 1948, *Meteorstome*, Weimar–Leipzig.
Jacchia, L. G., Unpublished data.
Lovell, A. C. B., 1954, *Meteor Astronomy*, Oxford University Press.
Lovell, A. C. B., and Clegg, J. A., 1948, *Proc. Phys. Soc.*, **60**, 491.
Whipple, F. L., 1954, *Ap.J.*, **59**, 201; 1955, *Ap.J.*, **121**, 241.

A RADIO ECHO METHOD OF METEOR ORBIT DETERMINATION

J. C. Gill and J. G. Davies

(Communicated by A. C. B. Lovell)

(Received 1955 October 29)

Summary

A radio echo system using three receivers spaced on the ground by 4 km has been used to determine the orbits of individual meteors. About 200 orbits can be calculated from the meteor echoes photographed during a 24 hour period of observation. An analysis of Geminid meteors observed in 1954 indicates that the accuracy obtainable is limited to about ± 2 km/sec in velocity by atmospheric deceleration, and to $\pm 3°$ in radiant position by turbulent winds in the meteor region.

---

1. *Introduction.*—Radio observations of meteors have been made since 1946. Velocity measurements based on the observation of diffraction patterns have been made both by pulsed (**1**) and continuous wave (**2, 6**) technique. These have yielded much information concerning both shower and sporadic meteors. In the case of showers, radio techniques are also available for delineation of radiant positions (**3**) and this has led to the discovery of daytime streams and the determination of orbits. In the case of sporadic meteors no measurement of individual radiants has been possible but, although information concerning their orbits has been of a statistical nature, it has been established that a large proportion move in orbits of short period, and that less than 1 per cent have an interstellar origin. For the more detailed analysis of the orbits of sporadic meteors, and the examination of radiant structure of showers, it is desirable to be able to measure both velocity and direction of motion for individual meteors. Following a suggestion by Kaiser, the pulse technique of velocity measurement (**1**) has recently been extended to accomplish this by the use of three spaced receivers.

2. *Theory.*—If two observing stations (A and B in Fig. 1) each with transmitter and receiver are used, there will be a time difference between reception of corresponding points on the diffraction patterns at the two stations equal to the time taken for the meteor to travel the distance between the specular reflecting points P_A, P_B. The velocity V of the meteor can be determined from either or both of the patterns, hence the length P_AP_B can be found if the time delay t is measured. The value of $\cos\theta$, where θ is the angle between AB and a line drawn through B parallel to the trail YX, can therefore be determined, since

$$\cos\theta = \frac{P_AP_B}{AB} = \frac{Vt}{AB}$$

and AB can be measured directly.

In the general case when XY and AB are not coplanar, $\cos\theta$ becomes the direction cosine between the line of flight XY of the meteor and the base-line AB. The addition of a third station enables a second direction cosine to be found, thus defining the flight direction and hence the radiant of the meteor. The

velocity is already known and, given the time of occurrence, the orbit can be computed.

The error in the measured angle θ is given by

$$\delta\theta = \cos\theta\left[\left(\frac{\delta V}{V}\right)^2 + \left(\frac{\delta t}{t}\right)^2\right]^{1/2}$$

where δV and δt are the errors of measurement in V and t respectively. The time delay is directly proportional to the base-line AB and thus the angular error will be reduced by an increase in base-line until this is such that the fractional error in t is small compared with the fractional error in V. For a typical case the two error terms are equal with a base-line of the order of 1·5 km.

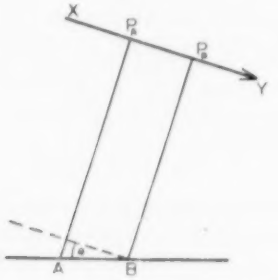

FIG. 1.—*Radio stations at A and B observe the meteor trail at the specular reflection points P_A, P_B. From the ratio of $P_A P_B$ to the baseline AB, the radiant direction can be determined in the two-dimensional case.*

In practice it is not necessary to use complete transmitting and receiving equipment at all three stations. If a transmitter at A is used with a remote receiver at B, the point of specular reflection lies at the mid-point of $P_A P_B$, provided that the range of the echo greatly exceeds AB. It can be shown that under these conditions the diffraction pattern received at B is for practical purposes the same as would be obtained at a complete transmitting and receiving station situated midway between A and B. The delay between patterns received at A and B is therefore half that for the case of two separate transmitting and receiving stations.

A single transmitting and receiving station, with two remote receivers, is thus sufficient to provide the three diffraction patterns necessary for orbit determination.

An equipment using a single transmitter and capable of recording the three diffraction patterns necessary for orbit determination has been constructed and was first used at Jodrell Bank in 1953 December.

3. *Apparatus.*—The basic equipment parameters are given below:

Radio frequency: 36·3 Mc/s.

Transmitter: 600 pulses per second are radiated; a pulse length of 15 microseconds and pulse power of 100 kW are usually employed.

Aerials: The transmitting aerial most frequently employed has an absolute power gain of 28, with a beam width of $\pm 12°$. The aerial is directed slightly north of east at an elevation of 30°. Reception at all stations is by aerials having absolute power gains of 12 in the direction of the main beam of the transmitting

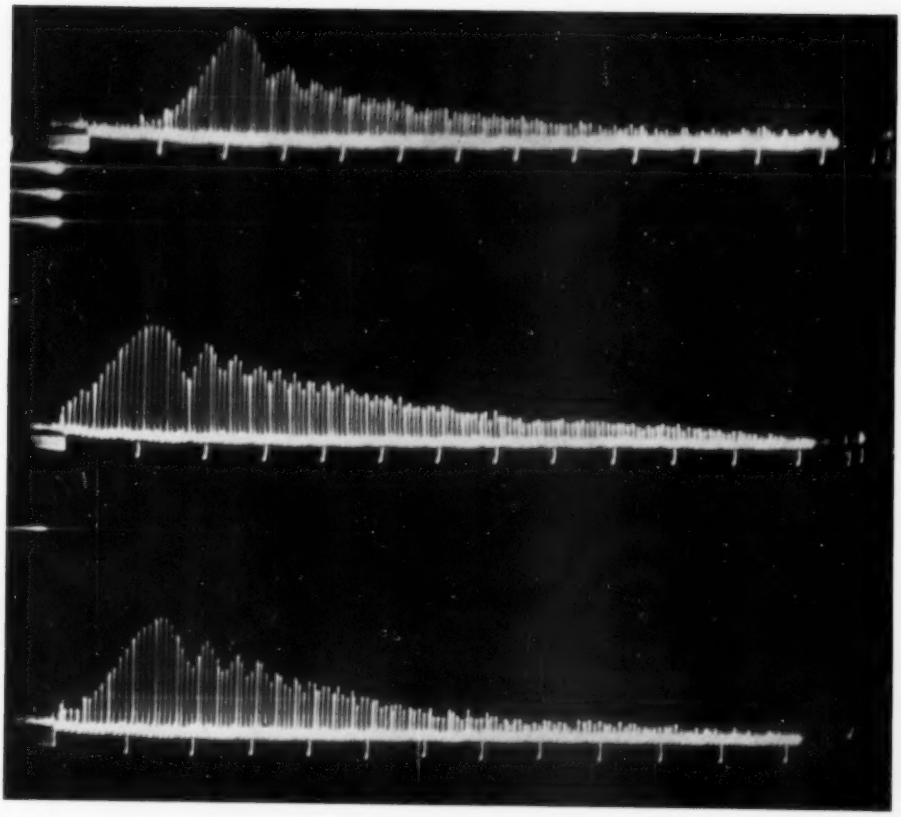

Specimen photographs showing the diffraction patterns observed at three receivers.

aerial; the latter determines the effective beam width of the system as a whole.

The transmitter and one receiver are located at Jodrell Bank; remote receivers are situated approximately south and east of this at distances of 3·5 kilometres. Signals received at the remote stations are amplified, converted to link frequencies in the 75–80 Mc/s band, and after further amplification are re-transmitted to the home station, where the signals received at all three stations are displayed on cathode-ray tubes, a fourth tube being used to record the range of the echo at one station.

The received pulses are recorded photographically using a moving film system triggered by reception of the echo itself. The echo pulses are recorded for a maximum time of 0·5 seconds, to ensure satisfactory reception of the patterns from all three stations for the slowest meteors.

The time of occurrence of the echo is also recorded. A specimen record obtained with this apparatus is shown in Plate 2.

With this equipment the majority of meteors for which orbits are determined lie in the magnitude range +6 to +8; in an average period of 24 hours some 200 sporadic meteors giving patterns satisfactory for orbit determination can be recorded.

4. *Reduction of results and computation of the orbit.*—The derivation of the orbit from the recorded information falls into two stages: the determination from the film records of the meteor velocity and the time delays between stations, and the computation of the orbit from these results.

The first stage involves fitting the best theoretical diffraction pattern to that observed; the velocity corresponding to this pattern and its separation from the other two are recorded. This is now achieved using an analogue computer, with considerable saving in time over alternative methods of computation using a desk machine.

The computation of the meteor orbit from the observed velocity and delays follows the method described by Porter (4), including corrections for atmospheric deceleration, diurnal aberration and zenith attraction. Since the calculation is a lengthy process and several hundred orbits may be computed from observations over a single 24-hour period, it was found necessary to use electronic computation. The Manchester University digital computer is used and is arranged to print the following information for each meteor:—

Corrected geocentric radiant position in altazimuth, equatorial and ecliptic co-ordinates.
Elongation of radiant from apex, and heliocentric velocity.
Heliocentric radiant in ecliptic coordinates.
Longitude and argument of perihelion.
Longitude of ascending node.
Inclination of orbital plane.
Semi-major axis, a.
Eccentricity, e.
Aphelion and perihelion distances.
The parameter of the orbit $p = a(1 - e^2)$.
Ecliptical coordinates of aphelion direction and pole of the orbit.

This process takes approximately 40 seconds for each meteor.

5. *The geminid shower, 1954.*—In order to determine the accuracy of the method an investigation of the Geminid shower of 1954 December has been made. Geminid meteors have previously been extensively observed both by radio and photographic techniques. The results of the most important measurements are summarized in Table I.

TABLE I

Observing station		Radiant (Sun's longitude = 260·6°) R.A. °	Dec. °	Diameter °	Velocity km/sec.	Observed spread in velocity km/sec
Jodrell Bank	1947	—	—	—	34·4	± 1·2
(Radio) (5)	1949–50	112·8	+31·8	—	35·9	± 4·6
Ottawa (Radio) (6)		—	—	—	35·2	± 2·3
Harvard (Photographic) (7, 8)		112·5	+32·8	0·22	36·4	± 0·2

In Table I the radiant positions have been corrected for the effects of diurnal aberration and zenith attraction; the velocity quoted is the mean observed velocity in the case of the radio determinations, and the mean velocity at the top of the atmosphere for the photographic results, after removal of the component due to the Earth's rotation. The figure given for the spread in velocity is the standard deviation of an individual observation, assuming the distribution to be Gaussian. In the case of the radio data the spreads are considerably larger than the random errors of measuring the velocity from the diffraction patterns. The radio results refer to +6th magnitude and fainter meteors; the Harvard data are for meteors brighter than zero magnitude.

6. *Radiants.*—Sixty-one Geminid meteors were recorded on 1954 December 13. The radiants of these are shown in Fig. 2 plotted separately for three consecutive periods. From considerations of the accuracy of measurement of velocity and time displacement of diffraction patterns errors of ±0·5 km/sec. in velocity and 1°·5 in radiant position would be expected. It is seen that, although the mean radiant agrees with previous photographic and radio results, the spread of individual radiants exceeds that anticipated from the errors in reading the diffraction patterns, and also the observed shape of the radiant changes with its position relative to the base-lines used, showing that the spread is not astronomical in origin.

It has been shown by Kaiser (9) that such a radiant spread can be caused by a uniform wind shear in the region of the trail. The chief effects of such a shear are found to be:—

(*a*) The diffraction pattern observed shows no distortion unless very high or second-order shears are present.

(*b*) The value of velocity obtained is slightly too high; the error, however, is negligible compared with the random errors of determination, for uniform shears.

(*c*) The displacements between diffraction patterns are seriously affected. The fractional error in delay is found to be

$$\frac{\delta}{2-\delta} \qquad \text{where} \qquad \delta = \frac{2R}{V}\frac{du}{ds}$$

R = echo range,
V = meteor velocity,
u = wind velocity parallel to line of sight from station to trail,
s = distance along trail.

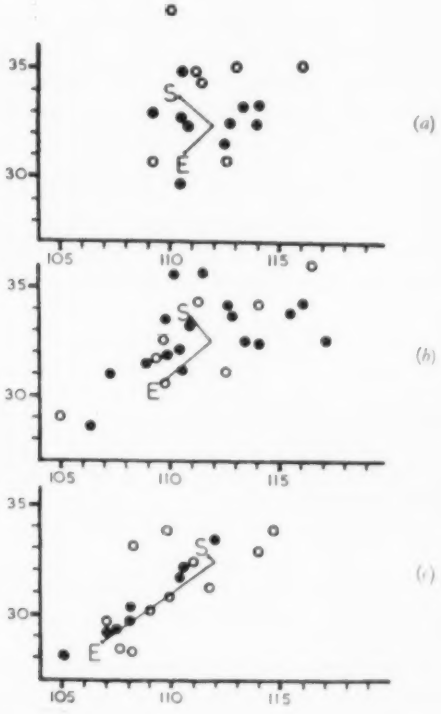

FIG. 2.—*Radiant points of Geminid meteors observed on 1954 December 13. Solid points represent undistorted diffraction patterns. Open circles represent diffraction patterns showing evidence of turbulent winds. The straight lines E and S represent the errors introduced by 10 per cent errors in estimating the time displacements of the eastern and southern remote station respectively from the home station.*

(a) Sidereal time $07^h\ 30^m$ *to* $09^h\ 30^m$
(b) Sidereal time $09^h\ 30^m$ *to* $10^h\ 30^m$
(c) Sidereal time $10^h\ 30^m$ *to* $12^h\ 00^m$
Abscissae : R.A. in degrees.
Ordinates : declination in degrees.

The effects on radiant position produced by 10 per cent errors in the time displacements between diffraction patterns are indicated for the central time of each period in Fig. 2. If the radiant is so placed that there is no time displacement

between the diffraction patterns observed at a pair of stations, then wind shear cannot affect the magnitude of this displacement, and this accounts for the very small S vector in Fig. 2(*c*). In this figure the radiants lie along a line parallel to the E vector with a spread of $\pm 1°$. The observed spread in radiants therefore does not conflict with Whipple's measurement of radiant diameter. The Geminid observations show that the radiant spread is equivalent to errors in displacements of about 5 per cent. Such errors would be caused by wind shears of 10 m sec^{-1} km^{-1}. Shears of this order are commonly observed by other methods, e.g. by photography of persistent meteor trails. The accuracy of radiant determination for individual meteors is therefore limited by this effect to $\pm 3°$ for an average case.

7. *Observed velocities.*—The observed velocity will be affected by errors of measurement and by atmospheric deceleration. Photographic velocity determinations by Whipple (**10**) indicate that for 3rd magnitude meteors at their maximum of ionization the loss in velocity due to atmospheric resistance is about 0·5 km/sec for meteors having an initial velocity of 35 km/sec. As the height of the meteor relative to its maximum of ionization is not known in this experiment, there is an uncertainty, of the same order as the loss in velocity at maximum ionization, in the correction to be applied and hence in the geocentric velocity of the meteor. The theory of Herlofson (**11**) predicts that the loss in velocity of a spherical meteor travelling through the atmosphere is

$$-\frac{6L}{V\Lambda}\ln\left(1-\tfrac{1}{3}e^{-h}\right)$$

where L = latent heat of evaporation of meteor,
Λ = heat transfer coefficient,
h = height of meteor above maximum of ionisation, measured in units of atmospheric scale height,
V = velocity of meteor on entering atmosphere.

The loss in velocity, following this theory, is independent of the meteor magnitude, and therefore the necessary correction should remain 0·5 km/sec for the fainter Geminid meteors.

The velocities of meteors from the Geminid radiant recorded during the period 1954 December 10–14 are shown in Fig. 3. It is apparent that these radio determinations are systematically lower and exhibit a larger spread than the photographic results, the mean observed radio velocity being only 34·1 km/sec. After applying the correction for the Earth's rotation, this becomes 34·3 km/sec compared with 36·4 km/sec found photographically. The spread of the radio observations is much greater than the error of reading the diffraction patterns, and exceeds by a factor of 4 the spread due to atmospheric deceleration predicted from Herlofson's theory.

The radio observations of velocity quoted in Table I have slightly higher values than those given above, although they are significantly lower than the photographic velocity. A large spread in velocity occurs for all the radio determinations. The difference between the 34·3 km/sec found here and the previous mean radio velocities probably arises from the inclusion of sporadic meteors in the earlier data. These would be likely to have higher velocities than

Geminids, and are excluded from the present results for which radiants have been determined.

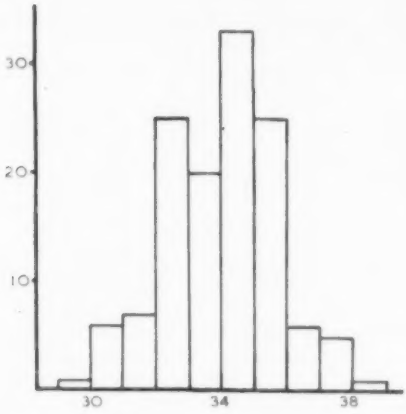

FIG. 3.—*Histogram of velocities of Geminid meteors recorded between 1954 December 10 and 14.*
Abscissae : velocity in km/sec.
Ordinates : number of meteors.

The difference between the radio and photographic observations can only be due to the difference in magnitude range covered. Either the true geocentric velocities of the fainter meteors are lower and exhibit a large scatter or they suffer much greater retardation in the Earth's atmosphere than do the brighter meteors. Since no systematic shift in radiant position with measured velocity is observed, it is unlikely that the cause of the lower velocities can be astronomical in nature. In the case of atmospheric retardation, the lowest observed velocities will be for meteors seen at the ends of their paths in the atmosphere, and consequently at the lowest observed heights. A marked correlation between height and velocity should be observed. If the velocity spread is astronomical, the only correlation between meteor velocity and height will be that given by the relation

$$P_{\max} \propto \frac{\cos^{2/3}\chi}{V^2}$$

where $P_{\max}$ = atmospheric pressure at maximum of ionization,
χ = zenith distance of radiant,
V = meteor velocity.

In Fig. 4 the measured velocities are plotted as a function of height. The latter has been obtained by an approximate method based on a knowledge of the radiant and range of the meteors. The errors in the plotted heights are of the order of ± 2 km. It is seen that the correlation between velocity and height is marked, and that the slope of the height-velocity curve is much greater than that expected if the observed velocity distribution were astronomical in origin. It must therefore be concluded that the spread in observed velocity is due to deceleration in the Earth's atmosphere, and that there is no reason for believing that the velocity at the top of the atmosphere of the faint Geminid meteors differs significantly

from that observed photographically for the brighter members of the stream. Assuming Whipple's value of the velocity to apply to the faint meteors, the median value of the correction for atmospheric deceleration is found to be 2·0 km/sec. There is, therefore, an uncertainty of this order in the geocentric velocity of meteors recorded with velocities around 35 km/sec.

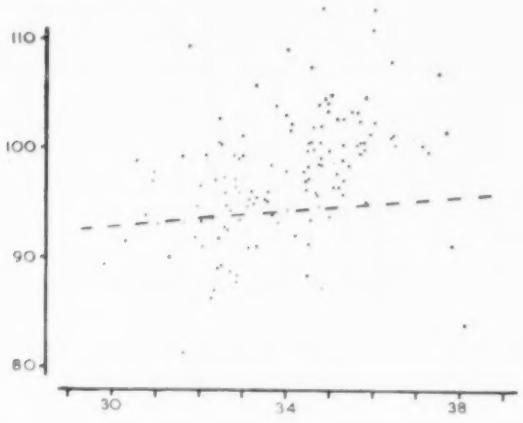

FIG. 4.—*Observed velocity of Geminid meteors as a function of height of point of observation. The dashed line indicates the relation between height of maximum ionization and velocity for sporadic meteors.*

Abscissae : velocity in km/sec.
Ordinates : height in km.

8. *Conclusions.* In the light of these results, it appears that the accuracy obtainable using this technique is limited, for 35 km/sec meteors, to ± 2 km/sec in velocity and $\pm 3^{\circ}$ in radiant position by atmospheric effects. These effects are expected to decrease for meteors of greater velocity.

This accuracy is amply sufficient for surveys of sporadic activity, but for more detailed work, such as investigations of the radiant structure of showers, greater accuracy is desirable. Corrections for the effects of wind shear on radiant determination could be derived from measurements of the wind components along the lines from the observing stations to the points of specular reflection on the trail. The error in geocentric velocity due to atmospheric retardation could be reduced if the velocity at a number of points spaced along the whole trail were measured. This would require a series of receiving stations spaced along each baseline, and would allow the velocity of the meteor before entering the atmosphere to be found by extrapolation. A simpler, though less accurate, method of correction would be to determine the height of the trail, and use the relation between height and retardation demonstrated in Fig. 4 to derive the necessary correction.

The apparatus has been used since 1954 May for a systematic survey of sporadic and summer daytime activity, the results of which will be published later. It is intended to continue and extend these observations in the future.

9. *Acknowledgments.*—This work has been carried out at the Jodrell Bank Experimental Station of the University of Manchester under the direction of Professor A. C. B. Lovell. We wish to thank Dr N. E. Hoskins of the Manchester University Computing Machine Laboratory for preparing the programme for computing the orbits. One of us (J. C. G.) is indebted to the Department of Scientific and Industrial Research for the award of a maintenance grant.

University of Manchester,
Jodrell Bank Experimental Station,
Cheshire:
1955 *November* 23.

References

(1) J. G. Davies and C. D. Ellyett, *Phil. Mag.*, **40**, 614, 1949.
(2) L. A. Manning, O. G. Villard and A. M. Peterson, *J. App. Phys.*, **20**, 475, 1949.
(3) J. A. Clegg, *Phil. Mag.*, **39**, 577, 1948.
(4) J. G. Porter, *Comets and Meteor Streams*, Chapman and Hall, London, 1952.
(5) G. S. Hawkins and Mary Almond, *M.N.*, **112**, 219, 1952.
(6) D. W. R. McKinley, *Ap.J.*, **113**, 225, 1951.
(7) F. L. Whipple and F. W. Wright, *M.N.*, **114**, 230, 1954.
(8) F. L. Whipple, *A.J.*, **59**, 201, 1954.
(9) T. R. Kaiser, *J. Atmos. Terr. Phys.* Suppl., **2**, on Meteors", 55, 1955.
(10) F. L. Whipple, *Private Communication.*
(11) N. Herlofson, *Reports on Progress in Physics*, **11**, 444, 1948.

THE DISSIPATION OF MAGNETIC ENERGY IN AN IONIZED GAS

T. G. Cowling

(Received 1955 December 2)

Summary

A general formula is derived for the rate of dissipation of magnetic energy in an ionized gas. The formula is used to confirm Piddington's value for the conductivity effective in producing dissipation. It is shown that, contrary to Piddington's assertions, an effective electric force must be taken into account when considering currents in the presence of a pressure gradient; however, this effective electric force has little effect on the dissipation. Piddington's results are completed by a general discussion of conductivity in a partially ionized gas. The results are applied to dissipation in interstellar gas; the effect of the magnetic field on the conductivity is shown to increase the rate of dissipation up to a point where the dissipation is not insignificant.

---

1. In recent papers J. H. Piddington (**1**) has studied certain problems of the dissipation of magnetic energy when an ionized gas moves in a magnetic field $\mathbf{H}$. He starts from the equation

$$\mathbf{j}=\sigma_0\mathbf{E}'_{\parallel}+\sigma_1\mathbf{E}'_{\perp}+\sigma_2 H^{-1}\mathbf{H}\times\mathbf{E}'_{\perp} \tag{1}$$

where $\mathbf{j}$ is the current-density, $\mathbf{E}_{\parallel}'$ and $\mathbf{E}_{\perp}'$ are respectively the components parallel and perpendicular to the magnetic field of the electric force on the moving material, and σ_0, σ_1 and σ_2 are appropriate conductivities. He finds that the rate of dissipation of magnetic energy per unit volume when currents flow perpendicular to the magnetic field is j^2/σ_3, where

$$\sigma_3=\sigma_1+\sigma_2^2/\sigma_1. \tag{2}$$

That is, σ_3 is the conductivity effective in dissipation in this case.

I do not query Piddington's result; I had, in fact, obtained an equivalent result a month or two before reading his paper. But his derivation appears unnecessarily complicated; I give below a simpler and more general derivation. Moreover, he accompanies his discussion by remarks suggesting that the "equivalent electric fields" introduced by myself (**2**) and Schlüter (**3**) are concepts which correspond to no essential physical reality, the true currents being always given by (1). Such a suggestion is incorrect; the relative diffusion of ions and electrons due to forces other than electric forces produces electric currents, and the equivalent electric force was introduced simply in order to take account of these currents. Schlüter, by skilful manipulation of such equivalent electric forces, was able to show that in certain cases the conductivity affecting the dissipation of electric energy was σ_0, not σ_3. Further investigation of the equivalent electric forces accordingly appears desirable, in order to be sure that they do not invalidate Piddington's results.

Piddington found that in a lightly ionized gas, when positive ions, as well as electrons, are free to spiral round the lines of magnetic force between collisions, σ_3 is much smaller than σ_0 (which is the conductivity in the absence of a magnetic field). This means that the magnetic field may increase the dissipation rate very appreciably in, for example, H I clouds in interstellar space and in the chromosphere above a sunspot. For the exact calculation of this important effect a further analysis of current-flow in a partially ionized gas is needed; this is also given below.

2. *Simple theory of dissipation.*—Assume first the validity of equation (1). The electric field $\mathbf{E}'$ of which $\mathbf{E}'_{\parallel}$ and $\mathbf{E}'_{\perp}$ are components is given in terms of the field $\mathbf{E}$ on matter at rest and the velocity $\mathbf{v}$ by

$$\mathbf{E}' = \mathbf{E} + \mathbf{v} \times \mathbf{H} \tag{3}$$

(e.m.u. are used throughout). The velocity $\mathbf{v}$ is taken to be the mass-velocity, defined as such that the total momentum per unit volume is the same as if every particle present had velocity $\mathbf{v}$.

The total magnetic energy is given by

$$W_{\mathrm{H}} = \int \frac{H^2}{8\pi} d\tau \tag{4}$$

integrated over the whole of space. Since $\partial \mathbf{H}/\partial t = -\operatorname{curl} \mathbf{E}$, the rate of change of the magnetic energy is

$$\begin{aligned} \frac{dW_{\mathrm{H}}}{dt} &= -\frac{1}{4\pi} \int \mathbf{H} \,.\, \operatorname{curl} \mathbf{E} \, d\tau \\ &= -\frac{1}{4\pi} \int \{ \operatorname{div} (\mathbf{E} \times \mathbf{H}) + \mathbf{E} \,.\, \operatorname{curl} \mathbf{H} \} \, d\tau. \end{aligned}$$

In this, by Green's theorem, the divergence term gives no contribution on integration over the whole of space, if one assumes a field which tends to zero sufficiently rapidly at infinity. Thus, since $\operatorname{curl} \mathbf{H} = 4\pi \mathbf{j}$,

$$\frac{dW_{\mathrm{H}}}{dt} = -\int \mathbf{E} \,.\, \mathbf{j} \, d\tau.$$

The changes in W_{H} are not wholly due to dissipation; the mechanical force $\mathbf{j} \times \mathbf{H}$ of electromagnetic origin does work on the material at a rate $(\mathbf{j} \times \mathbf{H}) \,.\, \mathbf{v}$ per unit volume, and this is done at the expense of the magnetic energy. Hence dW_{H}/dt includes a part $-(\mathbf{j} \times \mathbf{H}) \,.\, \mathbf{v}$ per unit volume due to the work done; the part of dW_{H}/dt due to dissipation is

$$\begin{aligned} -\int \mathbf{E} \,.\, \mathbf{j} \, d\tau + \int (\mathbf{j} \times \mathbf{H}) \,.\, \mathbf{v} \, d\tau &= -\int (\mathbf{E} + \mathbf{v} \times \mathbf{H}) \,.\, \mathbf{j} \, d\tau \\ &= -\int \mathbf{E}' \,.\, \mathbf{j} \, d\tau. \end{aligned} \tag{5}$$

That is, the dissipation of energy due to electrical resistance is $\mathbf{E}' \,.\, \mathbf{j}$ per unit volume and time.

For a current parallel to the magnetic field $\mathbf{j}=\sigma_0\mathbf{E}'$, so that the rate of dissipation is j^2/σ_0 per unit volume—the usual result. For a current perpendicular to the field $\mathbf{E}'$ reduces to $\mathbf{E}'_\perp$, and

$$\mathbf{E}'\cdot\mathbf{j}=\sigma_1 E_\perp'^2.$$

But, according to equation (1), $\mathbf{j}$ is now the sum of components $\sigma_1 E'_\perp$, $\sigma_2 E'_\perp$ at right angles. Thus

$$j^2=(\sigma_1^2+\sigma_2^2)E_\perp'^2$$

and the rate of dissipation per unit volume is

$$\sigma_1 j^2/(\sigma_1^2+\sigma_2^2)=j^2/\sigma_3.$$

This is Piddington's result.

3. *Equivalent electric force.*—In his reference to equivalent electric forces Piddington has confused the influence of a pressure gradient in causing diffusion and its effect in producing a state of motion, which reacts on the current equation through the term $\mathbf{v}\times\mathbf{H}$ in $\mathbf{E}'$. Clearly only the diffusion effect can be treated as an equivalent electric force; the effect on the state of motion is already adequately allowed for by the term $\mathbf{v}\times\mathbf{H}$ in $\mathbf{E}'$. Equally clearly equation (1) is incomplete until the diffusion effect is taken into account.

For a wholly ionized gas the diffusion effect is equivalent to adding to $\mathbf{E}'$ in equation (1) the electric force $\mathbf{E}''$ given by

$$\mathbf{E}''=(\operatorname{grad}p_e)/ne \tag{6}$$

where p_e is the electron-pressure, n the number-density of electrons, and e the electronic charge (2, p. 468). A simple derivation of (6) will be given for a binary mixture of positive ions of one type and electrons. From this it will be clear that the introduction of $\mathbf{E}''$ has no direct relation to Piddington's discussion of steady motion.

The gas is supposed to consist of ions of mass m_i and partial pressure p_i, and electrons of mass m_e and partial pressure p_e. The number-density of each is n; thus if the ion and electron gases are supposed to have the same temperature, $p_i=p_e$. Relative diffusion of the two gases occurs if the forces acting on them would, in the absence of diffusion and of collisions between ions and electrons, give them different accelerations $\mathbf{f}_i$ and $\mathbf{f}_e$; the velocity of diffusion is then proportional in magnitude to $\mathbf{f}_i-\mathbf{f}_e$. If the only applied forces are gravitational and electromagnetic,

$$\left.\begin{aligned} nm_i\mathbf{f}_i &= nm_i\mathbf{g}+ne\mathbf{E}'-\operatorname{grad}p_i \\ nm_e\mathbf{f}_e &= nm_e\mathbf{g}-ne\mathbf{E}'-\operatorname{grad}p_e \end{aligned}\right\} \tag{7}$$

It is to be noted that the partial pressures p_i, p_e alone enter into these equations; p_e, being due to the transport of momentum by electrons, affects ions only through collisions, which are neglected in deriving the equations.

Equations (7) give

$$\mathbf{f}_i-\mathbf{f}_e=\left(\frac{e}{m_i}+\frac{e}{m_e}\right)\mathbf{E}'-\frac{1}{nm_i}\operatorname{grad}p_i+\frac{1}{nm_e}\operatorname{grad}p_e.$$

Since m_e/m_i is negligibly small, this equation approximates to

$$\mathbf{f}_i - \mathbf{f}_e = \frac{e}{m_e}\left(\mathbf{E}' + \frac{1}{ne}\operatorname{grad} p_e\right)$$
$$= e(\mathbf{E}' + \mathbf{E}'')/m_e$$

by (6). The velocity of diffusion, and the resulting electric currents, are proportional in magnitude to $\mathbf{f}_i - \mathbf{f}_e$, and so to $\mathbf{E}' + \mathbf{E}''$. Thus, in calculating the electric currents, $\mathbf{E}'$ in equation (1) has to be increased by the equivalent electric force $\mathbf{E}''$.

4. *Dissipation and* $\mathbf{E}''$.—When $\mathbf{E}''$ is added in, equation (1) is replaced by

$$\mathbf{j} = \sigma_0(\mathbf{E}'_{\parallel} + \mathbf{E}''_{\parallel}) + \sigma_1(\mathbf{E}'_{\perp} + \mathbf{E}''_{\perp}) + \sigma_2 H^{-1}\mathbf{H} \times (\mathbf{E}'_{\perp} + \mathbf{E}''_{\perp}).$$

An argument similar to that at the end of Section 2 now shows that if $\mathbf{E}' + \mathbf{E}''$ is perpendicular to the magnetic field

$$(\mathbf{E}' + \mathbf{E}'') \cdot \mathbf{j} = j^2/\sigma_3.$$

Thus the rate of dissipation per unit volume is given by

$$\mathbf{E}' \cdot \mathbf{j} = j^2/\sigma_3 - \mathbf{E}'' \cdot \mathbf{j}. \tag{8}$$

Similarly if $\mathbf{E}' + \mathbf{E}''$ is parallel to the magnetic field

$$\mathbf{E}' \cdot \mathbf{j} = j^2/\sigma_0 - \mathbf{E}'' \cdot \mathbf{j}. \tag{8'}$$

In either case there is a new term $-\mathbf{E}'' \cdot \mathbf{j}$ representing the effect of the equivalent electric force.

The question is whether this term increases or diminishes the total dissipation. There is no universally valid reason why it should do either; it does so only if $\mathbf{E}''$ is related in some way to $\mathbf{j}$. And it is easy to see in the cases of most interest that $\mathbf{E}'' \cdot \mathbf{j}$ is, on an average, equal to zero.

Consider, say, a steady discharge. The current flowing in the discharge produces a magnetic field constricting the discharge, as a consequence of which the pressure inside the discharge column exceeds that outside. This gives rise to a pressure gradient, and an $\mathbf{E}''$, which are perpendicular to the current. Thus $\mathbf{E}'' \cdot \mathbf{j} = 0$ and (the magnetic field being perpendicular to $\mathbf{j}$) the dissipation is j^2/σ_3, just as if $\mathbf{E}''$ were not acting. This agrees with Schlüter's results (3), since in a wholly ionized gas σ_3 is (roughly) equal to σ_0, the conductivity in the absence of a magnetic field.

A case of greater astronomical interest is that in which the lines of force are nearly frozen into the material. The material motions bend the lines of force and the magnetic field reacts back on the motion; the currents flowing are not essentially determined by the conductivity, but by the changes in magnetic field, in accordance with the equation $\operatorname{curl}\mathbf{H} = 4\pi\mathbf{j}$. If ρ is the density, the equation of motion of the gas as a whole is

$$\rho\frac{d\mathbf{v}}{dt} = \rho\mathbf{g} - \operatorname{grad} p + \mathbf{j} \times \mathbf{H}. \tag{9}$$

The field reacts on the motion through the force $\mathbf{j} \times \mathbf{H}$; in part this force helps to accelerate the gas, but in part it tends at any time to be balanced by the pressure

gradient. Thus the part of $\mathbf{j}$ which is related to the pressure gradient can be expected to be perpendicular to it, and so to the equivalent electric force $\mathbf{E}''$. This means that, although the new term $-\mathbf{E}''.\mathbf{j}$ in the dissipation may fluctuate, its average value is likely to be zero.

Of course, as Schlüter and Biermann (**4**) have pointed out, the equivalent electric force $\mathbf{E}''$ may be able to build up a small magnetic field from nothing (so that $-\mathbf{E}''.\mathbf{j}$ corresponds to a negative dissipation). When $\mathbf{H}$ is very small, the connection of $\mathbf{j}$ with $\mathbf{E}''$ through the term $\mathbf{j}\times\mathbf{H}$ in (9) becomes unimportant. On the other hand, the equation of conduction now becomes $\mathbf{j}=\sigma_0(\mathbf{E}'+\mathbf{E}'')$, and a connection between $\mathbf{j}$ and $\mathbf{E}''$ is possible through this equation if $\mathbf{E}''$ is not balanced by an electrostatic field. However, this effect is important only when the magnetic field is very small.

5. *Partially ionized gas.*—To study electric currents in a partially ionized gas we must consider a mixture of at least three constituents—electrons, positive ions, neutral atoms. The general formulae governing diffusion in a multi-component gas in a magnetic field are excessively involved. However, relatively simple equations can be obtained in a first approximation.

Let the constituent particles of the rth gas have mass m_r, charge e_r and number-density n_r; let p_r and ρ_r be the partial pressure and density of the rth gas, and $\mathbf{V}_r$ be its velocity of diffusion relative to the mass. Then the velocities of diffusion are to be calculated from the equations *

$$\rho_r\frac{d\mathbf{v}}{dt}=\rho_r\mathbf{g}-\operatorname{grad}p_r+n_re_r(\mathbf{E}'+\mathbf{V}_r\times\mathbf{H})-\sum_s\theta_{rs}(\mathbf{V}_r-\mathbf{V}_s) \tag{10}$$

together with

$$\sum_r\rho_r\mathbf{V}_r=0. \tag{11}$$

Since in this case $\mathbf{j}=\Sigma n_re_r\mathbf{V}_r$, and $\Sigma n_re_r=0$, when the equation (10) is summed over all values of r the equation of motion (9) is obtained.

Equation (7) can be interpreted as follows (**3**). The velocities of diffusion are assumed to be small compared with the velocity $\mathbf{v}$ of the mass; thus $\rho_r d\mathbf{v}/dt$ gives the mass-acceleration of the rth gas per unit volume. Equation (7) equates this to the sum of the forces on the gas per unit volume – gravity $\rho_r\mathbf{g}$, the gradient of its partial pressure, the electric force on particles moving with average velocity $\mathbf{v}+\mathbf{V}_r$, and finally drag forces due to the diffusion relative to the other gases of the mixture. The drag due to diffusion relative to the sth gas is proportional to the relative velocity $\mathbf{V}_s-\mathbf{V}_r$, and to the number of collisions between particles of the rth and sth gases per unit volume and time.

Here it is sufficient to consider a gas composed of electrons, of charge $-e$ and mass m_e, positive ions, of charge e and mass m_i, and neutral atoms, of mass m_a. The electrons and ions spiral round the lines of magnetic force with spiral-frequencies ω_e, ω_i, where

$$\omega_e=eH/m_e, \qquad \omega_i=eH/m_i. \tag{12}$$

The number-densities of electrons and positive ions are each taken to equal n; the neutral atoms are supposed to contribute a fraction f to the total pressure p, and a fraction F to the total density.

* Such equations can be obtained, e.g., from (**2**), equation (22), on multiplying by $m_r\mathbf{C}_r$ and integrating, using equation (19) of (**2**) and evaluating the collision-integrals to a first approximation similar to that used in that paper.

The diffusion velocities of ions and electrons relative to the mass are taken to be $\mathbf{V}_i$, $\mathbf{V}_i+\mathbf{V}$. Since the mass-density of the electron-gas is negligible, equation (11) shows that the velocity of neutral atoms relative to the mass is $-(1-F)\mathbf{V}_i/F$; the velocities of ions and electrons relative to the neutral atoms are respectively $\mathbf{V}_i/F$ and $\mathbf{V}+\mathbf{V}_i/F$. The current-density is given by

$$\mathbf{j}=-ne\mathbf{V}. \tag{13}$$

By analogy with this we write

$$\mathbf{j}_i=ne\mathbf{V}_i. \tag{14}$$

Thus $\mathbf{j}_i$ denotes the current-density due to the diffusion velocity of ions (cancelled by an equal current-density due to the component $\mathbf{V}_i$ in the diffusion velocity of electrons).

If the mass-density of electrons is neglected, the electron equation of the set (10) takes the form

$$0=-\operatorname{grad}p_e-ne(\mathbf{E}'+(\mathbf{V}_i+\mathbf{V})\times\mathbf{H})-\theta_{ie}\mathbf{V}-\theta_{ae}(\mathbf{V}+F^{-1}\mathbf{V}_i). \tag{15}$$

In this, $-\theta_{ie}\mathbf{V}$ denotes the drag on the electron-gas due to collisions with ions. Conventionally a collision can be regarded as destroying, on an average, the relative motion of the colliding particles. Because of the smallness of m_e, this means effectively that each collision of electrons with ions results in a loss $m_e\mathbf{V}$ of momentum to the electrons. Thus if τ is the mean time between successive collisions of an electron with ions,

$$\theta_{ie}\mathbf{V}=n\tau^{-1}m_e\mathbf{V}, \qquad \theta_{ie}=nm_e\tau^{-1}. \tag{16}$$

Similarly if τ_e is the mean time between successive collisions of an electron with neutral atoms,

$$\theta_{ae}=nm_e\tau_e^{-1}. \tag{17}$$

On use of these expressions for θ_{ie} and θ_{ae}, equation (15) becomes

$$0=-\operatorname{grad}p_e-ne\{\mathbf{E}'+(\mathbf{V}_i+\mathbf{V})\times\mathbf{H}\}-nm_e(\tau^{-1}+\tau_e^{-1})\mathbf{V}-nm_e\tau_e^{-1}F^{-1}\mathbf{V}_i.$$

If $\mathbf{j}$ and $\mathbf{j}_i$ are introduced from equations (13) and (14) in place of $\mathbf{V}$ and $\mathbf{V}_i$, this becomes

$$0=-\operatorname{grad}p_e-ne\mathbf{E}'+(\mathbf{j}-\mathbf{j}_i)\times\mathbf{H}+(\kappa+\kappa_e)H\mathbf{j}-\kappa_eF^{-1}H\mathbf{j}_i, \tag{18}$$

where

$$\kappa=(\omega_e\tau)^{-1}, \qquad \kappa_e=(\omega_e\tau_e)^{-1}. \tag{19}$$

The quantities κ, κ_e are pure numbers; the condition for electrons to be able to spiral between collisions is that $\kappa+\kappa_e$ shall be small.

In the equation for ions in the set (10) one may similarly put

$$\theta_{ai}=nm_i\tau_i^{-1}. \tag{20}$$

However, τ_i is not exactly the mean time between collisions of an ion with neutral atoms. Each collision destroys only a fraction $m_a/(m_a+m_i)$ of its momentum $m_i\mathbf{V}_i/F$ relative to the neutral atoms; thus τ_i is $m_a/(m_a+m_i)$ times the collision-interval. On use of (17) and (20), the equation for ions becomes

$$(1-F)\rho\frac{d\mathbf{v}}{dt}=(1-F)\rho\mathbf{g}-\operatorname{grad}p_i+ne(\mathbf{E}'+\mathbf{V}_i\times\mathbf{H})+nm_e\tau^{-1}\mathbf{V}-nm_i\tau_i^{-1}F^{-1}\mathbf{V}_i.$$

Once again $\mathbf{V}$ and $\mathbf{V}_i$ are replaced by $\mathbf{j}$ and $\mathbf{j}_i$. Then if

$$\kappa_i = (\omega_i \tau_i)^{-1} \tag{21}$$

the equation becomes

$$(1-F)\rho \frac{d\mathbf{v}}{dt} = (1-F)\rho\mathbf{g} - \operatorname{grad} p_i + ne\mathbf{E}' + \mathbf{j}_i \times \mathbf{H} - \kappa H \mathbf{j} - \kappa_i F^{-1} H \mathbf{j}_i. \tag{22}$$

The equation for neutral atoms will not be used explicitly. Its place will be taken by (9), the equation of motion for the gas as a whole.

6. *The current equation.*—To obtain an equation giving $\mathbf{j}$, we must eliminate $\mathbf{j}_i$ between equations (18) and (22). Add the equations; then

$$(1-F)\rho \frac{d\mathbf{v}}{dt} = (1-F)\rho\mathbf{g} - \operatorname{grad}(p_i + p_e) + \mathbf{j} \times \mathbf{H} + \kappa_e H \mathbf{j} - (\kappa_e + \kappa_i) F^{-1} H \mathbf{j}_i. \tag{23}$$

Substitute for $d\mathbf{v}/dt$ from equation (9); then, since $(p_i + p_e) = (1-f)p$, one finds that

$$(\kappa_e + \kappa_i) F^{-1} H \mathbf{j}_i = F\mathbf{j} \times \mathbf{H} - (F-f) \operatorname{grad} p + \kappa_e H \mathbf{j}. \tag{24}$$

If this equation is used to eliminate $\mathbf{j}_i$ from equation (18), the desired equation for $\mathbf{j}$ is obtained; it is

$$ne\mathbf{E}' = \frac{\kappa\kappa_e + \kappa\kappa_i + \kappa_i\kappa_e}{\kappa_i + \kappa_e} H\mathbf{j} + (1 - 2\beta F)\mathbf{j} \times \mathbf{H} - \tfrac{1}{2}\{1 - f - 2\beta(F-f)\} \operatorname{grad} p$$
$$- \frac{F}{H(\kappa_i + \kappa_e)} \{F(\mathbf{j} \times \mathbf{H}) \times \mathbf{H} - (F-f) \operatorname{grad} p \times \mathbf{H}\} \tag{25}$$

where

$$\beta = \kappa_e / (\kappa_i + \kappa_e). \tag{26}$$

The case of a wholly ionized gas is obtained by making κ_e, κ_i, f and F tend to zero, their ratios remaining finite; this gives

$$ne\mathbf{E}' + \tfrac{1}{2} \operatorname{grad} p = \kappa H \mathbf{j} + \mathbf{j} \times \mathbf{H}. \tag{25'}$$

Since in this case $p_e = \frac{1}{2}p$, the term $\frac{1}{2} \operatorname{grad} p$ is responsible for the effective electric force $\mathbf{E}''$. The term $\mathbf{j} \times \mathbf{H}$ is responsible for the effect of the magnetic field on the conductivity (in spite of its apparent form, κH is actually independent of the magnetic field). If the terms $\mathbf{j} \times \mathbf{H}$ and $\operatorname{grad} p$ in the equation of motion are comparable (which is frequently the case in astronomical applications) the term $\frac{1}{2} \operatorname{grad} p$ must not be neglected in any problem in which the effect of the magnetic field on the conductivity has to be taken into account. This is the reason for insisting earlier on the importance of the equivalent electric force, in spite of its normally unimportant effect on the dissipation.

For a partially ionized gas, any equivalent electric force would have to include two terms proportional respectively to $\operatorname{grad} p$ and $\mathbf{H} \times \operatorname{grad} p$. However, because of the complication of the expression for such an equivalent electric force, there is little point in introducing it. The terms involving $\operatorname{grad} p$ and $\mathbf{H} \times \operatorname{grad} p$ in equation (25) are in general comparable with those of the other terms which involve the magnetic field unless the degree of ionization is small (f and F both nearly equal to unity).

7. *Dissipation in a partially ionized gas.*—Equation (25) can, if desired, be solved to give an equation like (1), with extra terms involving the pressure gradient. However, the dissipation $\mathbf{E}' \cdot \mathbf{j}$ per unit volume and time can readily be calculated direct from equation (25).

The term involving $\mathbf{j} \times \mathbf{H}$ in (25) makes no contribution to $\mathbf{E}' \cdot \mathbf{j}$. The term proportional to grad p, like that involving $\mathbf{E}''$ in Section 4, can be expected to make no contribution on an average, since grad p, in so far as it is affected by the electric currents, depends on them only through a component proportional to $\mathbf{j} \times \mathbf{H}$. Attention will therefore be confined to the other terms; these give a rate of dissipation per unit volume equal to

$$\{ne(\kappa_i+\kappa_e)\}^{-1}\{(\kappa\kappa_e+\kappa\kappa_i+\kappa_i\kappa_e)Hj^2+F^2H^{-1}\,|\,\mathbf{j}\times\mathbf{H}\,|^2 - F(F-f)H^{-1}\,\mathrm{grad}\,p\,.\,(\mathbf{j}\times\mathbf{H})\}. \qquad (27)$$

For currents flowing parallel to the magnetic field, (27) reduces to j^2/σ_0, where

$$\sigma_0 = \frac{ne(\kappa_i+\kappa_e)}{H(\kappa\kappa_i+\kappa\kappa_e+\kappa_i\kappa_e)}. \qquad (28)$$

As can be seen from equation (25), σ_0 (which is independent of H) denotes the conductivity parallel to the magnetic field, as in equation (1).

For currents flowing perpendicular to the magnetic field, the term involving grad $p\,.\,(\mathbf{j}\times\mathbf{H})$ in (27) can be expected in general to cancel an appreciable part of the term involving $|\,\mathbf{j}\times\mathbf{H}\,|^2$ when $F>f$, since grad p can be expected to have an appreciable part proportional to $\mathbf{j}\times\mathbf{H}$. (The condition $F>f$ implies that the ion-mass m_i is less than twice the neutral-atom mass m_a.) However, for a gas only slightly ionized F and f are both nearly equal to unity, and the term involving grad $p\,.\,(\mathbf{j}\times\mathbf{H})$ is relatively unimportant.

If this term is neglected, the dissipation (27) becomes j^2/σ_3 for currents perpendicular to the magnetic field, where

$$\frac{\sigma_0}{\sigma_3} = 1 + \frac{F^2}{\kappa\kappa_i+\kappa\kappa_e+\kappa_i\kappa_e}. \qquad (29)$$

The expression on the right of this equation gives the ratio in which the dissipation is increased by the magnetic field. If the neutral atoms are an appreciable fraction of the whole (F not small) and both electrons and ions spiral freely between collisions (κ_i, κ_e and κ all small) this ratio may be very large. The increased dissipation is due to collisions between neutral and charged particles, which tend to destroy the common velocity of diffusion $\mathbf{V}_i$ of the charged particles relative to the neutrals (the velocity of ambipolar diffusion, as Schlüter (3) calls it). As can be seen from equation (24), the "current" $\mathbf{j}_i$ due to $\mathbf{V}_i$ is large compared with $\mathbf{j}$ when electrons and ions are free to spiral (roughly in the ratio $F^2/(\kappa_e+\kappa_i)$); thus the corresponding dissipation can be expected to be large. In cases considered by Schlüter, the "current" $\mathbf{j}_i$ due to ambipolar diffusion was supposed not to flow; thus he did not find the increased dissipation given by equation (29). In the cases of interest in astronomy, however, there is nothing to prevent $\mathbf{j}_i$ from flowing, and the increased dissipation is certain.

Piddington obtained a special case of the result (29), when in a slightly ionized gas collisions between electrons and ions can be neglected. In this case $F=1$, $\kappa=0$, and in the increase in dissipation is roughly in the ratio $(\kappa_i\kappa_e)^{-1}=\omega_i\tau_i\omega_e\tau_e$,

for free spiralling; which is Piddington's result. However, in astronomical problems, even when the gas is only lightly ionized, it is normally not permissible to neglect the collisions between electrons and ions, because of their large electrostatic collision-radius.

8. *Application to interstellar clouds.*—The most immediate application of these results is to magnetic fields in interstellar clouds. An H I cloud can be supposed to consist of neutral hydrogen and ionized metal atoms; for illustrative purposes we assume the latter to be 10^{-4} of the whole number. The pressure in an H I cloud can perhaps be taken to be much the same as that in an H II cloud. Because of the lower temperature, this means that the density in an H I cloud is a hundred or so times that in an H II cloud; we assume a density of 100 atoms per cm^3, and a temperature of 100 deg. K.

In the absence of a magnetic field the conductivity would be about 7×10^{-12} e.m.u.; in spite of the fewness of the charged particles it is mainly determined by the collisions of electrons with ions. The time of decay of a magnetic field in a sphere of radius R is of order σR^2 if the conductivity σ of the material is unaffected by the field. Thus the time of decay would be 6×10^{19} years for an H I cloud of radius 5 pc if the effect of the field on the dissipation could be neglected.

On the other hand, assuming a magnetic field of order 10^{-5} gauss, one finds values of κ, κ_e and κ_i comparable with $3{\cdot}5 \times 10^{-6}$, 10^{-8} and $2{\cdot}3 \times 10^{-6}$; the last figure does not greatly depend on the mass m_i of the ions.* Thus the dissipation due to currents transverse to the magnetic field is, by equation (29), increased roughly in the ratio $1{\cdot}2 \times 10^{11}$ as a result of the effect of the field on the conductivity. Since currents must flow transverse to the field for an appreciable part of their course, the time of decay of a field in the cloud considered above is reduced in about the same ratio, i.e. to 5×10^8 years. These results should be compared with those of Gurevich (**5**), based on a less accurate formula for the reduced conductivity.

A time of decay of order 5×10^8 years is still very large, but it is not, like a time of order 6×10^{19} years, so large as to make dissipation effects altogether negligible. The calculated time of decay is admittedly very approximate. For example, κ, κ_i and κ_e are inversely proportional to H; thus if the field were only 10^{-6} gauss the time of decay would be increased 100-fold, making dissipation correspondingly less important. Likewise the assumed densities and collision-radii are somewhat uncertain. Perhaps the biggest ground for uncertainty is in a possible large increase in the dissipation by reason of turbulence, as suggested for different reasons by Sweet (**6**) and Elsasser (**7**). For these reasons, the possible effects of dissipation cannot be dismissed out of hand as certainly negligible in studies of galactic magnetic fields.

The assumption that the whole of the material, neutral as well as ionized, moves about with the lines of force is still reasonably obeyed, even in the conditions assumed above. The charged particles are closely attached to the lines of force by their spiral motions. The motion of the neutral atoms relative to these is comparable with $\mathbf{V}_i$, where

$$neV_i = j_i \sim j/(\kappa_e + \kappa_i).$$

* Details of the calculation are given in the Appendix.

But if R is the radius of the cloud, $j \sim H/4\pi R$, since $\operatorname{curl} \mathbf{H} = 4\pi \mathbf{j}$; thus

$$V_i \sim H\{4\pi neR(\kappa_e + \kappa_i)\}^{-1} \sim 10^2 \text{ cm/sec.}$$

That is, the motion of neutral atoms across the lines of force is fairly slow compared with the mass motions actually likely to be present. However, the lines of force are less securely frozen into the material than is usual in astronomical problems.

The figures quoted above refer to H I clouds. For H II clouds the situation is not altogether different, since even in these an appreciable fraction of the atoms can be expected to be neutral. The significant term in the dissipation (27) is the term $F^2\{Hne(\kappa_i + \kappa_e)\}^{-1} |\mathbf{j} \times \mathbf{H}|^2$. As compared with H I clouds, $\kappa_i + \kappa_a$ is reduced roughly in the ratio $F/100$ (being proportional to n_a, the number-density of neutral atoms); n is increased about 100-fold. This shows that the dissipation is decreased roughly in the ratio $F:1$. This even in H II clouds the rate of dissipation need not be altogether insignificant.

Note added 1956 *February*

A referee has invited me to clear up a difficulty implicit in the expression (27) for the dissipation of magnetic energy. The expression indicates a dissipation which tends to infinity like ρ^{-2} as the density ρ tends to zero. Such a result is clearly absurd; dissipation of electric currents occurs only because of collisions between ions, electrons and neutral atoms, and these become negligibly few as $\rho \to 0$.

The dissipation indicated by the expression (27) is proportional to ρ^{-2} only if the current $\mathbf{j}$ is independent of ρ. In fact, however, in the case of importance in magneto-hydrodynamics $\mathbf{j} \times \mathbf{H}$ is at most comparable with $\operatorname{grad} p$ (cf. equation (9)). Thus $\mathbf{j} \times \mathbf{H}$ must be regarded as proportional to ρ, and the dissipation given by (27) remains finite at low densities.

Even so, (27) overestimates the total dissipation at very low densities. Equation (10), on which it is based, is a diffusion equation, valid if the gas moves as a whole, the different constituents (electrons, ions, neutral atoms) having only relatively small velocities relative to the mass. In Section 8 this assumption was shown to be justified even in the rarefied interstellar medium. But if the density were further reduced, a point would be reached at which the assumption is no longer justified. According to equation (24), at low densities $\mathbf{j}_i$ is proportional to $\mathbf{j} \times \mathbf{H}/\rho$, and so is independent of the density; by equation (14), this implies that the velocity of diffusion $\mathbf{V}_i$ of ions relative to the mass increases like $1/\rho$. The increase cannot go on indefinitely. It goes on until $\mathbf{V}_i$ becomes comparable with the mass-motions present; when this is so the process ceases to be one of diffusion in a single gas, and instead there are a neutral gas and an ion gas moving independently. The mutual velocity of the two gases remains finite; electromagnetic dissipation, which is due to collisions between particles of the two gases, now drops off to zero as ρ^2, like the number of collisions.

It follows, therefore, that the expression (27) does not apply at vanishingly small densities. However, even the low densities of interstellar clouds are sufficient to make it applicable.

Appendix

The equation (29) for σ_3 can be written

$$\frac{1}{\sigma_3} = \frac{1}{\sigma_0} + \frac{F^2 H}{ne(\kappa_i + \kappa_e)}. \tag{30}$$

Under conditions of free spiralling the second term on the right is the important one; thus we need to determine κ_i and κ_e. On using equations (12), (17) and (19),

$$\kappa_e = \theta_{ae}/neH.$$

Also by reference (2), equation (36), θ_{ae} can be expressed in terms of the coefficient of diffusion D_{ae} of electrons relative to neutral atoms in the absence of ions by the equation

$$\theta_{ae} = \frac{nn_a kT}{(n+n_a)D_{ae}}.$$

The coefficient of diffusion D_{ae} is given in terms of the effective collision-distance r_{ae} by

$$D_{ae} = \left\{\frac{kT(m_a+m_e)}{2\pi m_a m_e}\right\}^{1/2} \frac{3}{8(n+n_a)r_{ae}^2}.$$

Combining these results

$$\kappa_e = \frac{8n_a r_{ae}^2}{3eH}\left\{\frac{2\pi kTm_a m_e}{m_a+m_e}\right\}^{1/2}. \tag{31}$$

Similarly

$$\kappa_i = \frac{8n_a r_{ai}^2}{3eH}\left\{\frac{2\pi kTm_a m_i}{m_a+m_i}\right\}^{1/2}. \tag{32}$$

The values of κ_e and κ_i quoted in the text are obtained by taking

$$r_{ai} = 7{\cdot}5 \times 10^{-8} \text{ cm}, \qquad r_{ae} = 2 \times 10^{-8} \text{ cm},$$

values suggested by mobility measurements. Since κ_i is large compared with κ_e, for purposes of calculating σ_3 we do not need to know κ_e very accurately. The mass m_a is taken to be that of a proton; κ_i is not sensitive to the exact value of m_i, and is calculated assuming m_i/m_a large. The value of κ can be calculated from a similar formula; the values of κ and σ_0 quoted in the text correspond to a collision-distance of about 4×10^{-5} cm for the (electrostatic) collisions between ions and electrons.

The University,
Leeds 2:
1955 *December* 1.

References

(1) J. H. Piddington, *M.N.*, **114,** 638 and 651, 1955.
(2) T. G. Cowling, *Proc. Roy. Soc.* A, **183,** 453, 1945.
(3) A. Schlüter, *Z. f. Naturforschung* **5A,** 72, 1950; **6A,** 73, 1951.
(4) A. Schlüter and L. Biermann, *Z. f. Naturforschung,* **5A,** 237, 1950.
(5) L. E. Gurevich, *Problems of Cosmogony* (Moscow, 1954), Vol. **2,** p. 151.
(6) P. A. Sweet, *M.N.*, **110,** 69, 1952.
(7) W. M. Elsasser, *Univ. of Utah Rep. on the Earth's Magnetism and Magnetohydrodynamics,* No. 7, 1954, *Amer. J. Phys.*, **23**, 590, 1955.

CONTENTS

PAGE

Meeting of 1956 January 13 :

Death of Professor W. M. H. Greaves 1

Award of the Gold Medal to Professor T. G. Cowling... 1

Fellows elected 1

Presents announced 2

A. J. Wesselink, Spectroscopic and photometric observations of S Doradus ... 3

B. E. J. Pagel, Results of a search for bright β Cephei variables in the southern sky 10

R. J. Tayler, The evolution of unmixed stars 25

A. B. Hart, Motions in the Sun at the photospheric level. VI. Large-scale motions in the equatorial region 38

D. E. Blackwell, A study of the outer solar corona from a high altitude aircraft at the eclipse of 1954 June 30. II. Electron densities in the outer corona and zodiacal light regions 56

C. W. Allen, Coronal photometry at the eclipse of 1954 June 30 69

T. D. Kinman, An attempt to detect deuterium in the solar atmosphere 77

J. v. B. Lourens, Astrometric observations of Eros during the 1954 opposition ... 88

G. S. Hawkins, A radio echo survey of sporadic meteor radiants 92

J. C. Gill and J. G. Davies, A radio echo method of meteor orbit determination ... 105

T. G. Cowling, The dissipation of magnetic energy in an ionized gas 114

Printed in London by Taylor & Francis, Ltd., 1956 November